

Thalamic and cortical contributions to physiological brain rhythms in vivo

Thalamische und kortikale Komponenten
physiologischer Hirnrhythmen *in vivo*

Dissertation
zur Erlangung des Doktorgrades
der Naturwissenschaften

vorgelegt beim Fachbereich 15
der Johann Wolfgang Goethe-Universität
in Frankfurt am Main

von
Joscha Tapani Schmiedt
aus Oxford, Großbritannien

Frankfurt (2016)
(D 30)



Ernst Strüngmann Institute for Neuroscience
in Cooperation with Max Planck Society



Vom Fachbereich 15 der Johann Wolfgang von Goethe-Universität als Dissertation angenommen.
Dekanin: Prof. Dr. Meike Piepenbring
Gutachter: Prof. Dr. Manfred Kössl und Dr. Michael Schmid
Datum der Disputation: 2.5.2016

Contents

Deutsche Zusammenfassung	iii
I General introduction and discussion	1
1 Introduction	3
1.1 Oscillations in dynamical systems	5
1.2 Rhythms of the brain	8
1.3 Anatomical and functional aspects of the thalamus	17
1.4 The primate visual system	20
2 Discussion and summary	25
2.1 Contribution of thalamus to slow waves	25
2.2 Contribution of primary visual cortex to extrastriate beta rhythms . .	28
2.3 Summary	30
II Contribution of thalamus to slow/delta rhythms	31
3 Essential thalamic contribution to slow waves of natural sleep	33
4 Rhythmic 1-5 Hz firing of pulvinar in behaving monkeys	47
III Contribution of primary visual cortex to extrastriate beta rhythms	55
5 Motion-sensitive responses in area V4 without V1	57
6 Beta oscillation dynamics in extrastriate cortex after removal of V1	65
IV Appendix	75
Bibliography	77
List of publications	85
Acknowledgements	87
CV	89

Deutsche Zusammenfassung

Rhythmen, d.h. periodische Abfolgen von Ereignissen und Zuständen, sind in physiologischen Systemen allgegenwärtig; sei es bedingt durch äußere Umwelteinflüsse, z.B. im zirkadianen System durch den Nacht-Tag-Wechsel, oder in raffinierten biomechanischen Volumenpumpen wie dem Herzen oder der Lunge. Auch im zentralen Nervensystem konnte seit der Entdeckung des Alpha-Rhythmus (10 Hz) im Elektroenzephalogramm des Menschen eine enorme Vielfalt elektrischer Rhythmen identifiziert werden, die auf unterschiedlichsten räumlichen wie zeitlichen Skalen in beinahe allen Hirnarealen operieren. Im Gegensatz zum Herzen oder der Lunge, bei denen eine gewisse Rhythmizität einen wesentlichen Teil ihrer Funktionsweise darstellt, ist es bei den Rhythmen des Gehirns schwierig eindeutige Funktionen zuzuordnen – einerseits durch die Komplexität in Hirnstruktur und möglichem Verhalten andererseits durch die Schwierigkeit experimentell die Rhythmizität isoliert zu manipulieren.

Um die mögliche funktionelle Relevanz neuronaler Rhythmen zu verstehen ist ein wesentlicher Schritt, ihre Generationsprozesse zu verstehen. Nach dem Aufdecken der zu Grunde liegenden Mechanismen können dann experimentelle Methoden entwickelt werden, die spezifisch auf die Rhythmen und nicht auf neuronale Aktivität als ganzes wirken. Ziel dieser Arbeit war es den Einfluss zweier Hirnareale auf die Entstehung zweier physiologischer *in vivo*-Rhythmen zu untersuchen: (1) die Rolle des Thalamus für die langsamen Delta-Rhythmen (0.5 bis 5 Hz) im Schlaf- und Wachzustand (**Kapitel 3** bzw. 4), (2) die Rolle des primären visuellen Kortex für Beta-Rhythmen (13 bis 30 Hz) im visuellen

Assoziationskortex (**Kapitel 5** und **6**). Dabei wurde in beiden Fällen das zu untersuchende Areal inaktiviert und die darauffolgende Entwicklung des Rhythmus in den efferenten Projektionsarealen aufgenommen.

Rolle des Thalamus für langsame Delta-Rhythmen

Der Thalamus im Mittelhirn ist die letzte Verarbeitungsstation sensorischer Signale bevor sie den Kortex erreichen, wo sie zu einer kohärenten Wahrnehmung integriert werden. Durch ihre besondere Physiologie können thalamische Nervenzellen zwischen zwei Feuermodi wechseln: (1) einem rhythmischen Modus bei leichter Hyperpolarisation der Membran, und (2) einem tonischen Modus bei normaler Membranspannung, der dem Verhalten anderer bspw. kortikaler Nervenzellen ähnelt. Dadurch eignen sich thalamische Zellen dazu, als Taktgeber für Rhythmen zu fungieren, besonders im Schlafzustand in dem das Membranpotential leicht gesenkt im Vergleich zum Wachzustand ist. Bei Hyperpolarisation der thalamischen Nervenzellen werden sogenannte T-Typ-Kalzium-Kanäle aktiv, die normalerweise inaktiv sind und in Wechselwirkung mit anderen Membranströmen zu rhythmischen Feuermustern führen.

Da ein einflussreiches Experiment gezeigt hatte, dass der kortikale langsame Rhythmus nach thalamischer Resektion weiterbestand wurde bis vor kurzem angenommen, dass der Thalamus nicht wesentlich zur Generation der physiologischen Schlafrhythmen abseits der sogenannten Schlafspindeln beiträgt. In der vorliegenden Arbeit konnte nun nun gezeigt werden, dass nach reversibler Inhibition des Thalamus durch lokale Applikation pharmakologischer Substanzen die Expression dieses Rhythmus im verbundenen kortikalen Areal dramatisch reduziert wurde (**Kapitel 3**). Dieser Effekt trat ebenfalls auf, wenn nur die Kalzium-Kanäle selektiv blockiert wurden. Dies deutet daraufhin, dass der Thalamus wesentlich zur Entstehung des Rhythmus im Kortex beiträgt.

Eine andere Studie konnte inzwischen zeigen, dass der Unterschied zum früheren Experiment vermutlich auf plastische Adaptationsprozesse nach der Resektion zurückzuführen ist. Dies lässt vermuten, dass so-

wohl Thalamus als auch Kortex isoliert langsame Rhythmen erzeugen können, es jedoch erst im Zusammenspiel *in vivo* zur vollständigen Expression des physiologischen Rhythmus kommt.

Im Wachzustand zeigen sich im Kortex unter bestimmten Umständen ebenfalls Rhythmen, die den langsamen Schlafrythmen ähneln. In **Kapitel 4** dieser Dissertation wird gezeigt, dass ein anderer Teil des Thalamus, der Pulvinar, der zwar keinen sensorischen Input bekommt aber ebenso als rhythmischer Taktgeber fungieren kann, wahrscheinlich zur Entstehung dieser langsamen Wachrhythmen beiträgt: Denn, der Pulvinar zeigt im Wachzustand Feuermuster, die denen während des Schlafes sehr stark ähneln.

Rolle des primären visuellen Kortex für Beta-Rhythmen im visuellen Assoziationskortex

Im visuellen System sind im aufmerksamen Wachzustand schnellere Rhythmen wie der Beta-Rhythmus (13 bis 30 Hz) und der Gamma-Rhythmus (>30 Hz) vorherrschend. Für den Gamma-Rhythmus gibt es inzwischen gute Modelle für seine Entstehung, die mit einer Vielzahl von Methoden untersucht wurden. Für den Beta-Bereich gibt es hingegen noch wenige Studien, die seine Generation zurückverfolgen konnten. Es wurde vermutet, dass Feedback-Prozesse, die von "höheren" in "niedrigere" Areale in der kortikalen Hierarchie projizieren, für die Generation der Beta-Rhythmen wesentlich sind. Um den Einfluss aus der entgegengesetzten Feedforward-Richtung zu überprüfen, wurde in der vorliegenden Arbeit der primäre visuelle Kortex (V1) chirurgisch entfernt und die verbleibende rhythmische Aktivität in verbundenen, efferenten Arealen untersucht. Dabei zeigte sich, dass der Beta-Rhythmus unabhängig von Aktivität in V1 bestehen kann, und durch Aktivierung von V1-umgehenden sensorischen Bahnen sogar verstärkt werden konnte (**Kapitel 5 und 6**).

Gleichzeitig verminderte die Entfernung von V1 das Auftreten von Gamma-Rhythmen in verbundenen Arealen. Diese Ergebnisse sprechen für differentielle Entstehungsmechanismen dieser beiden Rhythmen: Gamma-Rhythmen sind wesentlich von sensorischen Feedforward-Signalen, Beta-Rhythmen hingegen von internen Feedback-Signalen geprägt.

Zusammenfassung und Ausblick

In der vorliegenden Arbeit wurden die Generationsprozesse zweier Hirnrhythmen untersucht, den langsamen Delta-Rhythmen, und den Beta-Rhythmen im visuellen Kortex. Dabei wurde der Einfluss eines Hirnareals in den sensorischen Bahnen auf Rhythmen im Folgeareal untersucht.

Die vorliegende Arbeit konnte zeigen, dass thalamische Zellen durch ihre Kalziumkanäle ein wesentlicher Schrittmacher langsamer Hirnrhythmen im Kortex sind. Diese Erkenntnis wird es zukünftigen Studien ermöglichen durch spezifische experimentelle Manipulationen die funktionelle Relevanz dieser Rhythmen zu untersuchen. Für die Beta-Rhythmen hat sich gezeigt, dass der primäre visuelle Kortex nicht notwendig für die Expression dieses Rhythmus im visuellen Assoziationskortex ist. Vielmehr bedarf es der Aktivierung von Bahnen die entgegen der klassischen Reizbahn laufen um Beta-Rhythmen zu erzeugen. Im visuellen Kortex werden noch weitere Studien notwendig sein, um zu testen wie genau diese Feedbacksignale mit lokalen Prozessen wechselwirken und den Beta-Rhythmus generieren.

Part I

General introduction and discussion

Introduction

Rhythms, i.e. periodic sequences of events or states, are a ubiquitous feature of physiological systems such as the heart, the lungs or the brain (Keener and Sneyd, 2009). For the brain in particular, the diversity of rhythms is remarkable (Buzsáki, 2006), ranging from low frequency rhythms in the slow/delta band (0.5 to 4 Hz, Crunelli and Hughes, 2010) during sleep to gamma band oscillations (30 to 120 Hz, Fries, 2009) rhythms during alert behavior, all expressed in various brain areas and at various spatial scales. To understand whether these rhythms subserve a function for the organism it is important to also understand the underlying mechanisms that generate them. While the generation of some rhythms appear to be well-understood, e.g. sleep spindles, others such as the cortical beta rhythm (13 to 30 Hz) have remained elusive.

Understanding the generation of a brain rhythm involves multiple spatial scales, from identifying intracellular mechanisms such as the contribution of individual transmembrane currents to studying how specific neuronal populations or areas affect the full physiological rhythm present in the intact, highly interconnected brain. The aim of this work has been to delineate the mechanistic contributions of individual brain areas to the *in vivo* generation of two particular rhythms present in efferent areas: (1) The first part of this work studies the influence of thalamo-cortical neurons on cortical *slow/delta waves* (0.5 to 4 Hz) of sleep (Part

II, Chapter 3) that are sometimes also present in awake animals (Part II, Chapter 4). (2) The second part is about the contribution of primary visual cortex to the *beta rhythm* (13 to 30 Hz) in extrastriate cortex of awake behaving animals (Part III, Chapters 5 and 6).

Physiological systems such as neurons or the brain can often be described and analyzed with the tools of dynamical systems theory, which may help to understand the generation of rhythmic behavior. In this introduction I will therefore first consider how rhythms can be generated and shaped in simple theoretical models of dynamical systems (Section 1.1). Next, I will briefly overview the diversity of rhythms in the brain (1.2), and introduce anatomical and physiological aspects of the brain areas that were studied in Parts II (1.3) and III (1.4).

1.1 Oscillations in dynamical systems

In physics, the temporal dynamics of a system are often described using differential equations (Strogatz, 2014) of the form

$$\frac{d}{dt}x = \dot{x} = f(x, t) \quad , \quad (1.1)$$

where the temporal derivative \dot{x} of the n -dimensional state variable x is a function f of the current state and/or time t . More complex systems may involve coupled variables, and/or higher order derivatives, which, however, can always be reduced to the form in Equation (1.1). Differential equations can only for certain cases be solved analytically, but always with numerical simulations.

1.1.1 The harmonic oscillator

The simplest dynamical system that exhibits oscillatory behavior is the harmonic oscillator. The harmonic oscillator is characterized by counteracting feedback such that the driving force (i.e. acceleration, derivative of velocity v) is antiproportional to the current state x :

$$\ddot{x} = \dot{v} = -kx \quad (1.2)$$

In such a system, an increase in x will cause antagonistic feedback \ddot{x} . This type of differential equation is solved by sinusoidal functions

$$x(t) = A \sin(\omega t + \phi) \quad (1.3)$$

with amplitude A frequency $f = \frac{\omega}{2\pi}$ and phase ϕ because

$$\frac{d^2}{dt^2}A \sin(\omega t + \phi) = \frac{d}{dt}A\omega \cos(\omega t + \phi) = -\omega^2 \cdot A \sin(\omega t + \phi)$$

For example, for the ideal pendulum (Fig. 1.1A) of mass m and length l that is exposed to gravitation g and deflected little by ϕ , the force acting on the pendulum is given by

$$\begin{aligned} F = m \cdot \ddot{\phi} &= -\frac{mg}{l} \phi \\ \text{or} & \\ \ddot{\phi} &= -\frac{g}{l} \phi = -k\phi \end{aligned} \quad (1.4)$$

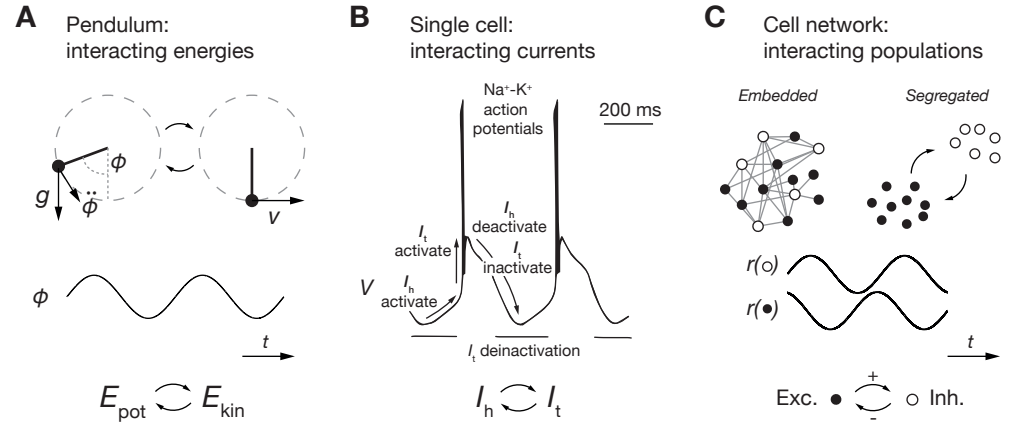


Figure 1.1 | Oscillations in dynamical systems are the result of feedback interactions.

A, An ideal pendulum exposed to gravitation g and displaced by ϕ from the resting equilibrium position will oscillate between a state of maximal potential energy at the highest point and maximal kinetic energy at the lowest.

B, Example for a cell-intrinsic oscillation. A thalamocortical cell released from hyperpolarization will oscillate between burst firing and hyperpolarization due to an interplay between trans-membrane currents. Reproduced with permission from McCormick and Pape (1990).

C, Network oscillations of (population) firing rate result from interacting populations. In this example an inhibitory population (open circles) and an excitatory population (filled circles) are coupled. By mutual feedback their firing rates r can oscillate (irrespective whether embedded in same area or segregated), possibly with a delay.

In other words, gravitation is providing negative feedback to the deflection, and pulls it back toward the non-deflected or relaxed state. When released from deflection ϕ_0 the pendulum will oscillate between maximum and minimum deflection and exhibit rhythmic behavior given by the sinusoidal function

$$\phi(t) = \phi_0 \cos(\sqrt{kt}) \quad . \quad (1.5)$$

In terms of energy, the pendulum oscillates between maximum potential energy

$$E_{\text{pot}} = \frac{1}{2}mk\phi^2 \quad (1.6)$$

at its highest point $\phi = \phi_0$ and maximum kinetic energy

$$E_{\text{kin}} = \frac{1}{2}m\dot{\phi}^2 \quad (1.7)$$

at its lowest point $\phi = 0$ where the velocity $\dot{\phi}$ is largest.

1.1.2 Anharmonic oscillations

Due to its simplicity, the harmonic oscillator is an attractive example that illustrates how oscillatory behavior results from an interplay of energies (kinetic and potential energy, Fig. 1.1A). In biological systems however, most oscillations are not sinusoidal but show pulse-like characteristics, such as the quick contraction of the heart muscles and the following slow release, or the quick discharge during neuronal firing and the following silence (see e.g. Buzsáki, 2006, and Fig. 1.1B). To understand such systems, more complex models such as the Van der Pol oscillator (Kanamaru, 2007) were developed. These *relaxation oscillators* capture more of the dynamics of typical biological systems; however, the basic necessary components that lead to oscillatory behavior – opposing forces interacting through a feedback mechanism – are similar to the harmonic oscillator (see Pikovsky et al., 2008, for an introduction).

1.1.3 Coupling of oscillators

When oscillators are coupled it is possible under specific conditions that they settle on a common rhythm, i.e., synchronize (Pikovsky and Rosenblum, 2007; Pikovsky et al., 2008). The final rhythm will depend on coupling (weak vs strong, positive vs negative) as well as the properties of the partaking oscillators (frequency, linear vs nonlinear, etc.). For example, two oscillators with not too different frequencies can synchronize with an intermediately rhythm under certain conditions (Fig. 1.2). In general however, n coupled nonlinear oscillators are not analytically tractable (Pikovsky et al., 2008; Strogatz, 2014).

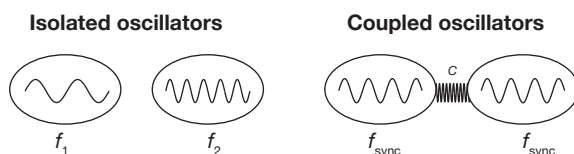


Figure 1.2 | Synchronization of coupled oscillators.

Two oscillators of different inherent frequencies f_1 and f_2 (left) can synchronize under certain conditions if coupled with coupling strength C , and settle on a common frequency f_{sync} (right). In general however, the extent of synchronization depends on many parameters of the coupling and individual oscillators.

1.2 Rhythms of the brain

Since Hans Berger's discovery of the alpha rhythm in the electroencephalogram (EEG) of his son (Berger, 1929), rhythmic phenomena were found in virtually all areas and at all spatial scales of the central nervous system, with diverse frequencies and properties. An excellent overview of the topic can be found in the book by György Buzsáki (2006) or the work of Mircea Steriade (e.g. Steriade, 1993) and only the aspects relevant for this thesis will be presented here.

In the brain, electrical rhythms can be observed at spatial scales ranging from the membrane potential of a single cell up to the summed synchronized activity of many populations in the EEG. Therefore, rhythmic phenomena are a reflection of rhythmic spiking of neurons, either individual pacemaking neurons, or populations that synchronize and engage in a rhythm at the population level. In other words, neural oscillators generate the rhythms that are detectable with electrodes (Steriade, 1993). In neural systems, two kinds of oscillators can be identified (Wang, 2003):

1. *cell-intrinsic oscillators* that can operate in isolation without rhythmic input, e.g., in a disconnected *in vitro* preparation (Fig. 1.1B)
2. *synaptic network oscillators* that result from coupling between (opposing) populations via chemical synapses (Fig. 1.1C)

Cell-intrinsic oscillators that act like pacemakers can be found mostly in subcortical areas such as the thalamus, (<1 to 10 Hz, Steriade and Deschenes, 1984; McCormick and Pape, 1990; Hughes et al., 2002, 2004), the substantia nigra (0.5 to 5 Hz, Fujimura and Matsuda, 1989; Harris et al., 1989; Grace and Onn, 1989) or the hippocampus (3 to 10 Hz, Goutagny et al., 2009). Probably due to its heavily interconnected structure with many different cell types, the cortex is the most prominent site that produces network oscillations, for example the slow oscillation (<1 Hz, Sanchez-Vives and McCormick, 2000) or gamma oscillations (>30 Hz, Buzsáki and Wang, 2012). In the fully connected, intact brain,

	Freq. (Hz)	Engaged brain areas
slow	0.1-1	Cortex, thalamus, (hippocampus)
delta	1-5	Cortex, thalamus
theta	4-8	Hippocampus, cortex
spindles	7-14	Thalamus, Cortex
alpha	8-13	Visual cortex, LGN
beta	13-30	Motor, parietal and visual cortex, basal ganglia
gamma	>30 Hz	Visual cortex, hippocampus

Table 1.1 | Incomplete list of common names for frequency bands of brain rhythms. See Steriade (1993) and Buzsáki (2006) for an overview.

these types of oscillators are connected, i.e. coupled, with each other and non-oscillating neural populations. Thus, the full physiological rhythms that can be observed *in vivo* are the result of complex network interactions with embedded oscillators.

The number of discovered brain rhythms has grown substantially since the alpha rhythm in the EEG. Unfortunately, the taxonomy has been based mostly on frequency range and order of discovery, not generative mechanisms (Buzsáki et al., 2013). A few common names that are used in this work are listed in Table 1.1.

A more or less general feature of brain rhythms is that low frequency rhythms such as the delta rhythms are associated with behavioral states of minimal arousal such as sleep or drowsiness. High frequency rhythms on the other hand are strongest in highly alert animals (Steriade, 1993). However, such an association is less clear for some intermediate rhythms, e.g. the alpha and beta rhythms.

1.2.1 Measuring brain rhythms

As rhythmic brain activity can occur at different spatial scales and in different brain areas, data acquisition approaches have to be optimized for each case. As most brain rhythms (~1 to 100 Hz requiring a sampling rate of at least 200 Hz) are faster than the temporal resolution of current functional magnetic resonance imaging techniques (sampling every ~2 s, i.e., up to a Nyquist frequency¹ of 0.25 Hz, Huettel et al., 2009), electrophysiological methods have to be employed. In electrophysiol-

¹half of the sampling frequency

ogy, the voltage between an active and a reference electrode is measured (Hubbard et al., 1969; Nunez and Srinivasan, 2006). Depending on the size, material and placement of these electrodes, it is possible to measure at different spatial scales ranging from the membrane potential or action potentials of a single cell (single-unit activity, SUA), action potentials of a small neuron population (multi-unit activity, MUA), summed synaptic activity of an intermediate sized population (local field potential, LFP) up to the synchronized activity of large cortical areas in the EEG. Whereas cortical regions can sometimes be sampled with non- or minimally invasive techniques, subcortical structures have to be reached with penetrating electrodes. In all cases, the reference electrode has to be placed with care such that the sampled voltage reflects the electric field of interest.

Rhythms of the brain can then be observed in the recorded signals, be it in a rhythmic sequence of action potentials (for pacemaker-like neurons) or in continuous field potentials. The key method in the quantification of these rhythms is the Fourier transform \mathcal{F} , which decomposes a signal $x(t)$ using sinusoidal functions of frequency $f = \omega/(2\pi)$:

$$\begin{aligned}\mathcal{F}_x(\omega) &= \frac{1}{\sqrt{2\pi}} \int_{-\infty}^{\infty} x(t) e^{-i\omega t} dt \\ &= \frac{1}{\sqrt{2\pi}} \int_{-\infty}^{\infty} x(t) (\cos(-\omega t)) + i \sin(-\omega t) dt\end{aligned}\tag{1.8}$$

In general, this decomposition from time into frequency domain is only valid for infinitely long, well-behaved² functions $x(t)$. To use this method for digitally sampled signals as it is the case with modern signal acquisition devices, one usually employs the Faster Fourier Transform algorithm (FFT, Cooley and Tukey, 1965), which is available in virtually all common signal processing packages. As the rhythms of the brain are generally non-sinusoidal and transient, care has to be taken to optimize analysis parameters such as the analysis window length and shape etc. Frequency decomposition with the FFT can then yield information

²differentiable, continuous, integrable in L^2 space

about the strength and (co)modulations of rhythms in the neuronal activity (see Torrence and Compo, 1998; Mitra and Bokil, 2007, for introduction and review). For each frequency (and time point if applied with a moving window) up to the Nyquist frequency, the FFT yields a complex coefficient \mathcal{F} , with

$$A = |\mathcal{F}| \quad (1.9)$$

$$\phi = \arctan \frac{\text{Re}(\mathcal{F})}{\text{Im}(\mathcal{F})} \quad (1.10)$$

representing the amplitude A and phase ϕ of each frequency component. Frequency components are often visualized and quantified with the power (squared amplitude) spectrum (see Fig. 1.3 for examples).

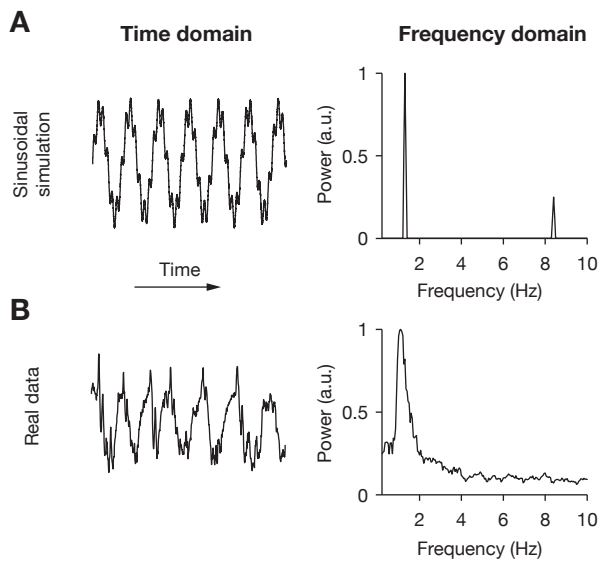


Figure 1.3 | Examples of frequency spectra.

A, 5 s of two summed sinusoids with frequencies $f_1 = 1.3$ Hz and $f_2 = 8.4$ Hz. The periodicity is apparent in time domain (left) and as two sharp peaks in the power spectrum (right) at the respective frequencies.

B, 5 s of real intracranial EEG data from somatosensory cortex of an anesthetized rat. Note the non-sinusoidal shape of the oscillation, i.e., sharpness of the downward transitions compared to the slow upward rises, which result in a blurred peak in the power spectrum (right) and nonzero energy at all frequencies.

1.2.2 Slow and delta rhythms in thalamus and cortex

Classically, the slow oscillation (0.1 to 1 Hz) and delta waves (1 to 5 Hz) in the EEG are the hallmark of deep sleep (Steriade, 1993; Crunelli and Hughes, 2010). Since the discovery of the slow oscillation in the pioneering work of Mircea Steriade (Steriade et al., 1993d,c,a) a large body of knowledge about the intracortical and single cell mechanisms underlying this rhythm was discovered (see Crunelli and Hughes, 2010, for review).

While it is generally acknowledged that the thalamus is a powerful generator of delta oscillations due to its physiology (see Section 1.3) it was assumed until recently that the thalamus does not contribute substantially to the generation of the slow oscillation visible at the cortical level (Steriade et al., 1993c; Sanchez-Vives and McCormick, 2000; Crunelli and Hughes, 2010). Although both thalamus and cortex engage strongly in the slow rhythm while it is present during sleep with strong activity during Up and silence during Down states (Steriade et al., 1993b,c; Crunelli and Hughes, 2010), an influential study showed that lesions of thalamic territories appear to leave the slow rhythm in cortex intact (Steriade et al., 1993c). A thalamus devoid of cortical input on the other hand did not display the slow rhythm anymore. However, more recent evidence showing that thalamocortical neurons can indeed exhibit an oscillation in the slow frequency range without rhythmic input (Hughes et al., 2002) questioned the assumption of a pure cortical origin of the slow oscillation (Crunelli and Hughes, 2010). In the study presented here (Chapter 3, David, Schmiedt et al., 2013) I and colleagues reassessed the role of the thalamus for the generation of physiological sleep slow waves.

Although delta waves are considered to be a feature of sleep, activity in the same frequency range can often also be observed during quiet wakefulness in the cortex of rodents (Castro-Alamancos and Calcagnotto, 2001; Petersen et al., 2003; Crochet and Petersen, 2006; Vyazovskiy et al., 2011) and humans (Sachdev et al., 2015), but not in the relay nuclei of thalamus (Ramcharan et al., 2000; Steriade, 2001a; Swadlow and Gusev,

2001; Ruiz et al., 2006). Where these waves originate from is unclear, in particular for humans. In Chapter 4 I provide evidence that the pulvinar nucleus of thalamus, a nucleus that does not (primarily) function as a relay of peripheral input, likely is a powerful contributor to the cortically observed delta waves during wakefulness.

1.2.3 Beta rhythms in visual cortex

Beta rhythms (13 to 30 Hz) can be observed both in cortical areas, in particular in sensorimotor cortex (Kilavik et al., 2013) but also visual cortex (Lopes da Silva et al., 1970), and subcortical areas such as the striatum (Courtemanche et al., 2003) of awake animals. They are generally strongest when the position of a body part is (actively) held in place such as during eye fixation or during stable grasp of a lever (Kilavik et al., 2013; Khanna and Carmena, 2015). Cognitive processes such as attention or working memory have been shown to modulate the beta rhythm in visual cortex and it was hypothesized to be involved in top-down processing (Wróbel, 2000; Engel and Fries, 2010; Bastos et al., 2015).

Although some studies point to a generator in the infragranular layers of cortex (Roopun et al., 2008; Sun and Dan, 2009; Buffalo et al., 2011; Maier et al., 2011; van Kerkoerle et al., 2014; Bastos et al., 2015) how the beta rhythm in visual cortex is generated is unclear. In the studies presented here (Chapters 5, Schmid, Schmiedt et al., 2013, and 6, Schmiedt et al., 2014) I and colleagues explored the role of the primary visual cortex for the generation of the beta rhythm in visual cortex.

1.2.4 Functional relevance of brain rhythms

For some physiological systems the function of rhythmic behavior is more or less apparent: systems that act as volume pumps such as the heart or the lung can only operate in an oscillatory manner due to energy and space constraints. Although they are virtually ubiquitous, the rhythms of the brain have been proven difficult to be assigned to particular functions. Correlational evidence led to the formulation of different hypotheses for different rhythms, for example the suppression of sen-

sory input by sleep spindles (Yamadori, 1971), binding of visual features by gamma oscillations (Eckhorn et al., 1988; Gray and Singer, 1989), routing of sensory signals by coherent gamma oscillations (Fries, 2005; Kreiter, 2006; Fries, 2015) or the transfer of memories from hippocampus to cortex through coherent slow oscillations (Diekelmann and Born, 2010). In all cases, rhythms are a sign of synchronized, correlated activity, which can be beneficial or detrimental to neuronal signals (Averbeck et al., 2006) depending on the specific rhythm (low vs high), behavioral state (sleep vs awake) and theoretical framework. A conclusive test of the functional relevance of a brain rhythm however is unfortunately very difficult or even impossible depending on the strictness of the criterion: An elimination of only the rhythmicity of signals without affecting any other experimental parameter is currently virtually impossible (Buzsáki, 2006) although it may become feasible with technological advancements. In this thesis, the focus was therefore on understanding the generative mechanisms of the rhythms under study, which is in any case an important step towards understanding their functional role.

1.2.5 Understanding rhythmogenesis by neuronal inactivation *in vivo*

In this thesis, the goal was to understand the generative mechanisms underlying two particular neuronal rhythms at the mesoscopic scale of individual brain areas. To study the contribution of a brain area to a rhythm I employed neuronal inactivation *in vivo* as method of choice, reversible by means of pharmacology for the case of the slow rhythm (Chapter 3) and permanent by means of surgical lesion for the beta rhythm in visual association cortex (Chapters 5 and 6).

Inactivation of neuronal tissue *in vivo* has been used for a long time to study its functional importance (Mountcastle, 1995; Lomber, 1999) as it may uncover the necessary components for a behavior or brain activity. Studying the symptoms of patients with brain damage was one of the key pillars of early neurology and has revealed the primary functions of many brain areas (Mountcastle, 1995). With time, more targeted methods were developed, in particular animal models with surgical lesions,

reversible pharmacological techniques (Lomber, 1999) and recently the genetic tools for optical manipulation of neurons (optogenetics, Packer et al., 2013).

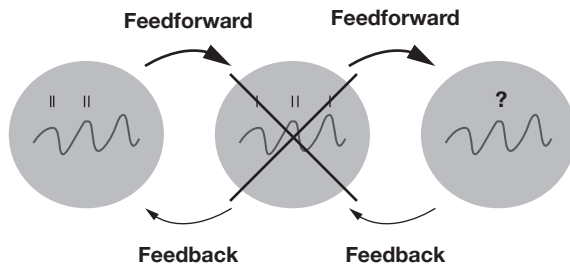


Figure 1.4 | Method of experimental intervention. In the studies presented here, the role of an area for a rhythm present in a connected downstream area was tested by removal of input to the downstream area. This was achieved by reversible pharmacological inactivation or permanent lesioning of the area under investigation.

Concerning tissue volume, surgical, chemical and electrolytic lesions or in animal models allow great flexibility ranging from small patches of tissue (e.g., Smirnakis et al., 2005) to whole cortical hemispheres (Nakamura and Mishkin, 1980). They also allow to study all kinds of behavior as they are performed on otherwise intact animals. However, since lesions are permanent and the brain is a highly adaptable and dynamic system, plasticity is likely to occur after the intervention, and is in fact also often observed (e.g., Cowey, 2010; Gilbert and Li, 2012). In addition, fibers of passage are affected as well (Lomber, 1999). Therefore, lesion studies should be interpreted with great care but can provide valuable first evidence towards understanding the precise origins of behavior and/or brain activity.

Reversible inactivation with drugs offers the advantage that an effect being due to long term plasticity can largely be excluded if normal activity recovers after drug wash-out. The affected volume is mostly dependent on substance diffusion and injection technique and ranges from small populations (Thiele et al., 2006) to whole brain areas (Lomber, 1999) to system-wide application. Measuring the affected area *in vivo* is difficult, but can be done (Boehnke and Rasmusson, 2001; David et al., 2013). A key feature of pharmacological interventions is that agonists and antagonists can be designed to specifically act on certain transmitter systems, which helps to unravel the molecular components of neural function.

Concerning control of time scales and neuronal specificity, optogenetics provide a new gold standard³ as selectivity is only constrained by the genetic markers and the time scale of operation depends on the chosen light-sensitive trans-membrane proteins (Packer et al., 2013). However, its use for larger volumes (>1000 neurons) of tissue such as primate V1 is still in its early days (Packer et al., 2013). As the rhythms under study are rather large scale phenomena that can be measured even in the EEG (Steriade, 1993), the studies in this thesis used more “old fashioned” methods that in the past were effective in unraveling the contributions of brain areas to rhythmogenesis, for example for the identification of the reticular nucleus and the suprachiasmatic nucleus as pacemakers for sleep spindles (Morison and Bassett, 1945; Steriade et al., 1985) and the circadian 24 h rhythm (Moore and Eichler, 1972; Stephan and Zucker, 1972), respectively.

Therefore, in this thesis, I tested the role of a brain area (somatosensory thalamus and primary visual cortex) for the generation of a rhythm (slow rhythm and beta rhythm) in a connected downstream area (somatosensory cortex and visual extrastriate cortex) by inactivation *in vivo*.

³*Ex vivo* preparations such as brain slices of course also provide excellent control of virtually all experimental parameters and can provide complementary and important insights about the (microscopic) generation of brain rhythms. To study *physiological* brain rhythms however the fully intact system should be the final subject of investigation (Steriade, 2001b)

1.3 Anatomical and functional aspects of the thalamus

1.3.1 Anatomy

The thalamus is a collection of nuclei in the midbrain that all project to cortex (Jones, 2012) and can be distinguished based on their input-output patterns. There are three kinds of nuclei (Fig. 1.5, Sherman and Guillery, 2009):

1. First order (FO) or relay nuclei primarily receive input from the periphery, e.g. the lateral geniculate nucleus (LGN) from the retina, or the ventrobasal nucleus (VB) from the lemniscal, somatosensory tract.
2. Higher order nuclei (HO) do not primarily receive direct sensory input, but have reciprocal connections with the cortex, e.g. the pulvinar nuclei, which are strongly connected with the visual cortex.
3. The reticular nucleus (NRT) is a sheath of inhibitory neurons that innervates all other thalamic nuclei, and receives input from both thalamic nuclei and cortex.

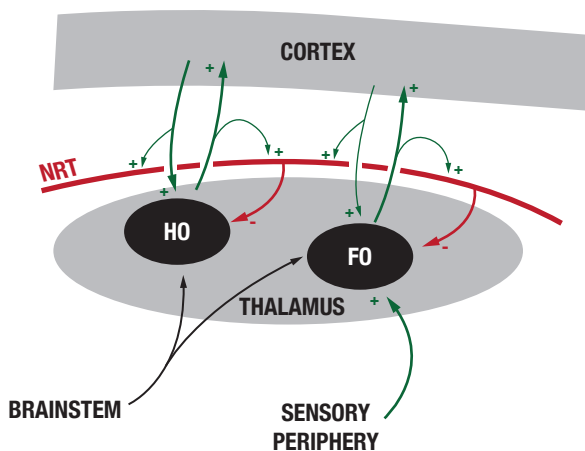


Figure 1.5 | Types of thalamic nuclei. First order nuclei (FO) relay sensory information from the periphery into cortex with strong *driving* synapses, while the input they receive from cortex is transferred through weaker *modulating* synapses. Higher order nuclei (HO) on the other hand do not receive sensory input and receive as well as send driving projections from and to cortex. Both types of nuclei are inhibited by the reticular nucleus (NRT), which receives collaterals from both corticothalamic as well as thalamocortical projections.

In addition, all nuclei receive neuromodulatory (cholinergic, dopaminergic, histaminergic, serotonergic, adrenergic and noradrenergic) projections from the brain stem to a varying extent (Jones, 2012). With respect to broad morphology, most thalamocortical neurons share a “bushy” appearance with highly branched and radially distributed dendrites (Clascá et al., 2012).

Within nuclei, at least three classes of cells can be distinguished based on their axonal patterns (see Jones, 2001; Clascá et al., 2012, for a review).

1. *Core*-type neurons target a single cortical area and their axons terminate mostly in layer 4 and 6, but never 1. They express parvalbumin, often carry high-fidelity, sensory signals and are most prominent in the relay nuclei such as the LGN.
2. *Matrix*-type neurons project to layers 5 and 1 of one or multiple cortical areas, but never layer 4. They express calbindin, never parvalbumin, and are most prominent in higher order nuclei such as the pulvinar.
3. *Intralaminar*-type neurons have a different morphology with few, often long dendrites and axons that project mostly to layers 5 and 6. These are mostly present in the intralaminar nuclei such as the central lateral nucleus.

1.3.2 Physiology

Thalamic neurons are special compared to cortical neurons in that they can operate in (at least) two different and now well-understood modes: (1) At depolarized membrane potential levels thalamic neurons fire in a tonic mode when stimulated, similar to cortical neurons; (2) when hyperpolarized however, thalamic neurons respond with rhythmic bursts of action potentials (Deschenes et al., 1982; Llinás and Jahnsen, 1982; Llinás and Steriade, 2006) (Fig. 1.6).

Since this discovery during the 1980s it could be established that a specific interaction between a T-type calcium current (I_t) and the hyperpolarization-activated current (I_h) allows thalamic neurons to switch be-

tween these modes (Crunelli et al., 1989; McCormick and Pape, 1990). At depolarized membrane potentials, the calcium channels mediating the I_t current are inactivated or blocked such that the cell dynamics and input-output response are dominated by sodium and potassium currents. Only after sufficiently long membrane hyperpolarization can they be de-inactivated or unblocked. The hyperpolarization will also activate the I_h current (Pape, 1996), which slowly depolarizes the cell. The (unblocked) I_t calcium current is then activated at a lower threshold than sodium and potassium channels, giving rise to a low-threshold calcium spike (LTS) with slower dynamics than classical action potentials (Fig. 1.1B). The LTS then depolarizes the cell further such that a burst of action potentials mediated by sodium and potassium channels will ride on top of the LTS. If the membrane potential was initially hyperpolarized for a long period the membrane potential will then fall again to a hyperpolarized level, de-inactivating the calcium channels, activating I_h etc. yielding a rhythmic sequence of spike bursts (Fig. 1.6)

This membrane potential-dependent switching of *modus operandi* is thought to allow thalamocortical neurons to act as gate for information transmission by switching between different functional dynamical regimes. Whereas the depolarized mode allows the high fidelity relay of sensory information, at hyperpolarized levels an input will lead to a stereotyped rhythmic pattern that contains little information about the input (Steriade, 1993). This idea is corroborated by the fact that neurons in the thalamic relay nuclei do not burst in attentive animals but only during sleep when the cortex is disconnected from the outside world.

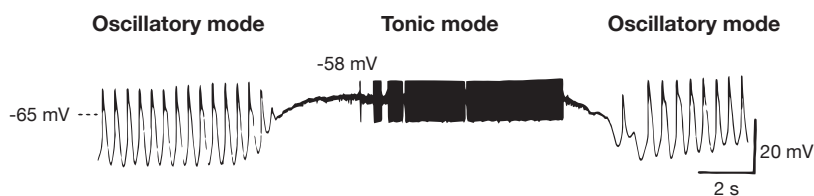
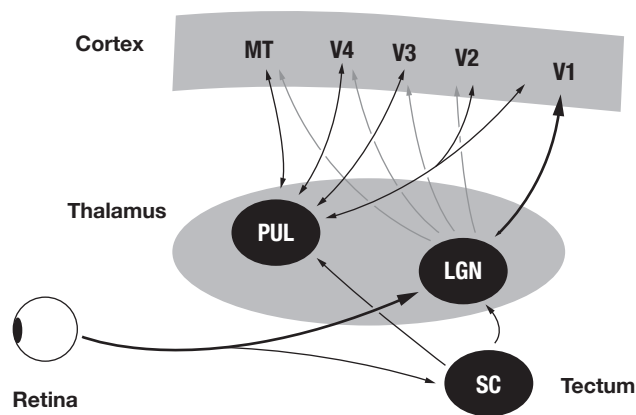


Figure 1.6 | Membrane potential-dependent switching of mode in thalamocortical neurons. A hyperpolarized thalamocortical neuron will operate in an oscillatory mode and switch to cortical-like tonic mode when brought to a slightly depolarized membrane potential. Reproduced with permission from McCormick and Pape (1990).

1.4 The primate visual system

The image-forming visual system processes sensory information about the world that enters the organism via photon absorption in the photoreceptors of the retina (Wurtz and Kandel, 2000). After intraretinal processing (see Wässle, 2004, for a review), retinal ganglion cells (RGCs) transmit the light information to the lateral geniculate nucleus (LGN) in the thalamus where it is relayed into visual cortex, strongest into primary visual cortex (V1). In addition, the RGCs project to the superior colliculus (SC) in the tectum, which controls saccadic eye movements.

Figure 1.7 | Schematic of the primate visual system. Visual information from the retina of the eye is primarily relayed through the lateral geniculate nucleus (LGN) into primary visual cortex (V1). From there it spreads through and is processed in the heavily interconnected visual cortex (intracortical connections are omitted for clarity). A second visual pathway goes into superior colliculus, which projects to pulvinar (PUL) and the LGN. Pulvinar is reciprocally connected with virtually all visual cortical areas. Branching of its projections to cortex is common. Next to the strong connection with V1, LGN projects weakly to extrastriate visual cortex (gray arrows).



1.4.1 Lateral geniculate nucleus

The LGN of thalamus is the first and primary relay station of visual information into visual cortex (Wurtz and Kandel, 2000). It has a layered structure in which each layer contains exclusively magnocellular (M), parvocellular (P) or koniocellular (K) cells (Fig. 1.8). These different cell types differ in their retinal afferents and hence response properties, as well as their thalamocortical efferents.

Whereas M cells are sensitive to luminance contrast, low spatial frequency and high temporal frequencies, P cells are sensitive to color contrast, high spatial frequency and low temporal frequencies. Both M and P cells project to layer 4 of V1, receive input from retina and layer 6 of cortex, and are the two main and well-characterized visual pathways (Wurtz and Kandel, 2000). Their receptive fields, i.e., parts of the visual

field that lead to neuronal responses, are small ($<1^\circ$) and have a characteristic center-surround structure, similar to their afferent RGCs but slightly larger.

The K cells on the other hand reside in between the M and P layers of LGN and form a third visual pathway. In contrast to the M and P cells, they project to the superficial layers of V1 (Hendry and Reid, 2000) and extrastriate areas such as area MT and V4 (Rodman et al., 2001; Sincich et al., 2004; Lyon and Rabideau, 2012). Also, they receive projections from the SC and extrastriate cortex (Hendry and Reid, 2000). Due to their heterogeneous response properties (Hendry and Reid, 2000) a clear contribution to vision however could not yet be identified. As they form a parallel V1-bypassing pathway for vision, it is conceivable that the K pathway plays a role in fast and less precise visual perception, for example the detection of motion.

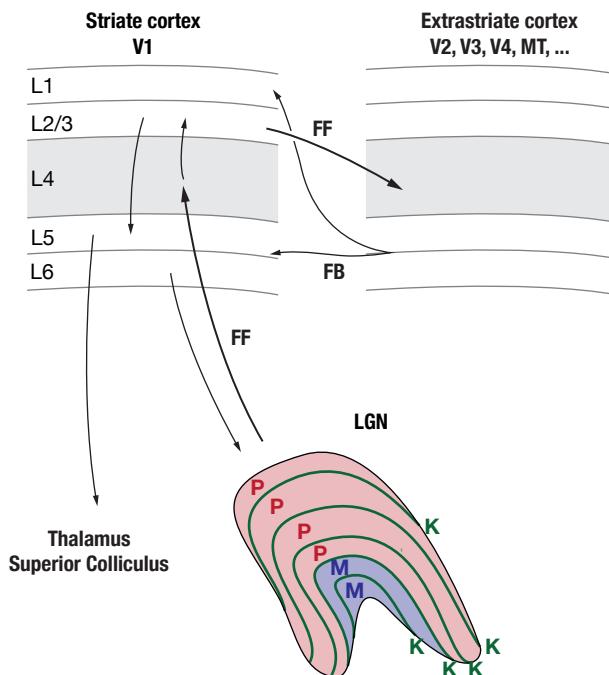


Figure 1.8 | Schematic of connectivity between thalamic and cortical layers of the visual system. LGN consists of four parvocellular (**P**) and two magnocellular layers (**M**) that project strongest to granular layer 4 of V1. From there visual information is processed within a microcolumn and output is sent to subcortical structures from layer 5, back to LGN from layer 6 and to extrastriate cortical areas from layer 2/3 in a feedforward manner (**FF**). Feedback (**FB**) from extrastriate cortex is received mainly from infragranular layers into supra- and infragranular layers. The koniocellular layers (**K**) of LGN in between the M and P layers project to supragranular layers of both striate and extrastriate cortex (omitted for clarity).

1.4.2 Visual cortex

The visual cortex forms a complex network of 6-layered areas that are strongly interconnected and partially hierarchical (Felleman and Van Essen, 1991; Markov et al., 2013) with the major entry point for visual information in the granular layer 4 of primary visual cortex (but see Constantinople and Bruno, 2013; Pluta et al., 2015, for direct thalamic projections into layer 5 in rodents) (Fig. 1.8). Layer 4 of V1 and LGN form strong synapses in a retinotopic connectivity pattern that displays convergence, i.e., V1 neurons integrate over a larger part of visual space than LGN or retinal neurons. From layer 4 of V1 onwards visual information is spread in a feedforward manner across the layers of a cortical microcolumn and sent from superficial layers to layer 4 of neighboring cortical areas such as area V2, V3, V4 or MT. Next to the feedforward processing stream of visual information, a prominent feature of visual cortex is the strong prevalence of feedback projections from “higher” visual areas such as MT to “lower” areas such as V1. These feedback projections differ in their laminar profile: they originate in the infragranular layers 5 and 6 and avoid layer 4 in the target area (Felleman and Van Essen, 1991; Markov et al., 2013). Due to its intracortical origin, this projection stream was suggested to carry top-down signals such as expectation or attention that modulate visual responses.

Throughout visual cortex, visual response fields become gradually more complex, specialized and heterogeneous than the stereotyped center-surround structures of retina and LGN. Visual cortex response fields range from “simple cells” in V1 that respond strongest to bar-like visual stimuli in specific parts of the visual field (Hubel and Wiesel, 1959) up to “Jennifer Aniston” neurons in the temporal lobe, which respond strongest to the presentation of a particular person’s face invariant of low-level features such as location or rotation (Quiroga et al., 2005). In other words, neurons in visual cortex are generally “tuned” to respond to a particular set of visual features. Neighboring neurons often share this tuning.

1.4.3 Pulvinar

The pulvinar complex represents the largest thalamic nucleus in primates that has grown substantially during evolution (Robinson and Cowie, 1997). As a higher order nucleus of thalamus, it does not primarily act as a relay of sensory information from the periphery into cortex, but rather receives input from and projects to multiple cortical areas, in particular with visual areas in the occipital cortex (Rockland et al., 1999).

Several subunits can be defined based on cytoarchitectonic (Walker, 1938; Olszewski, 1952), immunocytochemical (Gutierrez et al., 1995, 2000) or functional features (Bender, 1981; Shipp, 2003). Based on classical anatomical staining methods, a lateral, a medial, an inferior and an oral subdivision were identified (Fig. 1.9). The inferior and lateral parts are connected to visual areas including visual cortex and superior colliculus and exert neuronal responses to visual stimulation. The medial part on the other hand is associated with more parietal and frontal cortices that mediate visuo-motor behavior. The oral pulvinar is not connected with visual areas but the somatosensory system.

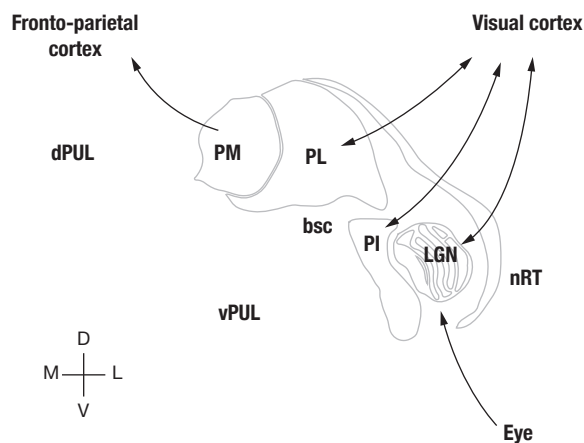


Figure 1.9 | Anatomical subdivisions of pulvinar. Inferior (PI) and most parts of dorsal lateral pulvinar (PL) are reciprocally connected with visual cortices. Medial pulvinar (PM) and some parts of PL are connected with frontal and parietal cortices. nRT, Reticular nucleus. LGN, Lateral geniculate nucleus. dPUL, Dorsal pulvinar, vPUL, Ventral pulvinar.

Puzzlingly, the functional properties of pulvinar neurons do not fully align with the anatomical subunits. For example, there are (at least) three representations of the visual field in pulvinar spread across lateral and medial pulvinar, and most neurons in pulvinar respond to visual stimulation. The tuning of pulvinar neurons is particularly heterogeneous and not strongly organized in space, potentially due to the widespread and reciprocal pulvinocortical connections. While the involvement of pulvinar in visual processing is generally accepted, there's no consensus on a specific role of pulvinar in vision. Numerous studies point to a role of pulvinar in the signaling of visual salience (Robinson and Petersen, 1992; Robinson and Cowie, 1997): (1) pulvinar lesions in humans and pulvinar inactivations in non-human primates can lead to neglect-like symptoms (Zihl and von Cramon, 1979; Ungerleider and Christensen, 1979) and attention-deficits (Snow et al., 2009; Petersen et al., 1985, 1987), (2) pulvinar neurons show enhanced visual responses to attended, i.e. relevant, visual stimuli (Petersen et al., 1985; Bender and Youakim, 2001; Saalman et al., 2012) similar to cortical neurons (Bender and Youakim, 2001). However, the exact mechanisms how the pulvinar contributes to the analysis of visual salience are not known.

A suggested candidate mechanism for the mediation of attentional selection of relevant stimuli in the cortex is selective rhythmic synchronization between areas (Fries, 2005; Kreiter, 2006; Fries, 2015); in this framework, communication between areas is facilitated by undergoing the same excitability fluctuations and thereby maximizing spike impact on the postsynaptic side. To achieve such “communication through coherence”, the areas to be connected to each other have to be synchronized. It was suggested that pulvinar could coordinate such coordination due to its widespread connectivity with cortex (Jones, 2001; Saalman and Kastner, 2011; Saalman et al., 2012). To act as a synchronizing hub it is necessary that individual neurons or populations produced rhythmic spiking patterns. In Chapter 4 I and colleagues studied the oscillatory behavior of individual pulvinar neurons in order to test to what extent they may contribute to cortical synchronization.

Discussion and summary

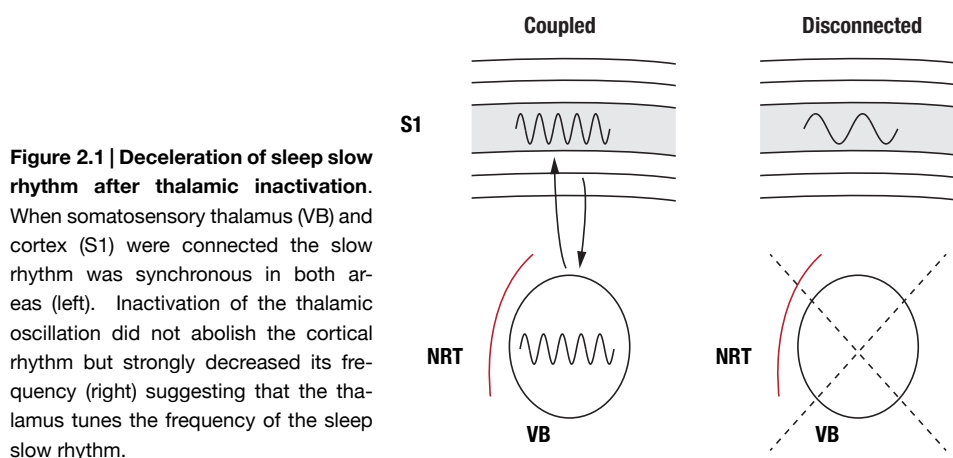
The work collected in this thesis was concerned with the contributions of individual brain areas to physiological brain rhythms present in efferent structures. Two rhythms in particular were subject of investigation: (1) the slow/delta waves (0.5 to 5 Hz) in cortex present during sleep (Chapter 3) and waking (Chapter 4), and (2) the beta rhythm in visual cortex (13 to 30 Hz) during attentive fixation (Chapters 5 and 6). For these rhythms the contributions of thalamus and primary visual cortex were tested, respectively.

2.1 Contribution of thalamus to slow waves

Sleep slow waves in cortex were found to crucially depend in their frequency on the presence of intact thalamic input (Chapter 3, David, Schmiedt et al., 2013). Although still present after inactivation of the somatosensory thalamus, slow waves in somatosensory cortex of anesthetized or naturally sleeping rats were decreased in frequency and number by ~50 % (Fig. 2.1). This deceleration of slow waves was shown to be strongly dependent on thalamic burst firing mediated by T-type calcium channels as a selective blockade with a T-type calcium channel antagonist induced similar effects as the full inactivation of thalamic spiking. Also optogenetic stimulation of thalamus could entrain cortical slow waves only in the presence of T-type calcium channels. As the activity in thalamus is

rhythmic itself during the presence of slow waves and slow waves were still present but slower after thalamic inactivation, the findings strongly suggest that the thalamic pacemaker neurons enforce their inherently faster rhythm onto the cortical rhythm by pushing the cortex phase-forward in its own cycle.

These findings are in contrast with an early study on the thalamic contribution to slow waves that did not find an alteration of slow waves in the cortex after destruction of large thalamic territories in cats (Steriade et al., 1993c). A recent study, which repeated the original experiment but monitored the presence of cortical slow waves immediately after the thalamic lesion and not only after a few days, was able to reproduce our result: Removal of thalamocortical afferents to cortical areas dramatically reduced the expression of slow waves (Lemieux et al., 2014; David and Schmiedt, 2014). However, within 12 h the authors found a resurgence of slow waves up to a nearly complete recovery. Therefore, the time of assessment could potentially explain the difference between the study by Steriade and colleagues and our own.



Although slow waves are classically the hallmark of deep sleep (Crunelli and Hughes, 2010), cortical recordings show low frequency rhythms (<5 Hz) also during waking (Sachdev et al., 2015), which may even couple to other frequency bands (Bosman et al., 2012; Landau et al., 2015) or behavior (Landau and Fries, 2012). Because the relay nuclei generally exhibit strong rhythmic activity during sleep and anesthesia mediated by calcium channels (Llinás and Steriade, 2006) but not during wakefulness (Swadlow and Gusev, 2001; Steriade, 2001a; Ruiz et al., 2006) it was assumed until recently that the thalamus would not contribute to delta rhythms present in cortex during waking. However, for higher order thalamic nuclei rhythmicity during waking was tested only sparsely. For example, for the pulvinar, which is connected with visual cortex, only one study investigated rhythmic behavior and did indeed find 10 out of 15 sampled neurons to exhibit rhythmic burst firing (Ramcharan et al., 2005) during active behavior. In Chapter 4 we tested the rhythmicity of macaque pulvinar firing during awake behavior on a large sample of neurons and found that ~20 % of the tested neurons exhibited rhythmic firing. The neurons with strong rhythmicity in their firing responded only weakly to visual stimulation and strongly decreased firing when the monkeys performed motor behavior. This substantial pacemaking activity is likely to influence connected cortical areas, making pulvinar are a possible contributor to cortical low frequency activity.

2.2 Contribution of primary visual cortex to extrastriate beta rhythms

Whereas the beta rhythm (13 to 30 Hz) in the sensorimotor system and its modulation by behavior is well studied (Kilavik et al., 2013; Khanna and Carmena, 2015), only few studies on the beta rhythm in visual cortex and its mechanisms exist (Lopes da Silva et al., 1970; Engel and Fries, 2010; Bastos et al., 2015). We here report (Chapters 5 and 6) the effects of surgical removal of primary visual cortex on spiking and oscillation dynamics in visual area V4, which receives direct and indirect feedforward projections from V1.

In the intact visual system, the beta rhythm present in the local field potential (LFP) of macaque V4 was strongest during active fixation awaiting the onset of a visual stimulus followed by reward (Chapter 6). Visual stimulation decreased the amplitude of the beta rhythm, but induced activity in the gamma range (>30 Hz). After an extensive lesion of primary visual cortex, the beta rhythm was still present, even slightly enhanced, which excludes the possibility that the beta rhythm at the level of V4 was generated in and inherited from V1.

Although the classical route of information transmission from LGN to V1 to V4 was eliminated by lesioning of V1, V4 neurons continued to show weak but consistent responses to visual stimulation (Chapter 5), which indicates that V4 receives visual input via a V1-bypassing route. Previous studies have shown the existence of projections from the koniocellular system of LGN to extrastriate cortex including direct and indirect pathways into V4 (Sincich et al., 2004; Lyon and Rabideau, 2012) as well as functional activations without V1 input (Schmid et al., 2009, 2010). Similar to the spiking activity, also the visually induced gamma rhythm was strongly reduced in amplitude yet not abolished (Chapter 6).

2.2. Contribution of primary visual cortex to extrastriate beta rhythms

In contrast to the spiking and the gamma rhythm, the dynamics of the beta rhythm with visual stimulation changed dramatically after the V1 lesion. Instead of decreasing the beta amplitude visual stimulation enhanced the beta rhythm.

The differential effect of the removal of feedforward input on spiking/gamma and beta amplitude dynamics suggests different generative mechanisms for the two rhythms with gamma relying on feedforward drive and beta on local and/or feedback input (Fig. 2.2). These results are in line with recent studies reporting that the two frequency ranges are associated with different streams of input: (1) microstimulation of V1 induced gamma activity in V4 and microstimulation of V4 alpha/beta activity in V1 (van Kerkoerle et al., 2014), (2) statistical analysis of directed influences revealed that beta and gamma act in a feedback and feedforward manner, respectively (Bosman et al., 2012; Bastos et al., 2015).

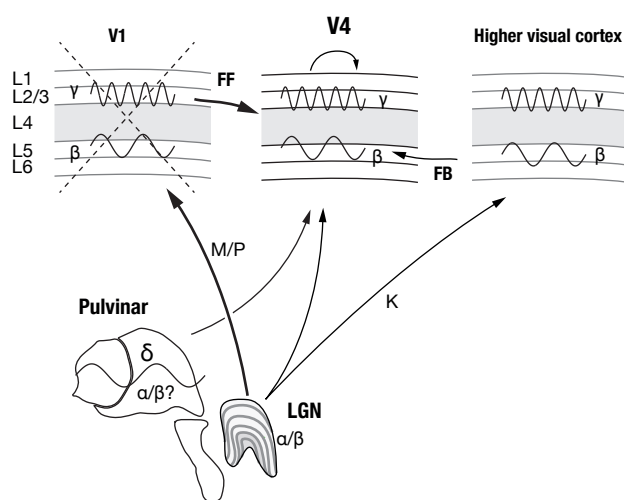


Figure 2.2 | Generation of awake beta rhythm in extrastriate cortex. Beta (β) rhythms in V4 survived a V1 lesion and were enhanced by post lesion visual stimulation indicating that beta originates from an interaction of local, remote cortical (feedback, FB) and/or thalamic oscillatory generators. LGN was shown to contain alpha/beta-generating networks (see Lőrincz et al., 2009; Bastos et al., 2014, and Chapter 4), which might contribute to extrastriate rhythms via the koniocellular system. Pulvinar was associated with alpha/beta activity (Saalman et al., 2012) but our own study did not find strong alpha/beta generators in pulvinar. V4 gamma (γ) rhythms and spiking were strongly diminished by removal of V1 indicating a reliance on feedforward (FF) projections.

2.3 Summary

Although brain rhythms have been the subject of neuroscientific research since more than 80 years, we have not deciphered their physiological function(s) and mechanisms, but instead have unraveled an astounding diversity and complexity, similar to the structure and functions of the brain itself.

One part of understanding the functional relevance of a biological rhythm involves the apprehension of its generative mechanisms. In this thesis, I attempted to delineate how the thalamus contributes to the cortical slow/delta rhythms (<5 Hz) and how primary visual cortex influences rhythms in the visual association cortex (beta, 13 to 30 Hz, and gamma, >30 Hz). I found that the thalamus acts as a powerful oscillator in the slow/delta range, both during sleep and waking, and is necessary for the full establishment of physiological sleep slow waves. Primary visual cortex on the other hand was not necessary for beta rhythms in visual association cortex, but important for gamma rhythm generation.

The generative mechanisms of the slow/delta rhythm now seem relatively well understood (Crunelli et al., 2014). However, its functional relevance is still a matter of debate and unresolved (Vyazovskiy and Harris, 2013; Diekelmann and Born, 2010). Targeting specific parts of the generative mechanism by modern, cell-specific experimental manipulations may hopefully provide new insights into this matter.

While a large body of evidence for the role of the gamma rhythm in visual processing could be collected in recent years (Fries, 2015), the beta rhythm in visual cortex has only recently received increased attention (Wróbel, 2000; Engel and Fries, 2010; van Kerkoerle et al., 2014; Spaak et al., 2014; Bastos et al., 2015). Further studies will be necessary to characterize which cells and networks generate it and how it influences processing and behavior.

Part II

Contribution of thalamus to slow/delta rhythms

CHAPTER **3**

Essential thalamic contribution to slow waves of natural sleep

Erklärung zu den Autorenanteilen

an der Publikation: Essential Thalamic Contribution to Slow Waves of Natural Sleep

Status: in press

Name der Zeitschrift: The Journal of Neuroscience

Beteiligte Autoren:

- | | |
|--|--------------------------|
| - Francois David (FD) | - Victor N. Uebele (VCN) |
| - Joscha T. Schmiedt (Promovierender) | - John J. Renger (JJR) |
| - Hannah L. Taylor (HLT) | - Régis C. Lambert (RCG) |
| - Gergely Orban (GO) | - Nathalie Leresche (NL) |
| - Giuseppe Di Giovanni (GDG) | - Vincenzo Crunelli (VC) |

Was hat der/die Promovierende bzw. was haben die Co-Autoren/Autorinnen beigetragen?

(1) zu Entwicklung und Planung

Promovierender 15%

FD 15%, VC 30%, HLT 8%, GO 8%, GDG 8%, RCL 8%, NL 8%

(2) zur Durchführung der einzelnen Untersuchungen und Experimente

Promovierender: Pharmakologische Experimente an anästhesierten und frei schlafenden Tieren (40%)

FD: Experimente an anästhesierten und frei schlafenden Tieren, Optogenetische Stimulations-Experimente in anästhesierten Tieren (40%)

GO: Vorläufige pharmakologische Experimente an anästhesierten Tieren (10%)

HLT: Optogenetische Stimulations-Experimente in anästhesierten Tieren (10%)

(3) zur Erstellung der Datensammlung und Abbildungen

Promovierender: Aufbau des Ableitsetups in allen Experimenten, Erstellung von Fig. 1-5 (50%)

FD: Aufbau des Ableitsetups in allen Experimenten, Erstellung von Fig. 6-9 (50%)

(4) zur Analyse und Interpretation der Daten

Promovierender: Analyse und Interpretation aller Daten, vorwiegend aus Experimenten unter Anästhesie (40%)

FD: Analyse und Interpretation aller Daten, vorwiegend aus Experimenten in frei schlafenden Tieren (40%)

VC: Interpretation aller Daten (20%)

(5) zur Verfassung des Manuskripts

Promovierender 33%:

FD 33%

VC 33%

Essential Thalamic Contribution to Slow Waves of Natural Sleep

François David,^{1,2,3*} Joscha T. Schmiedt,^{1,4*} Hannah L. Taylor,¹ Gergely Orban,¹ Giuseppe Di Giovanni,^{1,5} Victor N. Uebele,⁶ John J. Renger,⁶ Régis C. Lambert,^{2,3} Nathalie Leresche,^{2,3} and Vincenzo Crunelli¹

¹Neuroscience Division, School of Biosciences, Cardiff University, Cardiff CF10 3AX, United Kingdom, ²Unité Mixte de Recherche 7102 Centre National de la Recherche Scientifique and ³Université Pierre et Marie Curie, Université Paris 6, 75005 Paris, France, ⁴Ernst Strüngmann Institute for Neuroscience in Cooperation with Max Planck Society, 60528 Frankfurt, Germany, ⁵Physiology and Biochemistry Department, Malta University, 2080 Malta, and ⁶Merck & Company Inc., West Point, Pennsylvania 19486

Slow waves represent one of the prominent EEG signatures of non-rapid eye movement (non-REM) sleep and are thought to play an important role in the cellular and network plasticity that occurs during this behavioral state. These slow waves of natural sleep are currently considered to be exclusively generated by intrinsic and synaptic mechanisms within neocortical territories, although a role for the thalamus in this key physiological rhythm has been suggested but never demonstrated. Combining neuronal ensemble recordings, microdialysis, and optogenetics, here we show that the block of the thalamic output to the neocortex markedly (up to 50%) decreases the frequency of slow waves recorded during non-REM sleep in freely moving, naturally sleeping-waking rats. A smaller volume of thalamic inactivation than during sleep is required for observing similar effects on EEG slow waves recorded during anesthesia, a condition in which both bursts and single action potentials of thalamocortical neurons are almost exclusively dependent on T-type calcium channels. Thalamic inactivation more strongly reduces spindles than slow waves during both anesthesia and natural sleep. Moreover, selective excitation of thalamocortical neurons strongly entrains EEG slow waves in a narrow frequency band (0.75–1.5 Hz) only when thalamic T-type calcium channels are functionally active. These results demonstrate that the thalamus finely tunes the frequency of slow waves during non-REM sleep and anesthesia, and thus provide the first conclusive evidence that a dynamic interplay of the neocortical and thalamic oscillators of slow waves is required for the full expression of this key physiological EEG rhythm.

Introduction

Slow waves and their neuronal counterpart, the cortical and thalamic oscillations between depolarized UP states and hyperpolarized DOWN states (Steriade et al., 1993a; Contreras and Steriade, 1995; Petersen et al., 2003; Sirota and Buzsáki, 2005; Crunelli et al., 2012), are the main EEG hallmark of non-rapid eye movement (non-REM) sleep (Crunelli and Hughes, 2010; Brown et al., 2012) and are also observed during anesthesia (Chauvette et al., 2011). The physiological importance of these waves of natural sleep is emphasized by their ability to group together other EEG rhythms of non-REM sleep (Steriade, 1997) and by their putative role in the consolidation of recently acquired memories (Tononi and Cirelli, 2001; Marshall et al., 2006; Ji and Wilson, 2007).

The mechanisms underlying the generation of EEG slow waves, however, remain controversial. Because (1) lesions of thalamic nuclei do not suppress slow waves in anesthetized cats (Steriade et al., 1993b) and (2) UP and DOWN states are recorded in neocortical slices (Sanchez-Vives and McCormick, 2000; Cossart et al., 2003) and in an isolated cortical gyrus *in vivo* during anesthesia (Timofeev et al., 2000), these EEG slow waves are exclusively and consistently viewed as a cortically generated rhythm (Sanchez-Vives and McCormick, 2000; Timofeev et al., 2000; Chauvette et al., 2011; Brown et al., 2012). However, (1) increasing thalamic inhibition alters EEG slow waves in anesthetized rats (Doi et al., 2007) and suppresses whisking-induced cortical UP states in head-restrained mice (Poulet et al., 2012); (2) UP and DOWN states, and associated slow waves, can be recorded in thalamic slices (Hughes et al., 2002, 2004; Blethyn et al., 2006); and (3) selective thalamic degeneration modifies slow waves of non-REM sleep in humans (Gemignani et al., 2012). These findings, together with other mechanistic *in vitro* studies and investigations in anesthetized animals (for review, see Crunelli and Hughes, 2010), question the current corticocentric view of slow wave generation and led us to suggest that the full expression of these EEG waves of natural sleep requires a dynamic interplay of cortical and thalamic oscillators (Crunelli and Hughes, 2010). Unfortunately, the resolution of this controversy is still hampered by the lack of any study that has directly and systematically addressed this issue in unrestrained, naturally waking-sleeping

Received July 26, 2013; revised Oct. 22, 2013; accepted Nov. 6, 2013.

Author contributions: F.D., J.T.S., H.L.T., G.D.G., R.C.L., N.L., and V.C. designed research; F.D., J.T.S., H.L.T., and G.O. performed research; F.D., J.T.S., V.N.U., and J.J.R. contributed unpublished reagents/analytic tools; F.D. and J.T.S. analyzed data; F.D., J.T.S., and V.C. wrote the paper.

This work was supported by the Wellcome Trust (91882), ANR-MNMP-2009, and Centre National de la Recherche Scientifique (LEA 528). We thank Dr. K. Deisseroth for the channelrhodopsin-2 viral construct, Drs. W.M. Connelly and S.W. Hughes for critical comments on the manuscript, and Mr. T. Gould for histological processing.

V.N.U. and J.J.R. are employees of Merck and Co., Inc. and potentially own stock and/or stock options in the company. The remaining authors declare no competing financial interests.

*F.D. and J.T.S. contributed equally to this work.

Correspondence should be addressed to Dr. Vincenzo Crunelli, Neuroscience Division, School of Bioscience, Cardiff University, Cardiff CF10 3AX, United Kingdom. E-mail: crunelli@cardiff.ac.uk.

DOI:10.1523/JNEUROSCI.3169-13.2013

Copyright © 2013 the authors 0270-6474/13/3319599-12\$15.00/0

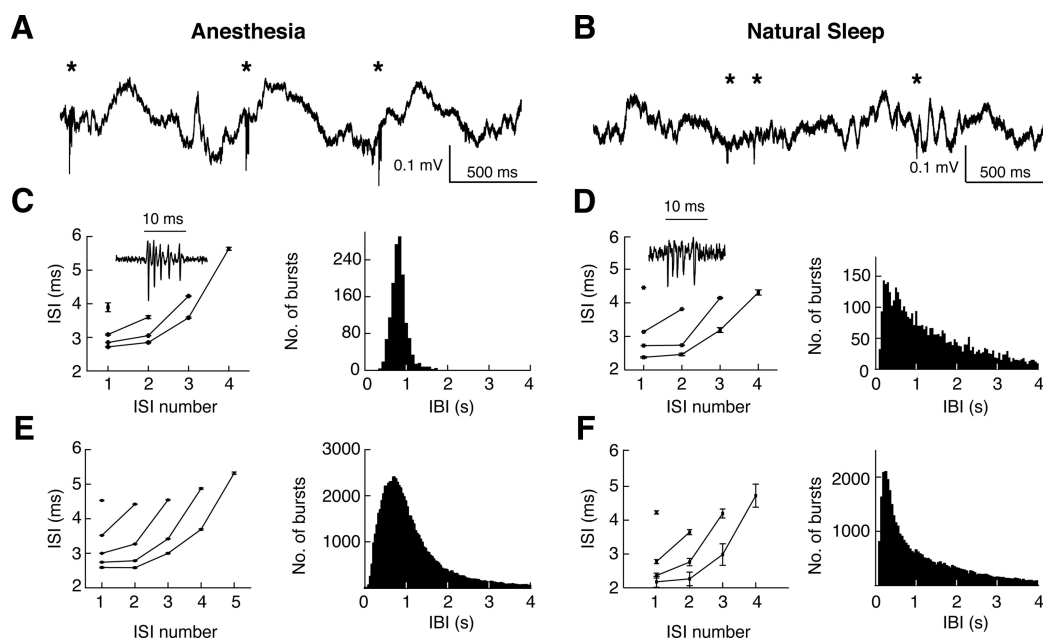


Figure 1. Properties of high-frequency bursts in VB TC neurons during ketamine-xylazine anesthesia and natural sleep. **A, B**, Local field potential in VB during anesthesia (**A**) and natural sleep (**B**). *Bursts. **C**, Burst properties of a representative TC neuron in the VB during anesthesia: ISIs for different burst lengths (left), and distribution of interburst intervals (IBI) (right) ($n = 5102$ bursts). **D**, Same as **C** for a different representative TC neuron in the VB during natural sleep ($n = 825$ bursts). **C, D** Insets, Representative bursts. **E, F**, Population data, as in **C** and **D**, for $n = 85$ and $n = 9$ TC neurons from $n = 18$ anesthetized and $n = 3$ naturally sleeping rats, respectively.

animals. Moreover, our current mechanistic knowledge of slow waves of natural sleep continues to be clouded by the speculative extrapolations of findings obtained in anesthetized conditions.

Using a combination of neuronal ensemble recordings, thalamus-selective pharmacological inactivation, and optogenetic activation of thalamocortical (TC) neurons in naturally sleeping or anesthetized rats, here we show, for the first time, that the thalamus is required for finely tuning the frequency of slow waves during non-REM sleep and anesthesia. Moreover, we demonstrate that the entrainment of EEG slow waves by selective thalamic activation is dependent on T-type calcium channels. Together, these results provide the first conclusive evidence that cortical and thalamic oscillators are necessary for the full expression of slow waves of non-REM sleep.

Materials and Methods

All experimental procedures were performed in accordance with the United Kingdom Animals (Scientific Procedure) Act 1986 and local ethics committee guidelines. All efforts were made to minimize animal suffering and the number of animals used. Experiments were performed on male adult Wistar rats (260–400 g, Harlan Laboratories), maintained on a normal diet and under a 8:00 A.M. to 8:00 P.M. light-on regimen.

Experiments in anesthetized rats

Surgery. After anesthesia induction with 5% isoflurane, rats received an intraperitoneal injection of ketamine (120 mg/kg) and xylazine (20 mg/kg). Anesthesia was then maintained with a constant flow of ketamine (42 mg/kg/h) and xylazine (7 mg/kg/h) delivered via an intraperitoneal catheter connected to a pump (NewEra NE-300 syringe pump). Body temperature was maintained at 37°C with a heating pad and rectal probe. Rats were implanted with gold-plated skull screws (diameter 1 mm, length 3 mm) for EEG recordings in S1: anteroposterior (AP) = -2.2 mm, mediolateral (ML) = ± 5.5 mm from bregma (Paxinos and Watson, 2007). An additional screw (ground electrode) was placed anterior to the bregma, and two other screws above the cerebellum were used as reference electrodes for EEG and thalamic recordings.

For measuring the spatial extent of the action of 3,5-dichloro-*N*-[1-(2,2-dimethyl-tetrahydro-pyran-4-ylmethyl)-4-fluoro-piperidin-4-ylmethyl]-

benzamide (TTA-P2), a potent and selective T-type channel antagonist (Uebele et al., 2009; Dreyfus et al., 2010), or of the sodium channel blocker TTX in the thalamus (i.e., see experiments illustrated in Fig. 3), a 1 mm hole was drilled unilaterally above the ventrobasal thalamic nucleus (VB), the dura was carefully removed, and a 32-channel silicone probe (10 mm length, 0.6 mm width, 1–4 M Ω) with four shanks (200 μ m recording point distance, 15 μ m thickness) (NeuroNexus Technologies) was slowly lowered in the VB (dorsoventral [DV] = -4.5 to -5.5 mm). A second hole in the same hemisphere was used to slowly lower (200 μ m every 5 min) a microdialysis probe (CMA 12 Elite, 2 mm dialysis membrane length, 20 kDa cutoff, with a 16° angle with respect to the vertical axis; see Fig. 3A) to a final position that was between 0.05 and 1 mm away from the silicone probe. The 16° angle positioning of the dialysis probe was dictated by the space constraints of the silicone and dialysis probes connecting devices on the animal skull.

For measuring the effect of TTX and TTA-P2 (applied by microdialysis in the VB) on slow and spindle waves during anesthesia (i.e., see experiments illustrated in Fig. 4), EEG electrodes were implanted as above, and two microdialysis probes (one in each VB) were slowly lowered fully vertically until their tips rested 6.5 mm below the skull (i.e., in the most ventral part of the VB). In some rats, a silicone probe was also inserted unilaterally in the VB with a 16° angle with respect to the vertical axis.

For measuring the effect of systemic TTA-P2 injection (i.e., see experiments illustrated in Fig. 5), rats were implanted with EEG electrodes and a unilateral silicone probe in the VB (as described above).

Systemic and microdialysis solutions. For intraperitoneal injection, TTA-P2 was dissolved in saline containing 4% DMSO and the pH adjusted with potassium hydroxide (1 mM). Control intraperitoneal injections contained 4% DMSO in saline. For reverse microdialysis injection, TTA-P2 was dissolved in aCSF with 4% DMSO. Tetrodotoxin citrate (TTX) was dissolved in aCSF. Flow rate of the microdialysis injection was set at 1 μ l/min.

Injections. For the systemic injections, once stable EEG slow waves were recorded for at least 30 min and high amplitude well isolated units were present in some of the silicone probe channels, a control period of at least 40 min was recorded before injecting intraperitoneally either saline/DMSO or TTA-P2 while continuing recording for at least another 2 h. For intrathalamic drug application, reverse microdialysis injection of aCSF was initiated as soon as the microdialysis probes were in position, and continued for at least 1 h before electrical recordings commenced. Once stable, high-amplitude, well-isolated units could be recorded from

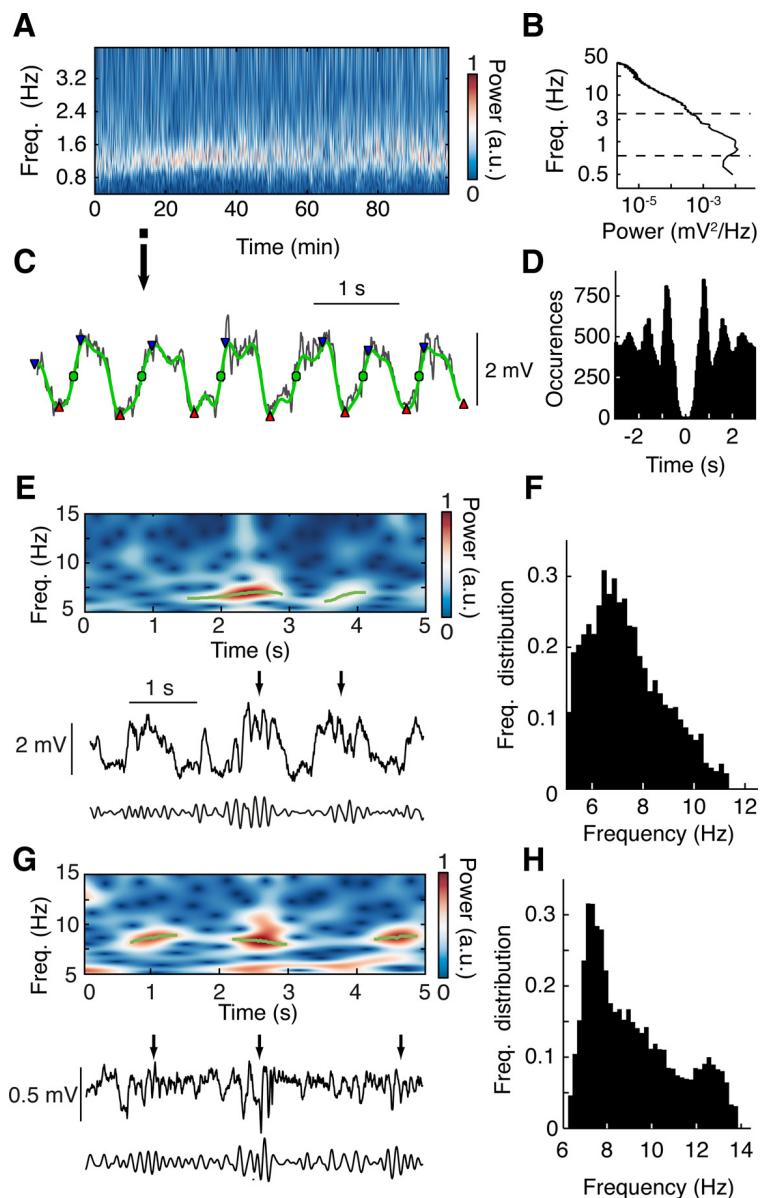


Figure 2. Detection of slow and spindle waves. **A**, Representative EEG wavelet power spectrum of slow wave frequency band (0.2–4.5 Hz) during ketamine-xylazine anesthesia. **B**, Representative EEG broadband power spectrum. Dashed lines indicate the frequency band shown in **A**. **C**, Expanded EEG trace (black) (from time period marked in **A** with arrow) illustrating the identification of slow waves (green circles) by means of negative to positive zero-crossing detection on the 0.2–4.5 Hz bandpass-filtered signal (green trace). Waves with peak-to-peak amplitude (red triangles to blue triangles) of $<60\%$ of the mean peak-to-peak amplitude were discarded. **D**, Autocorrelogram of EEG slow waves detected as shown in **C** from the first 20 min of data shown in **A**. **E**, Representative raw (middle), 5–12.5 Hz bandpass-filtered (bottom) EEG traces showing spindle waves (black arrows) and wavelet power spectrum (top) with detected spindle wave episodes (green lines) during anesthesia. **F**, Average frequency distribution of spindles during anesthesia ($n = 7$ rats). **G**, **H**, Data for spindles during natural sleep are illustrated in the same format as **E** and **F**, respectively ($n = 6$ rats).

some of the silicone probe channels, recording of a control period of at least 40 min was initiated. This was followed either by continuation of aCSF application or the inlet tubing was switched to a solution containing either TTX or TTA-P2. Recordings and dialysis application then continued for at least 1 h. At the end of the recording session, rats were transcardially perfused.

Recordings. Thalamic signals were amplified with an Omnetics preamplifier (gain 20, bandwidth 0.8 Hz to 54 kHz) and a Plexon recorder/64 channel amplifier (gain 7500–12,500, bandwidth 1–6000 Hz, Plexon).

The EEG signal was amplified with a combination of SuperTech Bio-AMP (Pecs) pre- (bandwidth 0.1–500 Hz) and main-amplifiers (bandwidth DC to 500 Hz). When combined unit and EEG recordings were made, signals were digitized with a Plexon recorder/64 system at 20 kHz with 16-bit resolution. EEG recordings were digitized using the Plexon

recorder input via the IP16 event input break-out panel. The digitized data were converted to Spike2 format (version 5.13, CED). For all further analyses, data were converted to a raw binary format using tools of the freely available Klusters, Neuroscope, and NManager software suite (Hazan et al., 2006). EEG data were low-pass filtered with a windowed sinc filter at 100 Hz and downsampled to 200 Hz.

Experiments in freely moving rats

Surgery. Rats were anesthetized and implanted with EEG electrodes, as described above, and an EMG electrode was positioned in the neck muscle. Two or four microdialysis guide cannulae (one or two in each VB, respectively) (i.e., see experiments illustrated in Fig. 6 for two probes in each VB) were slowly lowered fully vertically so their tip was just above the VB (DV = -4.4 mm) (Paxinos and Watson, 2007). When two guide cannulae were inserted in each VB, their AP coordinates were as follows: -2.6 and -3.8 mm (Paxinos and Watson, 2007). Both EEG electrodes and guide cannulae were fixed to the skull with dental acrylic cement. Rats were allowed at least 7 d to recover from surgery (single housed) and to habituate to the recording cage (4 h/d). At the end of the recording sessions, rats were transcardially perfused.

Injections. For the systemic injections, on the day of the experiment rats were transferred to the recording cage, connected to the electrical recording and microdialysis apparatus (as appropriate), and allowed to move freely in their cage for at least 1 h before any recording commenced. A control period of 1.5 h was then recorded before an intraperitoneal injection of either saline or TTA-P2 was made while continuing recording for at least another 2 h. Four days were allowed between two consecutive recording days in each rat. For intrathalamic drug application, 24 h before recording, microdialysis probes were slowly inserted into the brain to replace the dummy probe in the guide cannulae. On the day of the experiments, rats were transferred to the recording cage and connected to the dialysis probes and electrical recording apparatus. aCSF dialysis was initiated immediately while the rats were allowed to habituate for 1 h. A control period of 2.5 h was then recorded while administering aCSF (same conditions as described for the anesthetized condition). Animals were then recorded for an additional 2 h while receiving either aCSF or drug-containing aCSF (in a random order on consecutive recording days, each separated by at least 4 d). Video recording was performed simultaneously with electrical recordings in all experiments in freely moving rats.

TTA-P2 levels in the VB. The concentration of TTA-P2 in samples taken from the inlet and outlet dialysis tubes was measured, following protein precipitation with acetonitrile, by liquid chromatography-mass spectrometry under a validated analytical protocol (Shipe et al., 2008; Uebele et al., 2009). TTA-P2 concentration in the brain tissue outside the dialysis membrane was estimated according to the equilibrium equation described previously (Chan and Chan, 1999).

Optogenetics
Viral injection. pAAV-CaMKII α -hChR2(H134R)-mCherry plasmids (K. Deisseroth laboratory, Addgene plasmid 26975) were packaged into recom-

binant AAV2 vectors and serotyped with AAV1 coat proteins. Viral suspensions were titrated to 1.14×10^{13} genome copies/ml (GC) (University of Pennsylvania Vector Core). Concentrated stock virus was diluted with 0.1 M PBS tinted with Fast Green FCF (Sigma), giving a final viral concentration of 5.70×10^8 to 2.28×10^9 GC/ μ l for injection. The dorsal surface of the skull was exposed, a small craniotomy made over one VB (AP = -3.14 mm, ML = 2.80 mm from bregma) (Paxinos and Watson, 2007), and the dura reflected. A 10μ l Gastight Hamilton syringe and 34 Ga needle were front filled with mineral oil and diluted virus. Needles were then lowered slowly into the thalamus (DV = -5.75 mm from the pia) and left in place for 10 min. A 1μ l virus (5.70×10^8 to 2.28×10^9 infectious units) was injected at a rate of 100 nl/min using a programmable micro-pump (UMP3-1, WPI) and allowed to disperse for a further 10 min before the needle was slowly retracted. Rats were then individually housed and allowed to recover with *ad libitum* access to food and water for a minimum of 3 weeks to allow viral gene expression.

Optical stimulation and recording. Rats previously injected with rAAV-CaMKII α -hChR2 (H134R)-mCherry were anesthetized and EEG screws and two microdialysis probes (one in each VB) were implanted (as above) with a 16° angle with respect to the vertical axis. A 200μ m multimode (0.39 NA) optic fiber (CFM12L20; Thorlabs) was custom-glued to a 32-channel silicone probe, with the fiber tip $\sim 400 \mu$ m above the top recording sites. The fiber ferrule was connected to a compatible patch-cord and 473 nm laser diode (70 mW Stradus; Vortran Laser Technology), and the silicon probe and EEG wires connected to a Digital Lynx 10SX recording system (with Hybrid Input Boards; Neuralynx) via HS-36 unity gain preamplifiers. One optrode was slowly lowered to just above one VB, 300μ m posterior and medial to the virus injection site (AP = -3.44 mm, ML = 2.50 mm from bregma) (Paxinos and Watson, 2007), and DV = -4.60 mm from the pia, and then moved in small steps to locate light-responsive ChR2 $^{2+}$ cells exhibiting characteristic TC neuron bursts (see experiments illustrated in Figs. 9 and 10). Extracellular action potentials (sampling frequency: 32 kHz per channel, filtered from 600 Hz to 9 kHz), continuous extracellular signal (sampling frequency: 32 kHz per channel and broadband filtered from 0.1 Hz to 9 kHz), EEG signals (sampling frequency: 4 kHz, filtered from 0.1 Hz to 1 kHz), and light stimulation events were simultaneously recorded using Cheetah 5 Data Acquisition software (Neuralynx). Digital laser modulation was controlled with pClamp software and a 1322A Digidata (Molecular Devices), synchronized with the Digital Lynx 10SX. Laser output power for 5, 20, and 100 ms pulses was 40 mW, which equated to <10 mW at the fiber tip (dependent on stimulation frequency), quantified with a digital power meter and photodiode sensor (PM120D; Thorlabs).

Data analysis

Spike sorting and data preprocessing were performed with the Klusters, Neuroscope, NDManager software suite (Hazan et al., 2006). All other analyses were performed with routines based on the free toolboxes SciPy 0.8 (Jones et al., 2001), OpenElectrophy 0.2 (Garcia and Fourcaud-Trocmé, 2009), running under Python 2.6.6 and MATLAB (R2010b, MathWorks) on a 64-bit Linux computer.

Data preprocessing and spike sorting. To extract spikes from the extracellular field potential, the signal was high-pass filtered with median filter (0.5 ms window half-length). Spikes were detected by thresholding at 1.2 SD and

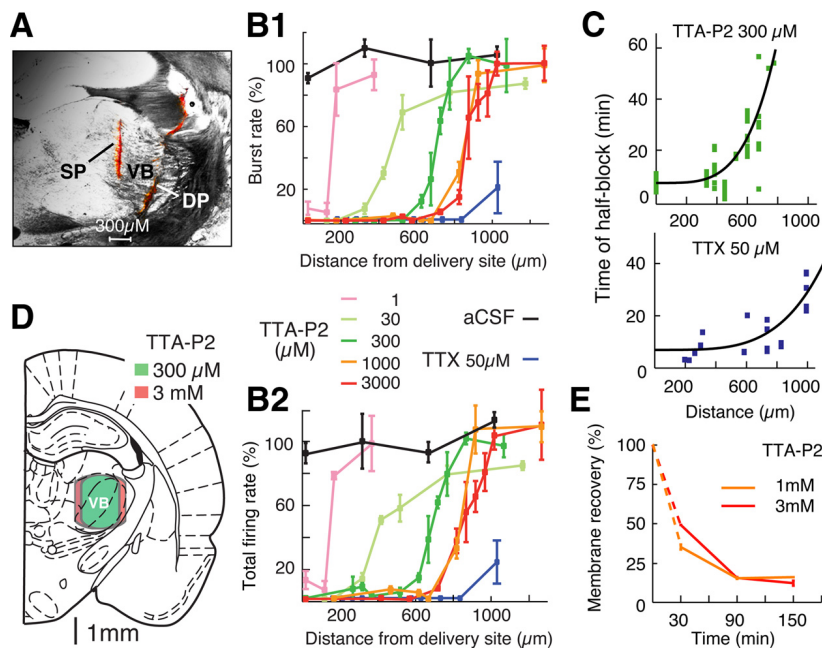


Figure 3. Block of TC neuron firing by TTA-P2 directly applied by reverse microdialysis in the thalamus under anesthesia. **A**, Coronal brain section showing the position of a microdialysis (DP) (inserted with a 16° angle with respect to the vertical axis, see Materials and Methods) and a silicone probe (SP) in the VB, both stained with a red fluorescent dye. **B1**, Distance–response curve of TTA-P2-elicited block of high-frequency bursts in VB TC neurons ($n = 533$ neurons from 37 rats). Burst rate was measured between 50 and 60 min from the start of TTA-P2 or TTX dialysis. Data are normalized to the burst rate measured during the last 10 min of the preceding 1 h of aCSF dialysis (see Materials and Methods). Different TTA-P2 concentrations are color-coded as illustrated and refer to the drug concentration in the inlet dialysis tube. There is similarity in the action of 1 and 3 mM TTA-P2. The effect of TTX is also depicted ($n = 33$ neurons from 11 rats). **B2**, Same as **B1**, but for total TC neuron firing (i.e., high-frequency bursts plus single action potentials). **C**, Distance dependence of time of half-block of high-frequency bursts by VB microdialysis of 300μ M TTA-P2 (top) and of time of half-block of total firing by VB microdialysis of 50μ M TTX (bottom). Black lines indicate the best fit of a fourth-order parabolic function. **D**, Schematic brain drawing (from Paxinos and Watson, 2007) showing that the area of burst firing block achieved with the dialysis of 300μ M TTA-P2 (green) (calculated from the data shown in **B2**) covers almost the entire VB. Only a small increase in the area of block (which now covers a small portion of the NRT) is achieved with 3 mM TTA-P2 (red). This drawing assumes a fully vertical position of the dialysis probe as it was used for all the experiments described in Figures 4, 5, 6, and 7. **E**, *In vivo* recovery of TTA-P2 applied by dialysis ($n = 6$ rats for both concentrations), which was estimated using the formula $([X]_{in} - [X]_{out})/[X]_{in}$, where $[X]_{in}$ and $[X]_{out}$ are the TTA-P2 concentration in the inlet and outlet dialysis tubes, respectively (Chan and Chan, 1999).

clustered by an expectation maximization algorithm (Klustakwik; Harris et al., 2000) on the basis of their first three principal components. All results of the automatic clustering were verified *post hoc* by visual inspection. Units were excluded from further analyses if more than one high amplitude cell was present on a single channel, if their autocorrelogram did not show a refractory period of at least 2 ms, and if their spike amplitude markedly changed during the experimental session.

Burst analysis. Bursts were defined as two or more spikes that were preceded by at least 100 ms of silence and had interspike intervals (ISIs) <10 ms, and were visually examined *post hoc*. For each burst, the following parameters were calculated (Fig. 1): (1) ISI, (2) interburst interval, (3) number of spikes per second in 5 min windows (spike rate), (4) number of bursts per second in 5 min windows (burst rate), (5) ratio of all spikes taking part in a burst, (6) number of spikes in each burst, and (7) ISI as a function of the ISI number within a burst (i.e., burst signature). Units with a *decelerando* burst signature (Fig. 1C,D) were classified as TC neurons, whereas those with a burst signature and spike autocorrelogram typical of thalamic reticular neurons (Huguenard and Prince, 1992) were discarded.

Detection of slow waves and spindles under anesthesia. To quantify EEG slow waves beyond power spectral analysis, a slow wave detection algorithm similar to those described previously (Mölle et al., 2009; Nir et al., 2011) was implemented (Fig. 2A–D). On the 0.2 to 4.5 Hz bandpass-filtered signal, all negative to positive zero-crossings were detected as slow waves. To discard spurious slow waves, the local minimum and maximum around a crossing were determined. If the difference between these was $<60\%$ of the mean maximum-to-minimum distance, the slow

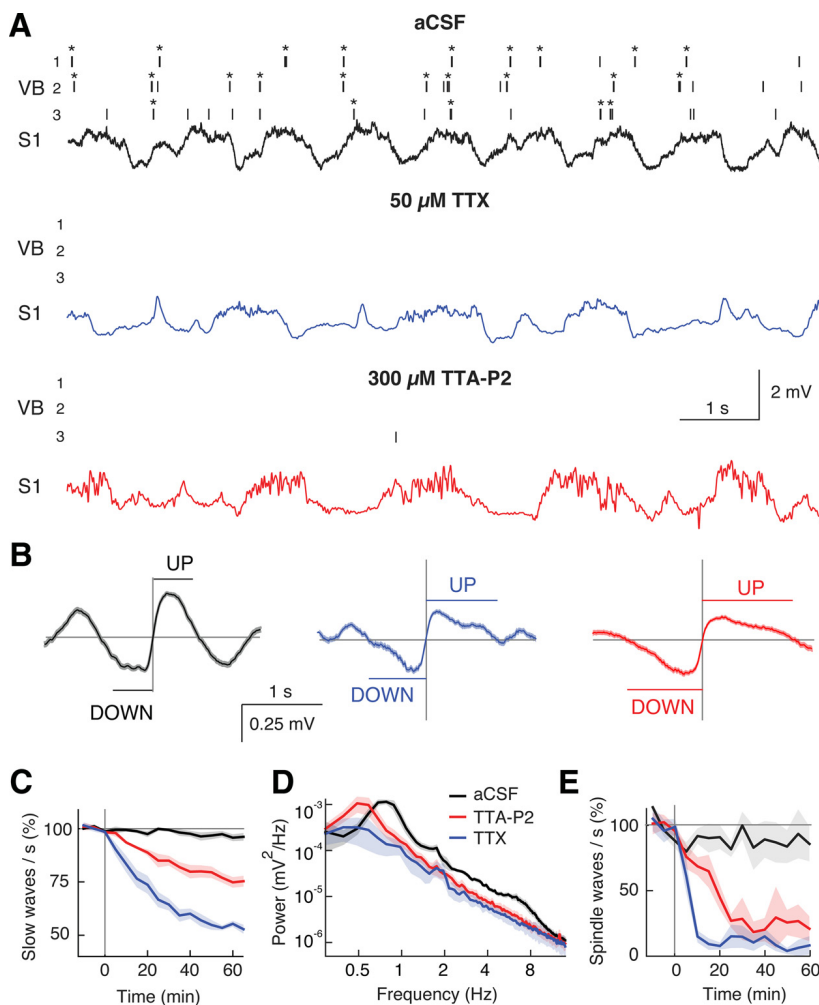


Figure 4. Block of thalamic firing decelerates EEG slow waves during anesthesia. **A**, Spike raster plots (top three traces; *bursts) from 3 VB TC neurons and EEG from S1 (bottom trace) show the effects of 50 μM TTX and 300 μM TTA-P2 dialysis in the VB. The predominant burst firing during aCSF is virtually abolished by TTX and TTA-P2, an effect accompanied by slowing of the EEG rhythm. **B**, Event-triggered averages of raw EEG traces centered on the middle point of DOWN to UP state transitions were calculated after 1 h of aCSF, TTX, and TTA-P2 dialysis ($n = 438, 243,$ and 222 transitions, respectively). **C**, Normalized (to predrug period), time-dependent decrease of slow waves by TTX ($n = 5$) and TTA-P2 ($n = 5$) (drug dialysis starts at 0). **D**, EEG power spectra 60 min after start of drug dialysis. **E**, Normalized (to predrug period), time-dependent reduction of spindle waves by TTX and TTA-P2. **C–E**, Solid lines indicate the mean; color shadings indicate SEM. In this and the following figures, illustrated drug concentrations during microdialysis are those of the inlet dialysis tube (for brain concentration delivered by dialysis probes, see Fig. 3E). In this experiment and those depicted in Figures 5, 6, and 7, the dialysis probes were inserted in a fully vertical position.

wave was discarded. For the analysis of UP and DOWN state duration, the periods above and below the midpoint of the DOWN to UP transitions in the bandpass-filtered signal were labeled as UP and DOWN states, respectively. States with a magnitude of $<25\%$ of the average magnitude during the control period were discarded and the neighboring states of equal type (UP or DOWN) merged. Spindle waves were detected in the frequency range 5–12.5 Hz (Fig. 2E,F).

Spectral analysis. Power spectral densities were estimated with Welch's average periodogram method using a Hanning window with length of 4096 data points. Total power in a frequency band was determined as the integral over that frequency band.

Detection of non-REM sleep epochs. The power of the EEG signal between 0.5 and 4 Hz was computed for every 10 s of recording. If the calculated power was higher than twice the power calculated during a period of active wakefulness, the 10 s epoch was classified as non-REM sleep. To ensure detection reliability and behavioral state stability over the selected periods, only consecutive epochs of sleep lasting at least 60 s were included in further analysis.

Detection of slow waves and spindles during natural sleep. The EEG signal was convolved with complex Morlet wavelets of 2.5 cycles for sleep

spindles and 1.0 cycle for slow waves at a frequency resolution of 0.1 Hz for spindles and 0.01 Hz for slow waves (Kronland-Martinet et al., 1987). Using a wavelet ridge extraction method, each oscillatory epoch of the EEG was extracted with an energy threshold to detect its beginning and end (see Figs. 2G, 6A, and 7A) (Roux et al., 2007; Garcia and Fourcaud-Trocmé, 2009). The boundary frequencies of wave detection were chosen as from 0.5 to 4 Hz for slow waves (see Fig. 6B) and from 6 to 14 Hz for spindle oscillations (see Fig. 2G,H). The threshold was defined as 3 times the average energy during a non-REM sleep period during the control session. Slow and spindle waves with <2 and 3 cycles, respectively, were discarded. When overlapping oscillations were detected, the wave with the highest energy was selected.

Statistical analysis. Group comparisons were performed using the Mann–Whitney U test. Paired data were tested with Wilcoxon's signed ranks test. All quantitative data in figures and text are given as mean \pm SEM.

Histology

Electrode and microdialysis probe tracking. Before insertion, silicone and microdialysis probes were immersed for 1/2 h and 5 min, respectively, in a 1% Vybrant Dil (Invitrogen) dye solution. At the end of the experiment, rats were injected with a lethal dose of urethane (40%), and the brains were removed and placed in a 4% PFA solution for 48 h. The brains were then transferred and stored in a 0.1 M PBS. Sections (100 μm thick) containing the VB were cut with a vibratome (Leica VT1000S) and mounted on coverslips to measure the relative position of microdialysis and silicone probes, which were visualized using a fluorescent microscope (Leica).

Immunofluorescence. Rats were given an overdose of ketamine-xylazine and transcardially perfused with 4% PFA. Brains were fixed in 4% PFA and then cryoprotected in 20% (w/v) sucrose in 0.1 M PBS. Each brain was blocked to give coronal sections, mounted onto a freezing microtome (Leica), and cut into 50 μm sections. Free-floating sections were processed for NeuN and RFP immunofluorescence. Briefly, sections were washed 3×10 min with fresh 0.1 M PBS and blocked for 1.5 h in $1 \times$ PGT [0.1 M PBS, 3% NGS, and 0.2% Triton X-100 (Sigma-Aldrich)]. Sections were gently shaken at room temperature for 2 h, then overnight at 4°C with primary antibodies against both NeuN (1:500 mouse monoclonal, Millipore), and RFP (1:1000 Living Colors DsRed rabbit polyclonal, Clontech) in $1 \times$ PGT. Sections were rinsed 3×10 min with fresh 0.1 M PBS and incubated for 2 to 3 h at room temperature with 1:200 goat anti-mouse AlexaFluor-488 (Invitrogen) and 1:200 goat anti-rabbit AlexaFluor-594 (Invitrogen) secondary antibodies in $1 \times$ PGT. Sections were washed 3×10 min in fresh 0.1 M PBS and mounted onto gelatin-subbed Superfrost Plus microscope slides (Thermo Scientific). Slides were coverslipped with VectaShield fluorescent mounting medium (Vector Laboratories) and visualized using a fluorescence microscope (Leica).

Results

Effect of thalamic inactivation on slow waves during anesthesia

We first abolished the somatosensory thalamic output to the cortex by bilateral reverse microdialysis of TTX in the ventrobasal thalamus (VB) of ketamine-xylazine anesthetized rats, while

simultaneously recording slow waves from primary somatosensory cortex (S1) and the firing of different single TC neurons in the VB. TTX abolished action potentials in TC neurons around the VB injection site (pre-drug: 2.51 ± 0.11 spikes/s, TTX: 0.001 ± 0.002 , $n = 11$ rats, $n = 33$ neurons, $p < 10^{-7}$, Wilcoxon signed-rank test) (Fig. 3B1,B2, blue lines, C, bottom plot; see also Fig. 4A, unit recordings). This effect led to a concomitant marked reduction ($45 \pm 1.4\%$) in the number of EEG slow waves after 1 h of drug dialysis (Fig. 4A,B) and thus to a frequency decrease from 1.19 ± 0.02 to 0.63 ± 0.03 slow waves/s ($n = 5$, $p = 0.0017$, Mann–Whitney U test compared with aCSF, $n = 6$) (Fig. 4A–D). The duration of both UP and DOWN states was increased by TTX from 0.40 ± 0.01 (UP) and 0.42 ± 0.03 s (DOWN) to 0.68 ± 0.07 and 0.58 ± 0.06 s, respectively ($p < 0.006$, Mann–Whitney U test compared with aCSF) (Fig. 4B). In the same rats, the simultaneously recorded spindle waves, which are a thalamically generated rhythm (Morison and Bassett, 1945; Steriade et al., 1985; De Gennaro and Ferrara, 2003; Astori et al., 2011), were abolished by TTX (pre-drug: 0.13 ± 0.02 spindles/s, TTX: 0.009 ± 0.008 , $p = 0.0016$) (Fig. 4E), indicating the effectiveness of our thalamic inactivation by microdialysis administration of TTX.

Because T-type calcium channels play a key role in the thalamic output to cortex (Llinás and Jahnsen, 1982; Crunelli et al., 1989; Deleuze et al., 2012) and underlie TC neuron UP states (Hughes et al., 2002), we next investigated the effect on slow waves of the potent and selective T-type calcium channel antagonist, TTA-P2 (Uebele et al., 2009; Dreyfus et al., 2010), directly applied in the VB by reverse microdialysis. This drug produced a block of high-frequency bursts of TC neurons, which was dependent on its concentration in the dialysis inlet tube and on the distance between the recorded neuron and the dialysis probe (Fig. 3B1; see also unit recordings in Fig. 4A). Interestingly, single action potential firing (which accounted for $\sim 18.4 \pm 1.2\%$ of the total firing) was also markedly decreased by TTA-P2 (Fig. 3B2) (see Fig. 4A, unit recordings) so that, at a distance of $500 \mu\text{m}$ from the dialysis probe, only $3.3 \pm 2.1\%$ of total spikes (i.e., in bursts and as single action potentials) remained after 1 h of TTA-P2 application. We chose a microdialysis inlet tube concentration of $300 \mu\text{M}$ TTA-P2 because: (1) it virtually abolished the total TC neuron firing in a region that almost fully covered the mediolateral extent of the VB (Fig. 3C,D), and (2) it resulted in a tissue concentration around the probe of $\sim 42 \mu\text{M}$ (based on a 14% recovery rate) (for explanation, see Fig. 3E), which is well in the range of concentrations that we previously showed to be required to abolish intrinsic and synaptically driven TC neuron firing in the VB *in vitro* (Dreyfus et al., 2010, their Fig. 1C). Thus, TTA-P2 applied in the VB at $300 \mu\text{M}$ elicited a clear reduction ($25 \pm 3\%$, $n = 5$, $p = 0.02$

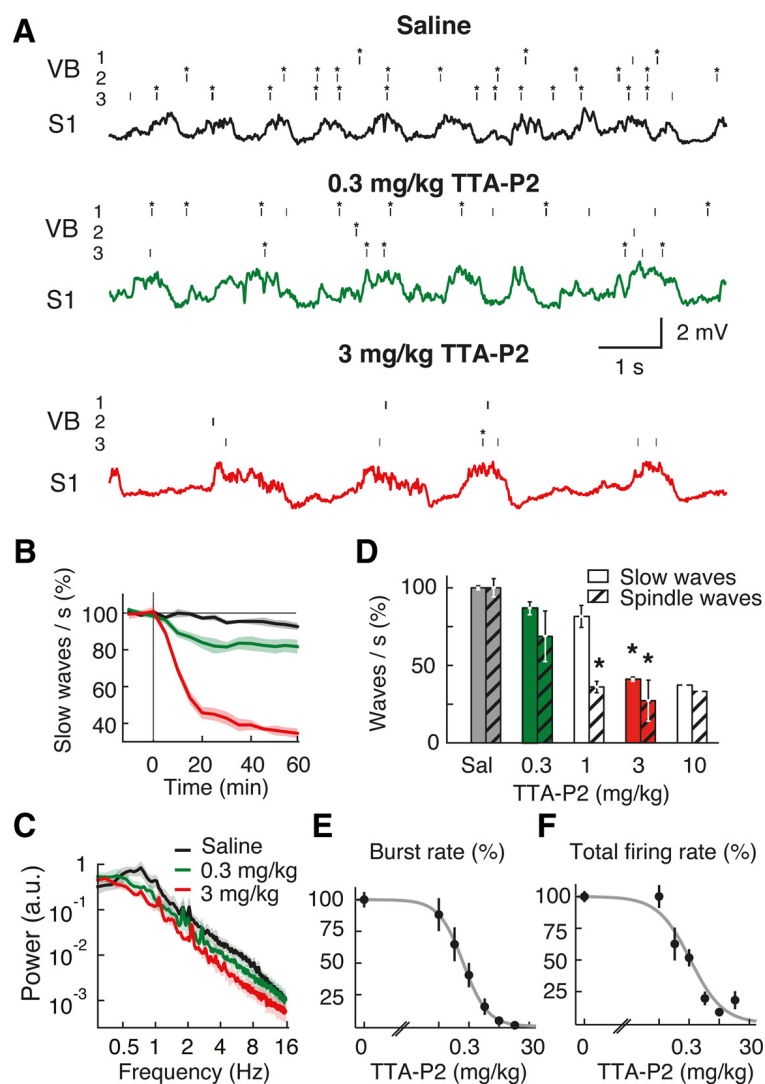


Figure 5. Systemic injection of TTA-P2 markedly decreases the frequency of slow and spindle waves during anesthesia. **A**, Spike raster plots (top three traces; *bursts) from 3 different TC neurons in the VB and EEG (bottom trace) from S1 show the effect of two doses of intraperitoneally injected TTA-P2 on neuronal firing and slow waves. **B**, Time-dependent block of slow waves after 0.3 and 3 mg/kg intraperitoneally of TTA-P2 injected at time 0. **C**, Power spectra calculated 1 h after TTA-P2 injection. **D**, Summary data showing the percentage reduction in slow and spindle waves produced by different doses of TTA-P2 (measured 1 h after intraperitoneal injection). Number of animals for saline (Sal) and TTA-P2 0.3, 1, 3, and 10 mg/kg injections are 4, 3, 3, 3, and 1, respectively. Error bars indicate SEM. * $p < 0.01$ compared with saline injection (Mann–Whitney U test). **E, F**, Dose–response curve of burst and total spike rate measured 40 min after systemic intraperitoneal injection of TTA-P2 (logistic regression fits, $p < 0.05$) (ED_{50} for bursts: 0.18 ± 0.05 mg/kg; ED_{50} for total spikes: 0.26 ± 0.06 mg/kg). The 3 and 10 mg/kg TTA-P2 abolish bursts ($p < 10^{-6}$ compared with saline injection, Mann–Whitney U test, $n = 40$ TC neurons). **B, C**, Solid lines indicate the mean; color shadings indicate SEM. Color code in **C** also applies to **B** and to the traces in **A**.

compared with aCSF, $n = 6$) of slow waves (Fig. 4A,B), leading to a frequency decrease from 1.00 ± 0.02 to 0.69 ± 0.03 slow waves/s ($p = 0.020$) (Fig. 4A,C,D). The durations of UP and DOWN states were both prolonged from 0.59 ± 0.04 (UP) and 0.58 ± 0.02 (DOWN) to 0.77 ± 0.06 and 0.70 ± 0.03 s, respectively ($p < 0.05$, Mann–Whitney U test compared with aCSF) (Fig. 4B). Moreover, in the same experiments, spindle waves were markedly suppressed ($88 \pm 5\%$) by microdialysis injection of TTA-P2 in the VB (aCSF: 0.15 ± 0.01 spindles/s; TTA-P2: 0.019 ± 0.008 ; $p = 0.02$) (Fig. 4E), indicating the effectiveness of our thalamic inactivation by microdialysis administration of TTA-P2.

TTA-P2 also elicited a dose-dependent decrease in slow waves when applied systemically (Fig. 5A–D), with a similar ED_{50} on burst (0.18 ± 0.05 mg/kg) (Fig. 5E) and total firing (0.26 ± 0.06 mg/kg) (Fig. 5F). In particular, at a dose (3 mg/kg) that abolished

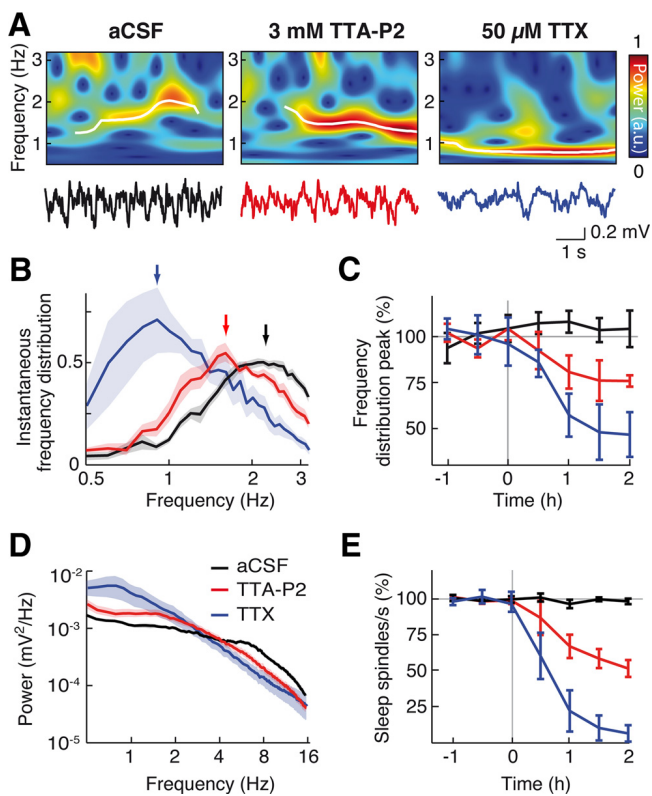


Figure 6. Block of thalamic firing decreases slow wave frequency during natural sleep. **A**, Non-REM sleep EEG (bottom) and corresponding wavelet spectra (top) during VB microdialysis of aCSF, 3 mM TTA-P2, and 50 μ M TTX. Transient slow waves (white lines) were detected as ridges in the wavelet spectra (see Materials and Methods). **B**, Slow wave frequency density distribution during aCSF, TTA-P2, and TTX dialysis, 1 h after the start of drug dialysis (arrows indicate the measured peaks). **C**, Time dependence of TTA-P2 ($n = 7$ rats) and TTX ($n = 5$ rats) effects on the normalized peak of the slow wave frequency distribution. **D**, Raw non-REM EEG power spectra show TTA-P2- and TTX-elicited decrease of power in sleep spindle frequency range and increase of power in slow wave frequency range. **E**, Time dependence of TTA-P2 and TTX effects on sleep spindles normalized count. **B, D**, Solid lines indicate the mean; color shading indicates SEM. **C, E**, Error bars indicate SEM.

burst firing in the VB (Fig. 5E), TTA-P2 produced a stronger decrease ($63 \pm 1\%$, $n = 3$, $p = 0.018$) of slow waves (Fig. 5B) than an equipotent (on burst firing) intra-VB application (compare with Fig. 3B1), indicating that T-type calcium channels in other thalamic nuclei and brain regions effectively contribute to the full expression of EEG slow waves in S1 during anesthesia.

Effect of thalamic inactivation on slow waves during natural sleep

Because anesthesia does not fully reproduce the spatiotemporal dynamics of slow waves during non-REM sleep (Chauvette et al., 2011; Nir et al., 2011; Vyazovskiy et al., 2011), we then applied TTX and TTA-P2 by reverse microdialysis in the thalamus of naturally sleeping-waking rats. The same inlet dialysis concentration of TTA-P2 (300 μ M) and one-probe-per-VB configuration that was effective during anesthesia had no effect on slow waves of natural sleep, nor did 1 and 3 mM TTA-P2, most likely because the volume of tissue where a firing block was achieved with these higher TTA-P2 concentrations was not much bigger than the region affected by 300 μ M (Fig. 3B1, B2, D). We therefore enlarged the thalamic area affected by microdialysis application by implanting a group of rats with four dialysis probes, so that in each VB one probe was close to its rostral and one to its caudal end (see Materials and Methods). In these animals, TTA-P2 (3 mM) in-

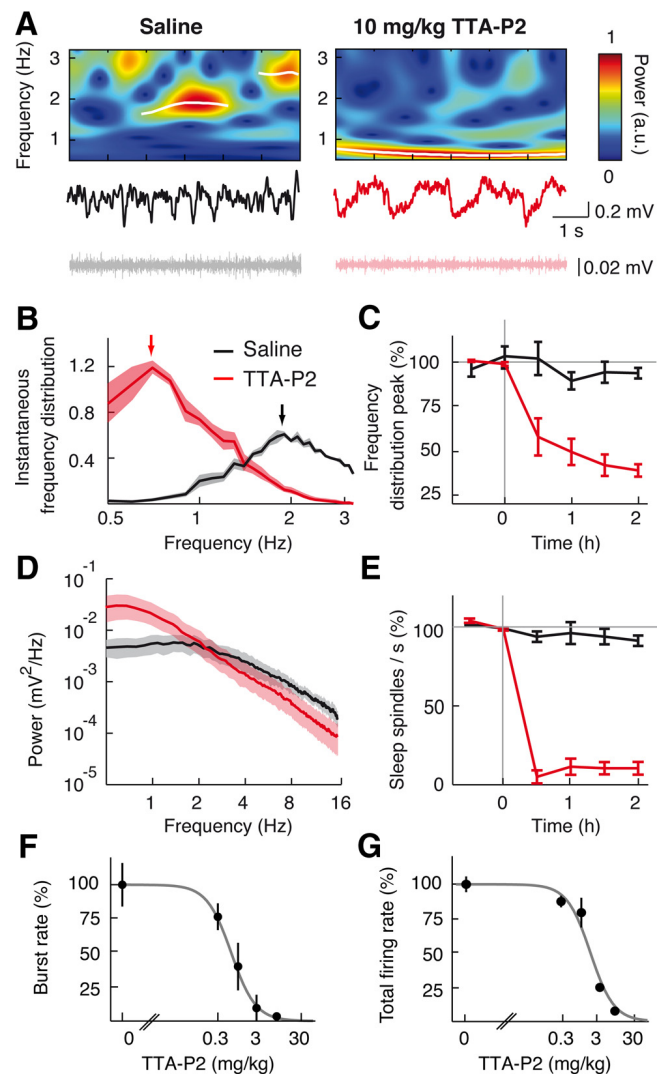


Figure 7. Systemic injection of TTA-P2 markedly decreases the frequency of slow waves and abolishes spindles during natural sleep. **A**, Non-REM sleep EEG (middle), corresponding wavelet spectra (top), and EMG (bottom) after intraperitoneal injection of saline (left) and 10 mg/kg TTA-P2 (right). Transient slow waves (white lines) were detected as ridges in the wavelet spectra as in Figure 2. **B**, Slow wave frequency distribution after saline and TTA-P2 injection. There is a shift of the peak (arrows) from ~ 2 Hz to ~ 0.7 Hz. **C**, Time dependence of TTA-P2 ($n = 4$ rats) and saline ($n = 6$ rats) effects on the normalized peak of the slow wave frequency distribution. **D**, Raw non-REM sleep EEG power spectra show TTA-P2-elicited decrease of power in sleep spindle frequency range and increase of power in slow wave frequency range compared with saline injection. **E**, Time dependence of TTA-P2 effects on sleep spindles normalized count. **F, G**, Dose-response curve of burst rate (**F**) and total spike (**G**) rate measured 40 min after systemic intraperitoneal injection of TTA-P2 (logistic regression fits, $p < 0.05$) (ED_{50} for bursts: 0.55 ± 0.03 mg/kg; ED_{50} for total spikes: 1.71 ± 0.11 mg/kg). The 3 and 10 mg/kg TTA-P2 abolish bursts recorded during natural sleep ($p < 10^{-6}$ compared with saline injection, Mann-Whitney U test, $n = 42$ TC neurons). **B, D**, Solid lines indicate the mean; color shading indicates SEM. **C, E–G**, Error bars indicate SEM.

duced a significant decrease ($23 \pm 7.8\%$, $n = 7$, $p = 0.0095$, Mann-Whitney U test compared with aCSF, $n = 12$) in the peak of the instantaneous frequency distribution of slow waves during non-REM sleep (predrug: 2.19 ± 0.09 Hz; TTA-P2: 1.72 ± 0.13 Hz), as did TTX (50 μ M) (TTX: 0.92 ± 0.13 Hz, $50 \pm 13\%$ reduction, $n = 5$, $p = 0.0061$) (Fig. 6A–D). As expected, in the same animals, sleep spindles were more potently decreased by TTX and TTA-P2 ($94 \pm 7\%$ and $48 \pm 6\%$, respectively) than slow waves (predrug: 0.36 ± 0.02 spindles/s; TTX: 0.05 ± 0.03 , TTA-P2: 0.19 ± 0.02 ; $p = 0.001$ for both compared with aCSF) (Fig. 6D, E).

As it was observed during anesthesia, also in naturally sleeping rats systemic injections of TTA-P2 dose-dependently blocked burst and total firing in VB TC neurons during non-REM sleep (with an ED_{50} of 0.55 ± 0.03 and 1.71 ± 0.11 mg/kg, respectively) (Fig. 7*F,G*), as well as slow waves and sleep spindles (Fig. 7*A–E*). In particular, a dose of 10 mg/kg of TTA-P2 markedly reduced slow wave (saline: 1.94 ± 0.13 Hz, $n = 6$; TTA-P2: 0.8 ± 0.01 Hz, $n = 4$ rats) and sleep spindle frequencies (saline: 0.32 ± 0.13 spindles/s, TTA-P2: 0.05 ± 0.01) by $73 \pm 5\%$ ($p = 0.0095$) and $86 \pm 4\%$ ($p = 0.00031$), respectively (Fig. 7*E*).

Entrainment of EEG slow waves by optogenetic stimulation of TC neurons during anesthesia

Because thalamic inactivation by either TTX or by selective block of thalamic T-type calcium channels with TTA-P2 decreased the frequency of slow waves during anesthesia and natural sleep, the thalamic input to the neocortex should be able to entrain these EEG waves. Because electrical stimulation of the thalamus leads to antidromic excitation of the somatotopic cortical region, which may in turn affect the cortical slow wave oscillator, we addressed this question using selective optogenetic activation of channelrhodopsin2-expressing TC neurons (Fig. 8) with short (5, 20, or 100 ms) 473 nm light pulses at stimulation frequencies that ranged from 0.75 to 4 Hz ($n = 7$ rats) (Fig. 9). At the cellular level, each light pulse elicited a single high-frequency burst of action potentials, which was invariably followed by a 100–250 ms period of electrical silence before firing resumed (Fig. 9*C*). For stimulation frequencies from 0.75 to 1.5 Hz, this pattern of TC neuron activation elicited a clear peak in the EEG wavelet (Fig. 9*A*) and FFT power spectrum (Fig. 9*D*) at the respective stimulation frequency, which had higher amplitude than the peak of the control EEG (i.e., with no light stimulation) (Fig. 9*D*, black line). As seen from the light-pulse triggered averages (Fig. 9*B*), light stimulation for frequencies >1.5 Hz not only failed to entrain EEG slow waves but also markedly flattened the power spectra eliminating the peak present at ~ 1 Hz during the control condition (i.e., without light stimulation; Fig. 9*D*, black line). When T-type calcium channels in VB were blocked by microdialysis of $300 \mu\text{M}$ TTA-P2 ($n = 3$ rats) (Fig. 10*A*), the cellular burst response during light stimulation was strongly reduced (burst reduction: $89 \pm 4\%$, $n = 1056$ pulses, $n = 11$ neurons, $p = 0.0020$, Wilcoxon signed-rank test), the TC neuron firing between stimulations was virtually abolished (Fig. 10*B*), and no entrainment of slow waves occurred for stimulation frequencies between 0.75 and 1.5 Hz (Fig. 10*C1,D*). Moreover, a similar block of EEG slow wave entrainment was observed after systemic injection of TTA-P2 (3 mg/kg) at these stimulation frequencies (data not shown). Finally, no significant effect of TTA-P2 injected locally (Fig. 10*C2,D*) or systemically (data not shown) was observed at stimulation frequencies ≥ 1.75 Hz.

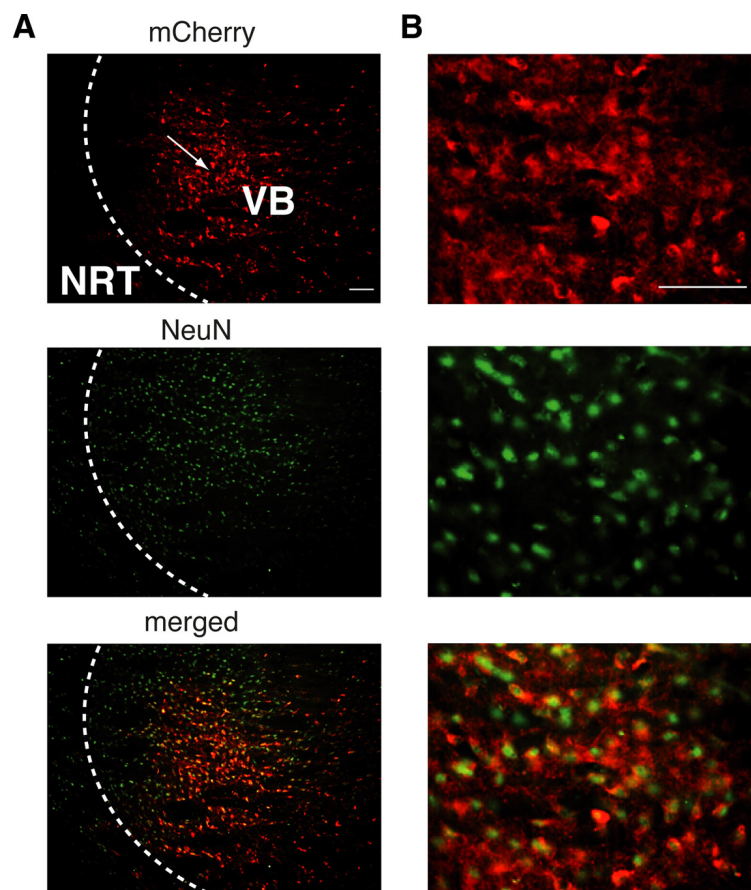


Figure 8. Channelrhodopsin-2 expression in VB TC neurons. *A*, Immunostaining of channelrhodopsin-2-mCherry (red) showing that the expression of the channelrhodopsin-2 protein is restricted to VB TC neurons and some TC axons passing through the NRT (top). Arrow indicates the putative site of the virus injection. NeuN staining (green) is evident in both VB and NRT somata (middle). Merged images (bottom) demonstrate colocalization of channelrhodopsin-2 and NeuN in TC, but not NRT, neurons. *B*, Higher magnification of a portion of the respective panels in *A*. Scale bars, *A*, *B*: $300 \mu\text{m}$.

Discussion

Our results conclusively demonstrate that the full manifestation of EEG slow waves during non-REM sleep in freely moving, naturally waking-sleeping rats requires a dynamic interplay of cortical and thalamic neuronal ensembles because inactivation of the thalamic output to the neocortex brings about a marked deceleration of slow waves and selective excitation of TC neurons entrains EEG slow waves.

Contribution of thalamic oscillators to sleep rhythms

There is a general consensus that an isolated neocortex can generate and maintain the UP and DOWN state dynamics that underlie EEG slow waves of natural sleep via an intricate balance of excitation and inhibition that is mostly generated by synaptically driven cortical slow wave oscillators (Sanchez-Vives and McCormick, 2000; Timofeev et al., 2000; Bazhenov et al., 2002; Cossart et al., 2003; Shu et al., 2003; Le Bon-Jego and Yuste, 2007; Beltramo et al., 2013). In line with this interpretation, the cortical firing (during UP states) and the electrical silence (during DOWN states) impose similar UP/DOWN state transitions on thalamic neurons, making the thalamus fully subservient to corticofugal activity. Over the last 10 years, however, this view has been challenged by solid experimental evidence demonstrating that an isolated thalamus as well as single TC and nucleus reticularis thalami (NRT) neurons *in vitro* can sustain slow waves and an intrinsic UP/DOWN states dynamics, respectively, which are similar to those observed during natural sleep (Crunelli

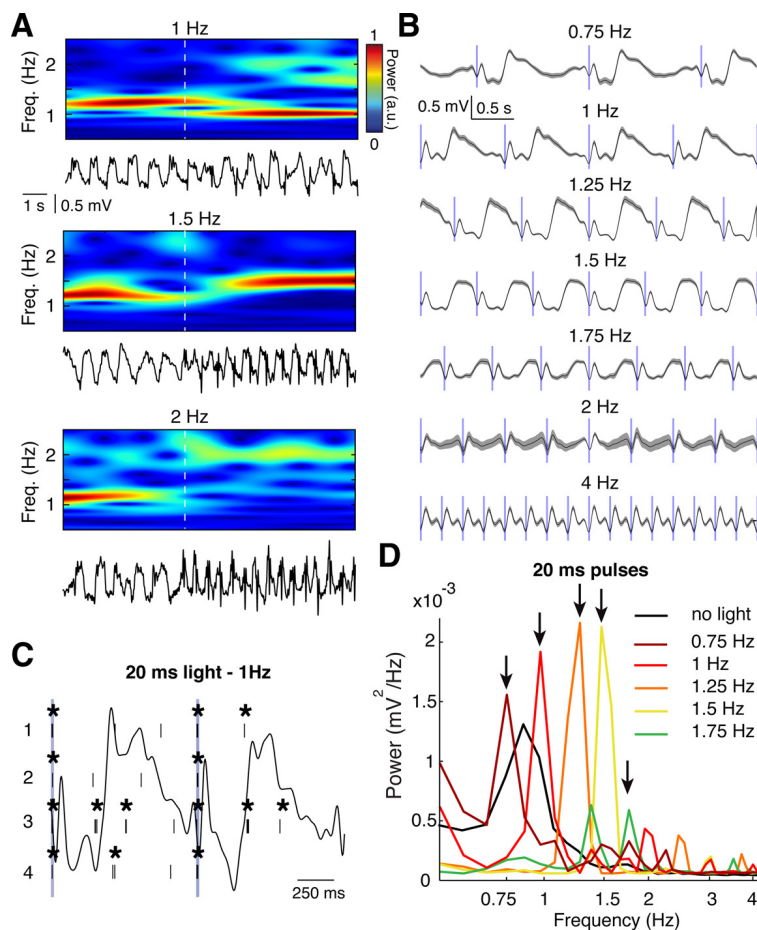


Figure 9. Thalamic entrainment of EEG slow waves during anesthesia. **A**, EEG trace (bottom) and wavelet transform (top) showing the effect of 20 ms, 473 nm light pulses at 1, 1.5, and 2 Hz. Dashed white line indicates the start of the first pulse. **B**, Event-triggered EEG averages centered on the 20 ms light pulses (blue vertical bars) for the illustrated stimulation frequencies. Gray areas indicate SEM. A total of 10 s of EEG was used for each average. **C**, Raster plots of firing of 4 VB TC neurons in responses to two consecutive 20 ms pulses (at 1 Hz) (blue vertical lines). *Bursts. The corresponding EEG trace is superimposed as a black line. **D**, EEG power spectra in response to 20 ms light pulses at the illustrated frequencies (indicated by arrows). There are frequency-dependent amplification and the shift of the peak of the power spectra compared with control (i.e., without light stimulation, black line).

and Hughes, 2010). This thalamic activity only occurs when the metabotropic glutamate receptors (which are present postsynaptically to the corticofugal terminals) of TC and NRT neurons (Godwin et al., 1996) are active, making these neurons “conditional oscillators” for slow waves (Crunelli and Hughes, 2010).

The present findings strongly support this hypothesis: removal of the thalamic input to cortex reduces the frequency of slow waves of non-REM sleep, demonstrating, for the first time, a necessary role for the thalamus in this physiological rhythm. The generation of slow waves during natural sleep, therefore, derives from cortical networks as primary oscillators with the thalamic oscillator providing a fine-tuning by imposing its faster frequency and phase properties to the cortical slow wave rhythm. The full physiological rhythm might, indeed, be the result of two competing oscillators (Gutierrez et al., 2013), with the thalamus being able to reset the phase of the slower cortical networks, as indicated by the ability of selective optogenetic excitation of thalamofugal fibers to entrain EEG slow waves (this work) and to induce isolated UP states in awake, head-restrained rats (Poulet et al., 2012). Importantly, the ability of the thalamus to modulate cortical UP states depends on thalamic T-type calcium channels, and in particular on the high-frequency burst of action potentials that invariably marks the start of TC neuron UP states (Contreras

and Steriade, 1995, their Fig. 9; Slézia et al., 2011; Ushimaru et al., 2012). The effect of this thalamic modulation will also be important in determining the slight acceleration of slow waves observed from sleep Stage 2 to 4 (Crunelli and Hughes, 2010; Brown et al., 2012) because the intrinsic slow wave thalamic oscillator increases its frequency with the progressive hyperpolarization that accompanies non-REM sleep deepening (Hughes et al., 2002; Crunelli and Hughes, 2010). Support to the thalamic modulation of EEG slow waves also comes from data showing that an acceleration of these waves is accompanied by a phase shift of the TC neuron firing toward the start of an UP state (Slézia et al., 2011).

In the same animals where slow waves of non-REM sleep were decreased in frequency, the simultaneously recorded sleep spindles, which are a thalamically generated rhythm (Morison and Bassett, 1945; Steriade et al., 1985; De Gennaro and Ferrara, 2003; Astori et al., 2011), were abolished by inactivation of the same thalamic region. This demonstrates that, whereas both cortex and thalamus are required for the full expression of slow waves and spindles of natural sleep, the relative contribution of these brain areas to these oscillations is markedly different, reflecting the diverse cellular/network generators that underlie these two EEG rhythms.

By comparing, for the first time, slow waves during natural sleep and anesthesia under the same laboratory conditions, we could identify that a larger area of thalamic inactivation was necessary to obtain

a significant effect on slow waves during non-REM sleep compared with anesthesia. This indicates that the thalamic modulation of slow waves during anesthesia is very different from that during natural sleep, stressing the diverse nature of the cortical and thalamic neuronal dynamics underlying these behavioral states, the limitations associated with extrapolating results from one experimental condition to the other, and a potentially different involvement of the “core” and “matrix” thalamic projection systems (Jones, 2001).

Thalamic T-type calcium channels and the slow rhythm

Our investigation is the first to provide direct evidence that the T-type calcium channels of thalamic (i.e., TC and NRT) neurons are required for the full expression of slow waves during natural sleep, although we could not distinguish between TC and NRT neuron contribution because of TTA-P2 spread to the latter neuronal population at the highest concentrations. A previous study reported an increased number of awakenings in mice carrying a supposedly thalamic-selective deletion of CaV3.1 T-type channels expression (Anderson et al., 2005). However, the presence of recombination in piriform cortex, some hypothalamic nuclei, and other brain areas questions the selectivity of this genetic approach and weakens its conclusions. Another study in anesthe-

tized CaV3.1 T-type calcium channel KO mice (Lee et al., 2004) suggested a contribution of these channels to δ waves (defined as power in the 1–4 Hz frequency band) but not to slow waves (defined as power in the <1 Hz frequency band). Our results in anesthetized rats instead indicate that slow waves peaking at ~ 1 Hz are decreased in number by TTA-P2, leading to a slowing down in frequency to ~ 0.6 Hz. Although these contradictory data may be the result of the use of different species or anesthetics, they may also result from the different wave classifications. Indeed, it is debatable (Luczak and Barthó, 2012) whether EEG waves occurring at the upper end of the δ frequency range (2–4 Hz) in naturally sleeping rats do represent a separate entity from slow (<2 Hz) waves because the underlying UP and DOWN state firing dynamics of slow waves in the 2–4 Hz band is similar to that in 0.5–2 Hz band (Ji and Wilson, 2007, their Fig. 2).

It is not surprising that the vast majority of the total TC neuron firing (i.e., high-frequency bursts plus single action potentials) depends on T-type calcium channels (i.e., it is blocked by TTA-P2). Indeed, although these channels are classically viewed as underlying only high-frequency bursts of TC neurons, recent evidence has indicated that the continuous opening of a very small number of T-type channels that occurs at ~ -60 mV generate a depolarizing window current (Dreyfus et al., 2010, their Fig. 2) that is crucial for the maintenance of the UP state (Hughes et al., 2002; Crunelli and Hughes, 2010). This strong reliance of the thalamic output on T-type channels also indicates that during slow waves synaptic activity, and in particular cortical inputs to the thalamus, are not sufficient to drive a TC neuron output in the absence of these channels.

Resetting and entrainment of EEG slow waves can be achieved by whisker stimulation (Civillico and Contreras, 2012) or by optogenetic activation of cortical neurons in anesthetized rats (Kuki et al., 2013), whereas long (>4 s) optogenetic stimulation of TC neurons in head-restrained mice can induce UP states in neocortical neurons that do not outlast the light stimulus (Poulet et al., 2012). Our results show that short (5 ms) optogenetic stimuli, which evoke high-frequency bursts in TC neurons, strongly entrain EEG slow waves, and that this response is only present when thalamic T-type calcium channels are functionally active. This strengthens the suggestion that thalamic T-type channel-mediated bursts may critically control UP states in related cortical territories during non-REM sleep by finely tuning the frequency of the EEG slow waves that occur during this behavioral state (Crunelli and Hughes, 2010). In contrast, a recent imaging study has reported that thalamic slow waves always follow cortical slow waves during anesthesia (Stroh et al., 2013). However, these results shed little light on the relative contribution of thalamic and cortical neuronal ensembles to slow waves of natural sleep, because, as indicated by Wester and Contreras (2013), they may be confounded by the experimental conditions, in

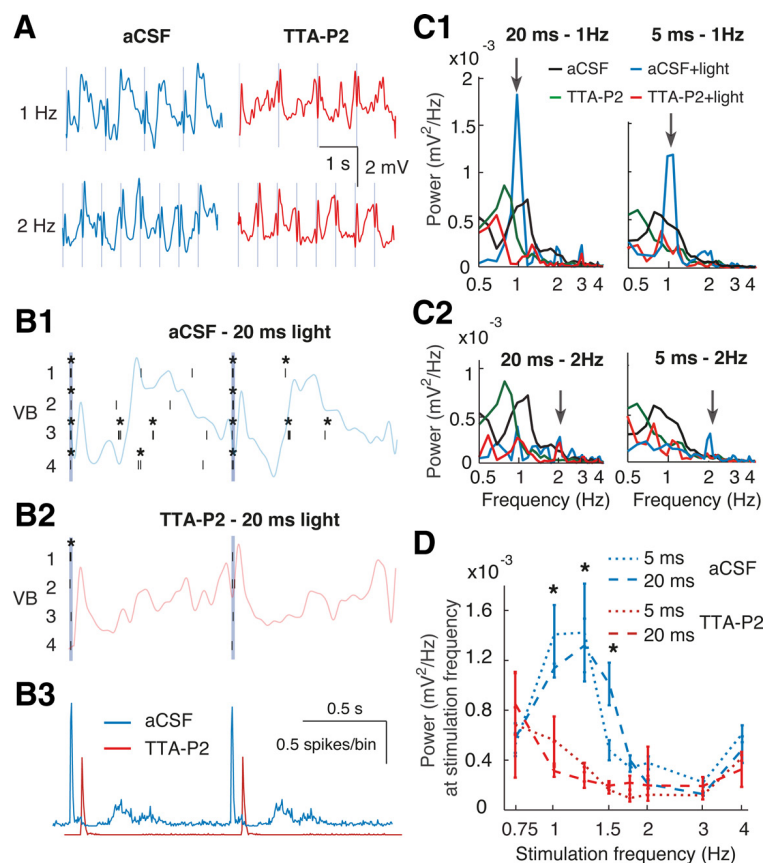


Figure 10. Thalamic entrainment of EEG slow waves requires thalamic T-type calcium channels during anesthesia. **A**, EEG traces showing the effect of 20 ms, 473 nm light pulses (vertical blue lines) at 1 and 2 Hz during aCSF and TTA-P2 dialysis in VB. **B**, Raster plots of firing of 4 VB TC neurons in responses to 20 ms pulses (at 1 Hz) during aCSF (**B1**) and TTA-P2 dialysis (**B2**). *Bursts. The corresponding EEG trace is superimposed. **B3**, Light pulse-triggered spike rates (red trace is right-shifted for clarity) from 41 stimulation epochs. **C**, EEG power spectra in response to 20 ms light stimulation at 1 (**C1**) and 2 (**C2**) Hz (arrows) during thalamic aCSF (blue, $n = 7$ rats) and TTA-P2 (red, $n = 3$ rats) dialysis compared with power spectra without light stimulation. Black represents aCSF; green represents TTA-P2. **D**, The power values at a given stimulation frequency (obtained from spectra as in **C**) for different light stimulation frequencies are plotted during aCSF and TTA-P2 dialysis. Error bars indicate SEM. * $p < 0.05$ for 5 and 20 ms pulses (Mann–Whitney U test).

particular the use of an anesthetic agent that is known to markedly block T-type calcium channels (Joksovic and Todorovic, 2010; Eckle et al., 2012).

In conclusion, these findings provide conclusive demonstration of our hypothesis (Crunelli and Hughes, 2010) that both cortical and thalamic population activities are required for the full manifestation of EEG slow waves of natural sleep, and suggest that a decreased thalamic output to the neocortex resulting from thalamic pathologies (Schmahmann, 2003; Kopelman et al., 2009; Parnaudeau et al., 2013) will bring about a slowing down of slow waves during non-REM sleep with deleterious consequences for memory processes.

References

- Anderson MP, Mochizuki T, Xie J, Fischler W, Manger JP, Talley EM, Scammell TE, Tonegawa S (2005) Thalamic Cav3.1 T-type Ca^{2+} channel plays a crucial role in stabilizing sleep. *Proc Natl Acad Sci U S A* 102:1743–1748. [CrossRef Medline](#)
- Astori S, Wimmer RD, Prosser HM, Corti C, Corsi M, Liaudet N, Volterra A, Franken P, Adelman JP, Lüthi A (2011) The $\text{Ca}(\text{V})3.3$ calcium channel is the major sleep spindle pacemaker in thalamus. *Proc Natl Acad Sci U S A* 108:13823–13828. [CrossRef Medline](#)
- Bazhenov M, Timofeev I, Steriade M, Sejnowski TJ (2002) Model of thalamocortical slow-wave sleep oscillations and transitions to activated States. *J Neurosci* 22:8691–8704. [Medline](#)
- Beltramo R, D’Urso G, Dal Maschio M, Farisello P, Bovetti S, Clovis Y, Lassi

- G, Tucci V, De Pietri Tonelli D, Fellin T (2013) Layer-specific excitatory circuits differentially control recurrent network dynamics in the neocortex. *Nat Neurosci* 16:227–234. [CrossRef Medline](#)
- Blethyn KL, Hughes SW, Tóth TI, Cope DW, Crunelli V (2006) Neuronal basis of the slow (<1 Hz) oscillation in neurons of the nucleus reticularis thalami in vitro. *J Neurosci* 26:2474–2486. [CrossRef Medline](#)
- Brown RE, Basheer R, McKenna JT, Strecker RE, McCarley RW (2012) Control of sleep and wakefulness. *Physiol Rev* 92:1087–1187. [CrossRef Medline](#)
- Chan SHH, Chan JYH (1999) Application of reverse microdialysis in the evaluation of neural regulation of cardiovascular functions. *Anal Chim Acta* 379:275–279. [CrossRef](#)
- Chauvette S, Crochet S, Volgushev M, Timofeev I (2011) Properties of slow oscillation during slow-wave sleep and anesthesia in cats. *J Neurosci* 31:14998–15008. [CrossRef Medline](#)
- Civillico EF, Contreras D (2012) Spatiotemporal properties of sensory responses in vivo are strongly dependent on network context. *Front Syst Neurosci* 6:25. [CrossRef Medline](#)
- Contreras D, Steriade M (1995) Cellular basis of EEG slow rhythms: a study of dynamic corticothalamic relationships. *J Neurosci* 15:604–622. [Medline](#)
- Cossart R, Aronov D, Yuste R (2003) Attractor dynamics of network UP states in the neocortex. *Nature* 423:283–288. [CrossRef Medline](#)
- Crunelli V, Hughes SW (2010) The slow (1 Hz) rhythm of non-REM sleep: a dialogue between three cardinal oscillators. *Nat Neurosci* 13:9–17. [CrossRef Medline](#)
- Crunelli V, Lightowler S, Pollard CE (1989) A T-type Ca^{2+} current underlies low-threshold Ca^{2+} potentials in cells of the cat and rat lateral geniculate nucleus. *J Physiol* 413:543–561. [Medline](#)
- Crunelli V, Lörincz ML, Errington AC, Hughes SW (2012) Activity of cortical and thalamic neurons during the slow (<1 Hz) rhythm in the mouse in vivo. *Pflugers Arch* 463:73–88. [CrossRef Medline](#)
- De Gennaro L, Ferrara M (2003) Sleep spindles: an overview. *Sleep Med Rev* 7:423–440. [CrossRef Medline](#)
- Deleuze C, David F, Béhuret S, Sadoc G, Shin HS, Uebele VN, Renger JJ, Lambert RC, Leresche N, Bal T (2012) T-type calcium channels consolidate tonic action potential output of thalamic neurons to neocortex. *J Neurosci* 32:12228–12236. [CrossRef Medline](#)
- Doi A, Mizuno M, Katafuchi T, Furue H, Koga K, Yoshimura M (2007) Slow oscillation of membrane currents mediated by glutamatergic inputs of rat somatosensory cortical neurons: in vivo patch-clamp analysis. *Eur J Neurosci* 26:2565–2575. [CrossRef Medline](#)
- Dreyfus FM, Tschertner A, Errington AC, Renger JJ, Shin HS, Uebele VN, Crunelli V, Lambert RC, Leresche N (2010) Selective T-type calcium channel block in thalamic neurons reveals channel redundancy and physiological impact of I(T) window. *J Neurosci* 30:99–109. [CrossRef Medline](#)
- Eckle VS, Digruccio MR, Uebele VN, Renger JJ, Todorovic SM (2012) Inhibition of T-type calcium current in rat thalamocortical neurons by isoflurane. *Neuropharmacology* 63:266–273. [CrossRef Medline](#)
- Garcia S, Fourcaud-Trocmé N (2009) OpenElectrophy: an electrophysiological data- and analysis-sharing framework. *Front Neuroinform* 3:14. [CrossRef Medline](#)
- Gemignani A, Laurino M, Provini F, Piarulli A, Barletta G, d’Ascanio P, Bedini R, Lodi R, Manners DN, Allegrini P, Menicucci D, Cortelli P (2012) Thalamic contribution to sleep slow oscillation features in humans: a single case cross sectional EEG study in fatal familial insomnia. *Sleep Med* 13:946–952. [CrossRef Medline](#)
- Godwin DW, Van Horn SC, Eriir A, Sesma M, Romano C, Sherman SM (1996) Ultrastructural localization suggests that retinal and cortical inputs access different metabotropic glutamate receptors in the lateral geniculate nucleus. *J Neurosci* 16:8181–8192. [Medline](#)
- Gutierrez GJ, O’Leary T, Marder E (2013) Multiple mechanisms switch an electrically coupled, synaptically inhibited neuron between competing rhythmic oscillators. *Neuron* 77:845–858. [CrossRef Medline](#)
- Harris KD, Henze DA, Csicsvari J, Hirase H, Buzsáki G (2000) Accuracy of tetrad spike separation as determined by simultaneous intracellular and extracellular measurements. *J Neurophysiol* 84:401–414. [Medline](#)
- Hazan L, Zugaro M, Buzsáki G (2006) Klusters, NeuroScope, NDManager: a free software suite for neurophysiological data processing and visualization. *J Neurosci Methods* 155:207–216. [CrossRef Medline](#)
- Hughes SW, Cope DW, Blethyn KL, Crunelli V (2002) Cellular mechanisms of the slow (<1 Hz) oscillation in thalamocortical neurons in vitro. *Neuron* 33:947–958. [CrossRef Medline](#)
- Hughes SW, Lörincz M, Cope DW, Blethyn KL, Kékesi KA, Parri HR, Juhász G, Crunelli V (2004) Synchronized oscillations at α and θ frequencies in the lateral geniculate nucleus. *Neuron* 42:253–268. [CrossRef Medline](#)
- Huguenard JR, Prince DA (1992) A novel T-type current underlies prolonged Ca^{2+} -dependent burst firing in GABAergic neurons of rat thalamic reticular nucleus. *J Neurosci* 12:3804–3817. [Medline](#)
- Ji D, Wilson MA (2007) Coordinated memory replay in the visual cortex and hippocampus during sleep. *Nat Neurosci* 10:100–107. [CrossRef Medline](#)
- Jokovic PM, Todorovic SM (2010) Isoflurane modulates neuronal excitability of the nucleus reticularis thalami in vitro. *Ann N Y Acad Sci* 1199:36–42. [CrossRef Medline](#)
- Jones EG (2001) The thalamic matrix and thalamocortical synchrony. *Trends Neurosci* 24:595–601. [CrossRef Medline](#)
- Jones E, Oliphant T, Peterson P (2001) SciPy: Open Source Scientific Tools for Python. Available at: <http://www.scipy.org>.
- Kopelman MD, Thomson AD, Guerrini I, Marshall EJ (2009) The Korsakoff syndrome: clinical aspects, psychology and treatment. *Alcohol* 44:148–154. [CrossRef Medline](#)
- Kronland-Martinet R, Morlet J, Grossmann A (1987) Analysis of sound patterns through wavelet transforms. *Int J Pattern Recogn* 1:273–302. [CrossRef](#)
- Kuki T, Ohshiro T, Ito S, Ji ZG, Fukazawa Y, Matsuzaka Y, Yawo H, Mushiaki H (2013) Frequency-dependent entrainment of neocortical slow oscillation to repeated optogenetic stimulation in the anesthetized rat. *Neurosci Res* 75:35–45. [CrossRef Medline](#)
- Le Bon-Jego M, Yuste R (2007) Persistently active, pacemaker-like neurons in neocortex. *Front Neurosci* 1:123–129. [CrossRef Medline](#)
- Lee J, Kim D, Shin HS (2004) Lack of δ waves and sleep disturbances during non-rapid eye movement sleep in mice lacking $\alpha 1G$ -subunit of T-type calcium channels. *Proc Natl Acad Sci U S A* 101:18195–18199. [CrossRef Medline](#)
- Llinás R, Jahnsen H (1982) Electrophysiology of mammalian thalamic neurons in vitro. *Nature* 297:406–408. [CrossRef Medline](#)
- Luczak A, Barthó P (2012) Consistent sequential activity across diverse forms of UP states under ketamine anesthesia. *Eur J Neurosci* 36:2830–2838. [CrossRef Medline](#)
- Marshall L, Helgadóttir H, Mölle M, Born J (2006) Boosting slow oscillations during sleep potentiates memory. *Nature* 444:610–613. [CrossRef Medline](#)
- Mölle M, Eschenko O, Gais S, Sara SJ, Born J (2009) The influence of learning on sleep slow oscillations and associated spindles and ripples in humans and rats. *Eur J Neurosci* 29:1071–1081. [CrossRef Medline](#)
- Morison R, Bassett D (1945) Electrical activity of the thalamus and basal ganglia in decorticate cats. *J Neurophysiol* 309–314.
- Nir Y, Staba RJ, Andrillon T, Vyazovskiy VV, Cirelli C, Fried I, Tononi G (2011) Regional slow waves and spindles in human sleep. *Neuron* 70:153–169. [CrossRef Medline](#)
- Parnaudeau S, O’Neill PK, Bolkan SS, Ward RD, Abbas AI, Roth BL, Balsam PD, Gordon JA, Kellendonk C (2013) Inhibition of mediodorsal thalamus disrupts thalamofrontal connectivity and cognition. *Neuron* 77:1151–1162. [CrossRef Medline](#)
- Paxinos G, Watson C (2007) The rat brain in stereotaxic coordinates. San Diego: Academic.
- Petersen CC, Hahn TT, Mehta M, Grinvald A, Sakmann B (2003) Interaction of sensory responses with spontaneous depolarization in layer 2/3 barrel cortex. *Proc Natl Acad Sci U S A* 100:13638–13643. [CrossRef Medline](#)
- Poulet JF, Fernandez LM, Crochet S, Petersen CC (2012) Thalamic control of cortical states. *Nat Neurosci* 15:370–372. [CrossRef Medline](#)
- Roux SG, Cenier T, Garcia S, Litaudon P, Buonviso N (2007) A wavelet-based method for local phase extraction from a multi-frequency oscillatory signal. *J Neurosci Methods* 160:135–143. [CrossRef Medline](#)
- Sanchez-Vives MV, McCormick DA (2000) Cellular and network mechanisms of rhythmic recurrent activity in neocortex. *Nat Neurosci* 3:1027–1034. [CrossRef Medline](#)
- Schmahmann JD (2003) Vascular syndromes of the thalamus. *Stroke* 34:2264–2278. [CrossRef Medline](#)
- Shipe WD, Barrow JC, Yang ZQ, Lindsley CW, Yang FV, Schlegel KA, Shu Y, Rittle KE, Bock MG, Hartman GD, Tang C, Ballard JE, Kuo Y, Adarayan

- ED, Prueksaritanont T, Zrada MM, Uebele VN, Nuss CE, Connolly TM, Doran SM, et al. (2008) Design, synthesis, and evaluation of a novel 4-aminomethyl-4-fluoropiperidine as a T-type Ca^{2+} channel antagonist. *J Med Chem* 51:3692–3695. [CrossRef Medline](#)
- Shu Y, Hasenstaub A, McCormick DA (2003) Turning on and off recurrent balanced cortical activity. *Nature* 423:288–293. [CrossRef Medline](#)
- Sirota A, Buzsáki G (2005) Interaction between neocortical and hippocampal networks via slow oscillations. *Thalamus Relat Syst* 3:245–259. [CrossRef Medline](#)
- Slézia A, Hangya B, Ulbert I, Acsády L (2011) Phase advancement and nucleus-specific timing of thalamocortical activity during slow cortical oscillation. *J Neurosci* 31:607–617. [CrossRef Medline](#)
- Steriade M (1997) Synchronized activities of coupled oscillators in the cerebral cortex and thalamus at different levels of vigilance. *Cereb Cortex* 7:583–604. [CrossRef Medline](#)
- Steriade M, Deschênes M, Domich L, Mulle C (1985) Abolition of spindle oscillations in thalamic neurons disconnected from nucleus reticularis thalami. *J Neurophysiol* 54:1473–1497. [Medline](#)
- Steriade M, Nuñez A, Amzica F (1993a) A novel slow (< 1 Hz) oscillation of neocortical neurons in vivo: depolarizing and hyperpolarizing components. *J Neurosci* 13:3252–3265. [Medline](#)
- Steriade M, Nuñez A, Amzica F (1993b) Intracellular analysis of relations between the slow (< 1 Hz) neocortical oscillation and other sleep rhythms of the electroencephalogram. *J Neurosci* 13:3266–3283. [Medline](#)
- Stroh A, Adelsberger H, Groh A, Rühlmann C, Fischer S, Schierloh A, Deisseroth K, Konnerth A (2013) Making waves: initiation and propagation of corticothalamic Ca^{2+} waves in vivo. *Neuron* 77:1136–1150. [CrossRef Medline](#)
- Timofeev I, Grenier F, Bazhenov M, Sejnowski TJ, Steriade M (2000) Origin of slow cortical oscillations in deafferented cortical slabs. *Cereb Cortex* 10:1185–1199. [CrossRef Medline](#)
- Tononi G, Cirelli C (2001) Some considerations on sleep and neural plasticity. *Arch Ital Biol* 139:221–241. [Medline](#)
- Uebele VN, Nuss CE, Fox SV, Garson SL, Cristescu R, Doran SM, Kraus RL, Santarelli VP, Li Y, Barrow JC, Yang ZQ, Schlegel KA, Rittle KE, Reger TS, Bednar RA, Lemaire W, Mullen FA, Ballard JE, Tang C, Dai G, et al. (2009) Positive allosteric interaction of structurally diverse T-type calcium channel antagonists. *Cell Biochem Biophys* 55:81–93. [CrossRef Medline](#)
- Ushimaru M, Ueta Y, Kawaguchi Y (2012) Differentiated participation of thalamocortical subnetworks in slow/spindle waves and desynchronization. *J Neurosci* 32:1730–1746. [CrossRef Medline](#)
- Vyazovskiy VV, Olcese U, Hanlon EC, Nir Y, Cirelli C, Tononi G (2011) Local sleep in awake rats. *Nature* 472:443–447. [CrossRef Medline](#)
- Wester JC, Contreras D (2013) Generating waves in corticothalamic networks. *Neuron* 77:995–997. [CrossRef Medline](#)

Rhythmic 1-5 Hz firing of pulvinar neurons in behaving monkeys

Abstract

The pulvinar nucleus of thalamus is one of the most enigmatic structures of the primate brain. Due to its widespread connectivity with cortex it has been hypothesized to act as a hub contributing to synchronization of cortical areas. In the dorsal and ventral pulvinar of macaque monkeys performing a detection task, we found strong rhythmic firing of single neurons in the delta frequency range (1 to 5 Hz) in ~20 % of the recorded units ($n=198$), but not in other frequency bands except one cell in the alpha range (~10 Hz). The units with rhythmic spike trains showed only weak visual responses and decreased their firing rate with motor action. Due to their strong connectivity with cortex, it is likely that the rhythm present in pulvinar neurons contributes to the generation of low-frequency rhythms in cortex, which were shown to be modulated by cognitive processes such as attentional state and hypothesized to affect interareal communication.

The chapter is a manuscript in preparation with co-authors Melanie Wilke, David A. Leopold and Michael Schmid. J.T.S. analyzed data and wrote the manuscript.

Introduction

One of the hallmark features of thalamocortical cells is that they can operate in two membrane potential-dependent modes: high-fidelity, tonic firing at depolarized levels, or bursty, rhythmic firing in the delta frequency range (1 to 5 Hz) at hyperpolarized states (Jahnsen and Llinás, 1984b,a; Deschenes et al., 1982; Llinás and Steriade, 2006, for a review). It is now well-established that the underlying mechanism mediating these modes is the interplay of the hyperpolarization-activated I_h and T-type Ca^{2+} transmembrane currents (McCormick and Pape, 1990; Llinás and Steriade, 2006), which leads to a rhythmic oscillation of the membrane potential and associated firing.

Despite some controversy on the presence of burst firing in relay nuclei (first order nuclei) of awake behaving animals (Swadlow and Gusev, 2001; Sherman, 2001; Steriade, 2001a), the two thalamic firing modes have been assigned to different states of vigilance: irregular firing during the awake behaving state and rhythmic firing during states of sleep and drowsiness (Llinás and Steriade, 2006). However, only few studies investigated the extent of rhythmic burst firing in thalamic nuclei that do not receive input from the sensory periphery (higher-order nuclei). Two studies using extracellular recordings did find rhythmic firing in the medio-dorsal and pulvinar nuclei of awake behaving monkeys (Fuster and Alexander, 1973; Ramcharan et al., 2005), which also have a higher density of burst-mediating T-type Ca^{2+} channels (Wei et al., 2011) leading to stronger burst propensity. However, a study using intracellular hyperpolarizing current pulses failed to elicit burst firing in the lateral posterior-pulvinar complex of conscious cats (Woody et al., 2003).

Here, we provide evidence for a substantial amount of rhythmic burst firing (~20 %) in the pulvinar nucleus of macaque monkeys during a detection task involving the maintenance of fixation and performing motor actions as a response to visual task events. The neurons exhibiting rhythmic firing responded only weakly to visual stimulation and decreased their discharge rates with motor behavior.

Materials and Methods

Subjects. Two healthy adult female rhesus monkeys (*Macaca mulatta*, Monkey B and Monkey E) were used in this study. All experimental procedures were performed in accordance with the Institute for Laboratory Animal Research Guide for the Care and Use of Laboratory Animals and approved by the Animal Care and Use Committee of the National Institute of Mental Health.

Behavioral Task. As described in Wilke et al. (2009). Briefly, monkeys fixated (0.7° radius) on a blue central fixation spot on a dark screen and reported the appearance of a target stimulus by pulling a lever. Target stimuli were presented mono- or binocularly in the parafoveal visual field (eccentricity 0.4 to 7.7°, size 0.3 to 6°) after 1.5 s of fixation for 2 s. Later in the trial, monkeys had to release the lever if the target disappeared physically or perceptually (Wilke et al., 2009); this part of the trial was not considered here.

Data acquisition. Data were acquired as described in Wilke et al. (2009) in 78 recording sessions (48 and 30 for monkey B and E, respectively) using 4 to 8 microelectrodes (Thomas Recording GmbH) that were lowered into the visual thalamus on a daily basis. Unit activity and local field potential were collected using the MAP recording system (Plexon Inc.). Spikes were detected by manually setting a threshold above background

activity and sorted offline (Offline Sorter, Plexon Inc.). If not otherwise noted, single- and multi-unit activity were pooled together. Electrodes were positioned in ventral (vPUL, ventral of brachium of superior colliculus, bsc) and dorsal (dPUL, dorsal of bsc) portions of pulvinar and in the lateral geniculate nucleus (LGN) based on anatomical MRI scans and electrode drive coordinates (see Wilke et al., 2009, for details).

Data analysis. All data were analyzed in MATLAB (Mathworks Inc., R2011b) using custom-written routines and the Fieldtrip toolbox (Oostenveld et al., 2011).

Firing rates were determined by convolution of the spike trains with a Gaussian kernel (SD 50 ms). To compare responses of neurons with different baseline firing rates, firing rates were z-scored based on the 1.5 s fixation period.

Autocorrelation histograms (ACHs) of the spike trains were calculated by counting the inter-spike intervals between all spikes up to a lag of 1.35 s in 1 ms bins and normalized to the total number of spike time differences (Fieldtrip function `ft_spike_xcor`). Data from all periods of each trial were used. For visualization, ACHs were smoothed with a Gaussian kernel (SD 50 ms).

Rhythmicity of spike trains was quantified by calculating a score value based on the power spectrum of the ACH, similar to Mureşan et al. (2008): After removal of offset and linear trend, the part of the ACHs from 0.1 to 1.35 s was spectrally decomposed with a hanning-tapered Fourier transform (zero padding to 3 s leading to a frequency resolution of 1/3 Hz). The power spectrum was then determined as the absolute value of the complex Fourier coefficients and normalized by the average power across all frequencies. The maximum peak power value in the frequency range 1 to 50 Hz was then used as the rhythmicity score.

To assess significance of the rhythmicity scores we compared them to scores based on an inhomogeneous Poisson process. For each unit, we generated 1000 random data sets from an inhomogeneous Poisson process with the same firing rate profile and number of trials as the unit. This yielded 1000 random rhythmicity scores. The ratio of randomly generated score values larger than the actual value is given as *p*-value for each unit's score, indicating the probability of being explained purely by Poissonian firing.

Results

Delta rhythm in pulvinar spike trains of awake monkeys

We recorded spiking activity from 198 units in the pulvinar nucleus of thalamus in awake behaving monkeys and assessed the extent of rhythmicity in their spike trains. In a subset of units, we found very strong rhythmic burst firing apparent in single trial raster plots (Fig. 4.1A). In those units, the autocorrelation histograms (ACHs, Fig. 4.1B) showed periodic and strong side lobes indicating a rhythmic inter-dependency of inter-spike intervals. Other units displayed only weak (Fig. 4.1D-E, 4.1G middle row) or no periodicity (Fig. 4.1 bottom row) in their ACHs.

To quantify this spike train rhythm, we computed the power spectrum of the ACH (see Material and Methods; see Fig. 4.1C and F for examples and Fig. 4.2A for the average) and used the strongest peak of the ACH spectrum as a score for rhythmicity. In total, 36 of 198 (18.2%; monkey B: 31 of 151, 19.8%; monkey E: 6 of 47, 12.8%) units displayed supra-Poissonian rhythmicity ($p < 0.01$ compared to a rate-matched inhomogeneous Poisson process, see Materials and Methods).

4. RHYTHMIC 1-5 Hz FIRING OF PULVINAR IN BEHAVING MONKEYS

The frequency of the significantly rhythmic spike trains was limited to the delta range (1.3 to 5.7 Hz) with a mean frequency of 3.30 ± 0.43 Hz with one exception at 12.3 Hz. Fig. 4.2A shows the distribution of frequency and rhythmicity score. Units with rhythmic spiking were present in both dorsal and ventral parts of pulvinar (see Fig. 4.2B).

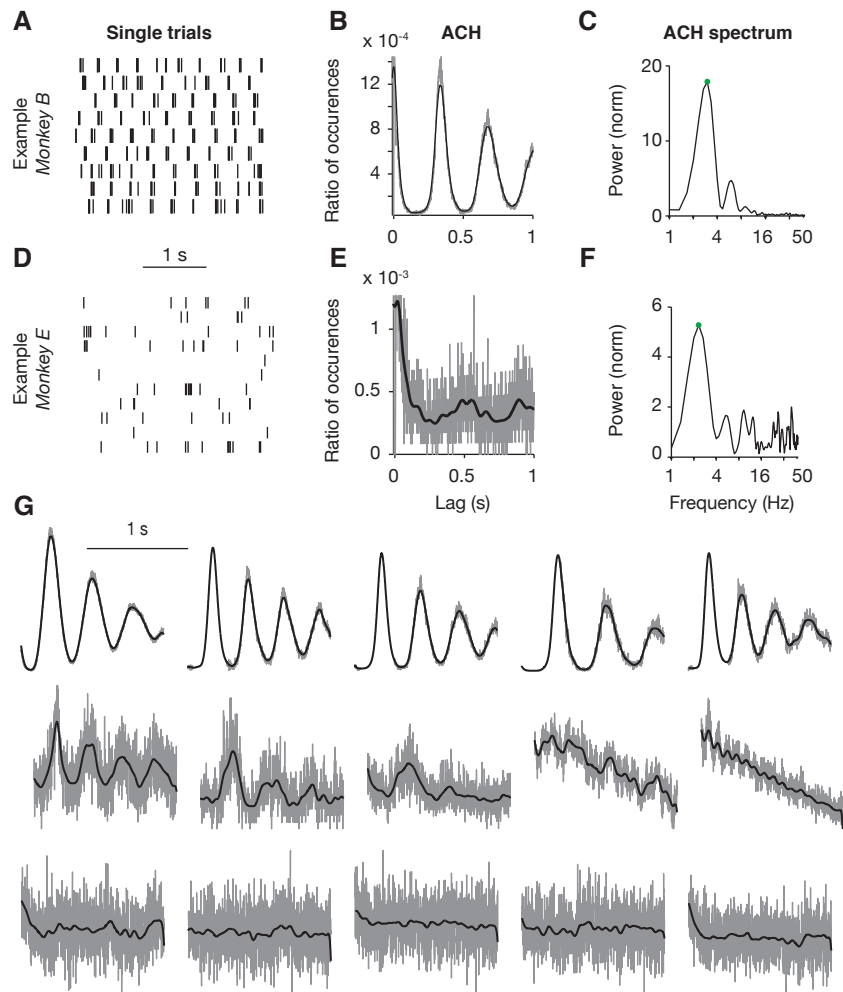


Figure 4.1 | Rhythmic firing of pulvinar neurons during awake behavior.

A-C, Example raster plot (**A**), autocorrelation histogram (ACH, **B**) and spectrum of the ACH for an example neuron from monkey B with very strong rhythmicity (score 17.9, peak frequency 3.0 Hz, $p < 10^{-3}$ compared with Poissonian firing). ACH was smoothed with Gaussian kernel (SD 50 ms) for visualization. Rhythmicity score was determined as the peak power in 1 to 50 Hz (green dot in **C**).

D-F, Same as **A-C** for an example neuron from monkey E with weak but significant rhythmicity (score 5.3, peak frequency 2.3 Hz, $p < 10^{-3}$ compared with Poissonian firing).

G, Example ACHs for strong (top row), weak (middle row) and absent rhythmicity (bottom row) in spike trains. ACHs are scaled to asymptote of ACH (lag > 50 ms).

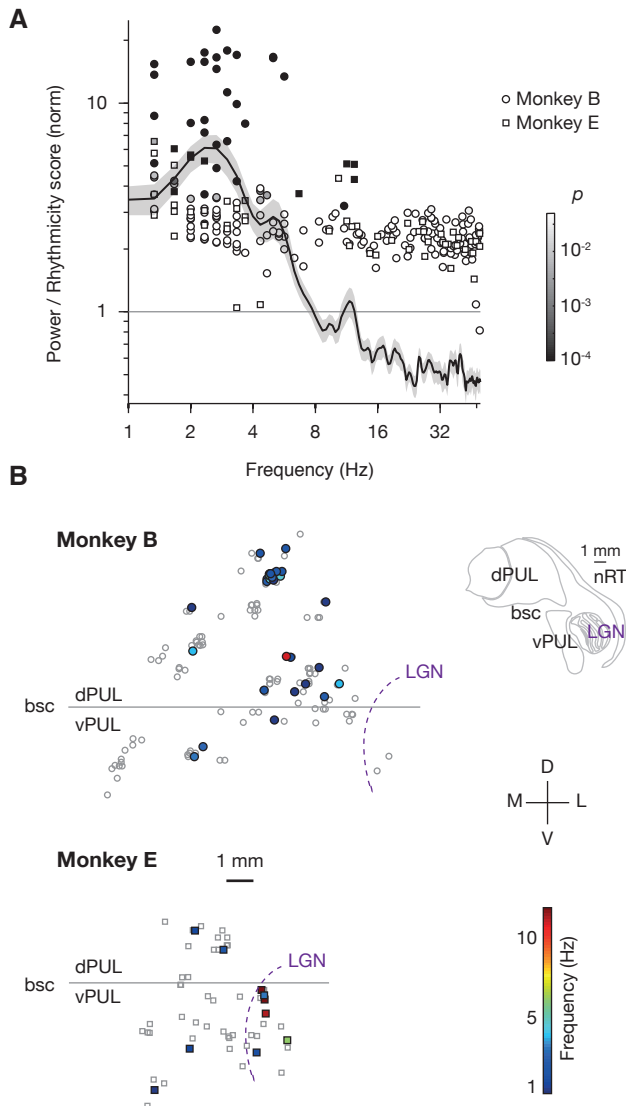
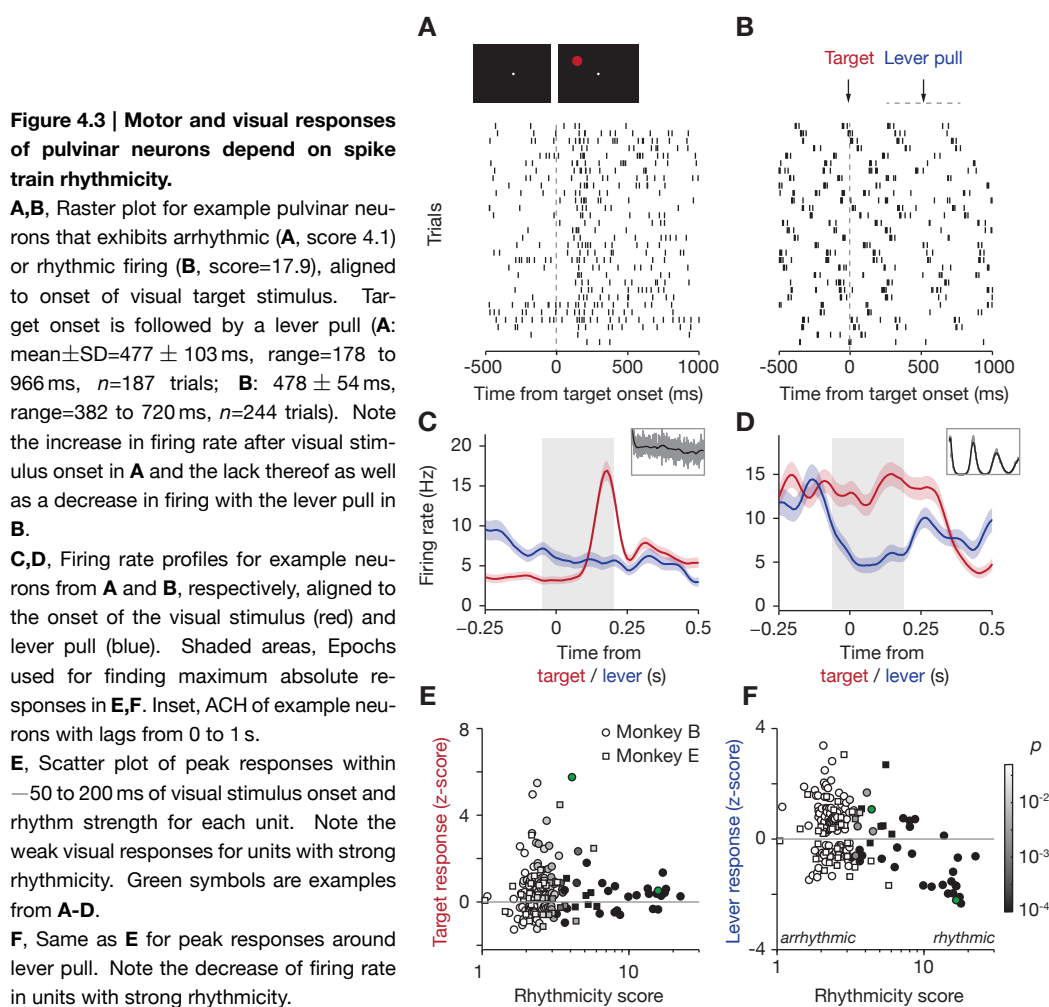


Figure 4.2 | Population overview of rhythmic firing in visual thalamus.

A, Rhythmicity scores with peak frequency for all units recorded in visual thalamus (pulvinar and LGN) ($n=248$ units) and average ACH power spectrum of units with significant spike train rhythms ($p < 0.01$ compared to Poissonian firing). Gray value of symbols indicates p -value compared with Poissonian firing.

B, Anatomical distribution of rhythmic ($p < 0.01$, filled, colored symbols, color indicates peak frequency) and arrhythmic units (gray symbols) in a medio-lateral (ML) plane collapsed over the anterior-posterior (AP) axis. For visualization, a random jitter (uniform $250 \mu\text{m}$) was added orthogonally to electrode track. Inset, Schematic drawing of visual thalamus at AP=6, based on Saleem and Logothetis (2012). Abbreviations: bsc, brachium of superior colliculus; dPUL, dorsal pulvinar; vPUL, ventral pulvinar; nRT, nucleus reticularis thalami; LGN, lateral geniculate nucleus.



Pulvinar responses to visual stimuli and motor action depend on rhythmicity

The monkeys performed a target detection task that involved maintaining fixation on a dark screen, the onset of a visual target stimulus and responding to it with a lever pull (see Materials and Methods and Wilke et al., 2009, for details). The responses of the pulvinar neurons to these events depended on the degree of rhythmicity present in their spike trains (Fig. 4.3).

Pulvinar units with weak rhythmicity in their spike trains (Fig. 4.3A,C) could show very strong responses to the visual target stimulus (up to 6 SD from baseline firing rate). Those units that displayed rhythmic activity ($p < 0.01$ compared with rate-matched Poissonian firing) however did only show weak responses (0.60 ± 0.32 SD from baseline, $p = 0.043$, Wilcoxon signed rank test, $n = 36$) and a receptive field based on manual mapping procedures could not be determined.

In contrast, the units that exhibited rhythmic firing decreased their firing rate by up to 2.3 SD below baseline firing rates (Fig. 4.3B,D,E, mean = -0.30 ± 0.27 SD, $p = 0.032$, same units as before.). The decrease in firing rate around the lever pull was correlated with the strength of spike train rhythmicity ($R = -0.54$, $p = 7.3 \times 10^{-4}$).

Discussion

The results presented here demonstrate that a substantial subset of neurons located in both ventral and dorsal parts of macaque pulvinar are engaged in a delta rhythm (1 to 5 Hz) during awake behavior. These neurons showed only weak responses to visual stimuli, but drastic reductions in firing rate associated with motor behavior.

Only few studies on rhythmic burst patterns in higher-order thalamic nuclei exist. During sleep, silent and active states of pulvinar were shown to be synchronous with cortical slow waves (Thieffry et al., 1977) indicating that the classical rhythmic bursting of thalamic neurons during sleep is present in pulvinar as well. For the awake state however, only one previous study reported bursting in 9 of the 15 (60 %) sampled pulvinar neurons displayed a 3 Hz rhythm in their spike pattern (Ramcharan et al., 2005) as quantified by visual inspection of the autocorrelation histogram. Based on a much larger sample size ($n=198$ neurons) and compared to rate-matched Poissonian spike trains we here report that ~20 % of the pulvinar neurons have rhythmic spike trains. Although this number is below the previous finding, it is still a substantial amount, especially when compared to relay nuclei, in which virtually no rhythmic bursting exists during waking (Swadlow and Gusev, 2001; Steriade, 2001a; Ruiz et al., 2006). A possible explanation is the increased expression of T-type calcium channels in pulvinar neurons compared to geniculate neurons (Wei et al., 2011) as it is known that bursting of thalamocortical neurons is mediated by the interplay of the T calcium (I_t) and hyperpolarization-activated currents (I_h) (Llinás and Steriade, 2006).

On a functional level, it is possible that the rhythmic sleep-like patterns observed in pulvinar are merely a reflection of decreased arousal (Vyazovskiy et al., 2011; Nir et al., 2011) as the well-trained monkeys could perform the detection task nearly effortlessly. The cessation of rhythmic bursting with the lever pull could then be interpreted as a change of awareness state since the monkeys had to perform a (possibly conscious) motor action. On the other hand, since delta rhythms (<5 Hz) can be observed in cortex (Bosman et al., 2012; Sachdev et al., 2015; Bastos et al., 2015), are modulated by attentional demands, and co-modulate higher rhythms associated with activated states (Bosman et al., 2012), it's conceivable that the pulvinar rhythm is influencing cortical processing. A direct test could involve the selective block of T-type calcium currents in pulvinar and observing the effects on cortical rhythms, sensory processing and ultimately behavior.

Part III

Contribution of primary visual cortex to extrastriate beta rhythms

CHAPTER **5**

**Motion-sensitive responses in visual
area V4 in the absence of primary
visual cortex**

Erklärung zu den Autorenanteilen

an der Publikation: Motion-sensitive responses in visual area V4 in the absence of V1

Status: in press

Name der Zeitschrift: The Journal of Neuroscience

Beteiligte Autoren:

- | | |
|--|-----------------------------|
| - Michael C. Schmid (MCS) | - Richard C. Saunders (RCS) |
| - Joscha T. Schmiedt (Promovierender) | - Alexander Maier (AM) |
| - Andrew J. Peters (AJP) | - David A. Leopold (DAL) |

Was hat der/die Promovierende bzw. was haben die Co-Autoren/Autorinnen beigetragen?

(1) zu Entwicklung und Planung

MCS 60%, AM 10%, DAL 30%

(2) zur Durchführung der einzelnen Untersuchungen und Experimente

MCS: Aufnahme der Daten (85%)

DAL: Durchführung der OPs (5%)

RCS: Durchführung der OPs (5%)

AJP: Aufnahme der Daten (5%)

(3) zur Erstellung der Datensammlung und Abbildungen

Promovierender: Erstellung aller Abbildungen (80%)

DAL: Aufbau des Setups (5%)

MCS: Aufbau des Setups (15%)

(4) zur Analyse und Interpretation der Daten

Promovierender: Analyse und Interpretation aller Daten (90%)

MCS: Vorläufige Datenanalysen und Interpretation aller Daten (10%)

(5) zur Verfassung des Manuskripts

Promovierender 45%:

MCS 45%

DAL 10%

Motion-Sensitive Responses in Visual Area V4 in the Absence of Primary Visual Cortex

Michael C. Schmid,^{1*} Joscha T. Schmiedt,^{1*} Andrew J. Peters,² Richard C. Saunders,⁴ Alexander Maier,³ and David A. Leopold^{4,5}

¹Ernst Strüngmann Institute for Neuroscience in cooperation with Max Planck Society, 60528 Frankfurt, Germany, ²University of California San Diego, La Jolla, California 92093-0634, ³Vanderbilt University, Department of Psychology, Nashville, Tennessee 37240, ⁴Laboratory of Neuropsychology, National Institute of Mental Health, Bethesda, Maryland 20892, and ⁵Neurophysiology Imaging Facility, National Institute of Mental Health, National Institute of Neurological Disorders and Stroke, and National Eye Institute, Bethesda, Maryland 20892

Neurons in cortical ventral-stream area V4 are thought to contribute to important aspects of visual processing by integrating information from primary visual cortex (V1). However, how V4 neurons respond to visual stimulation after V1 injury remains unclear: While electrophysiological investigation of V4 neurons during reversible V1 inactivation suggests that virtually all responses are eliminated (Girard et al., 1991), fMRI in humans and monkeys with permanent lesions shows reliable V1-independent activity (Baseler et al., 1999; Goebel et al., 2001; Schmid et al., 2010). To resolve this apparent discrepancy, we longitudinally assessed neuronal functions of macaque area V4 using chronically implanted electrode arrays before and after creating a permanent aspiration lesion in V1. During the month after lesioning, we observed weak yet significant spiking activity in response to stimuli presented to the lesion-affected part of the visual field. These V1-independent responses showed sensitivity for motion and likely reflect the effect of V1-bypassing geniculate input into extrastriate areas.

Introduction

The visual system is thought to operate via serially and hierarchically organized processes (Felleman and van Essen, 1991) where damage to earlier stages leads to loss of function in later stages. However, at the level of primary visual cortex (V1), lesions do not abolish all visual function: Humans and nonhuman primates can retain residual vision in the form of “blindsight” (Cowey, 2010), a term that was coined to describe the ability to detect and respond to visual stimuli in the absence of conscious visual experience. Research over the past years has established that activity in higher cortical areas, most prominently in motion-sensitive area V5/MT, is correlated with blindsight (Rodman et al., 1989; Zeki and Ffytche, 1998; Baseler et al., 1999; Goebel et al., 2001; Azzopardi et al., 2003; Schmid et al., 2010). However, the extent to which ventral stream cortex retains responsiveness without V1 input remains controversial. Here we address this question at the

level of V4, an area thought to be primarily important for shape and object processing (Roe et al., 2012). Previous assessment of neuronal activity during temporary V1 cooling under anesthetized conditions concluded that V4 is entirely dependent on V1 input (Girard et al., 1991). However, this finding is in apparent conflict with reports of reliable fMRI responses in V4 of awake monkeys and humans with chronic V1 lesions (Baseler et al., 1999; Goebel et al., 2001; Schmid et al., 2010). These V1-independent fMRI responses were shown to depend on the lateral geniculate nucleus (LGN) of the thalamus (Schmid et al., 2010) and thus most likely rely on a geniculo-extrastriate pathway (Rodman et al., 2001; Sincich et al., 2004) that draws its input from the superior colliculus (Harting et al., 1991). To resolve the apparent conflict between electrophysiology and fMRI and to control for some of the methodological differences that may have contributed to these discrepant findings, we chose an approach in which we longitudinally recorded the multiunit spiking activity (MUA) in behaving monkeys before and after permanently lesioning V1.

Materials and Methods

Subjects. Two healthy adult female rhesus monkeys (*Macaca mulatta*, Monkey B and Monkey F) with prior V1 lesions in the right hemisphere were used in the study. All procedures were in accordance with the Institute for Laboratory Animal Research Guide for the Care and Use of Laboratory Animals and approved by the Animal Care and Use Committee of the National Institute of Mental Health.

Surgical procedures. A large occipital bone flap over the left hemisphere was created to warrant access to areas V1 and V4. A chronic 10 × 10 “Utah” array of microelectrodes (Blackrock Microsystems) was subdurally inserted on the prelunate gyrus, ~2 mm dorsal of the lateral tip of the

Received Sept. 12, 2013; revised Oct. 15, 2013; accepted Oct. 19, 2013.

Author contributions: M.C.S., A.M., and D.A.L. designed research; M.C.S., A.J.P., R.C.S., A.M., and D.A.L. performed research; M.C.S. and J.T.S. analyzed data; M.C.S., J.T.S., and D.A.L. wrote the paper.

This work was supported by the Intramural Research Program of the National Institute of Mental Health (D.A.L.) and a Deutsche Forschungsgemeinschaft Emmy Noether grant (M.C.S.). The authors thank Alex Cummings, David Hu, Charles Zhu, Frank Ye, George Dold, Andy Mitz, Rachel Reoli, Katy Smith, and James Yu for technical assistance; Michele Cox for help with experiments and analysis; Georgios Spyropoulos for preliminary analysis; and Pascal Fries for support.

The authors declare no competing financial interests.

*M.C.S. and J.T.S. contributed equally to this work.

Correspondence should be addressed to Dr. Michael C. Schmid, Ernst Strüngmann Institute for Neuroscience in cooperation with Max Planck Society, Deutschordenstrasse 46, 60528 Frankfurt, Germany. E-mail: michael.schmid@esi-frankfurt.de.

DOI:10.1523/JNEUROSCI.3923-13.2013

Copyright © 2013 the authors 0270-6474/13/3318740-06\$15.00/0

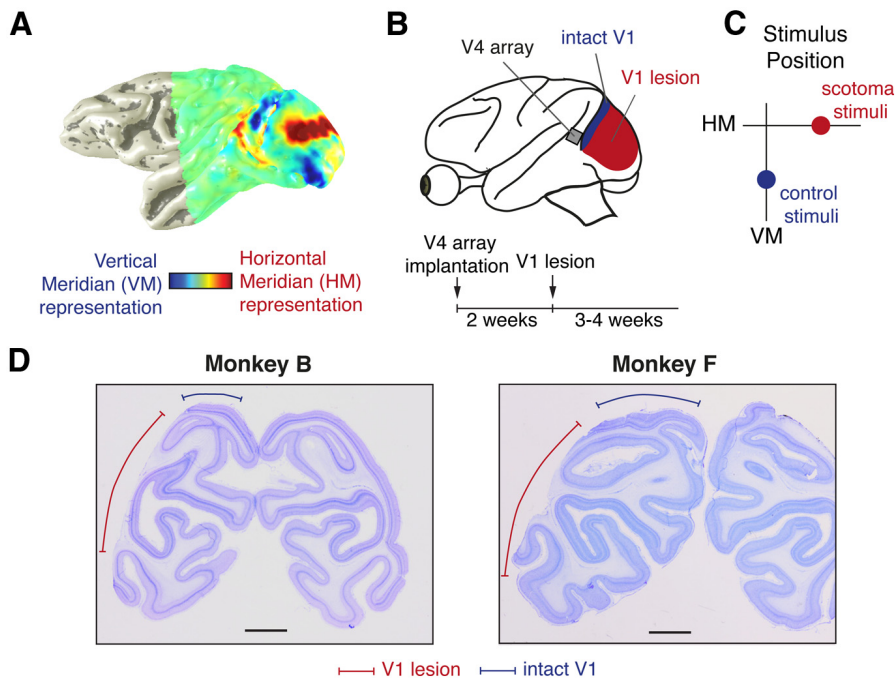


Figure 1. Longitudinal investigation of V4 neuronal responses before and after V1 lesion. **A**, fMRI-based retinotopic map of visual cortex for Monkey B, acquired before lesioning V1 using alternating rotating checkerboard wedges. **B**, The lesion was targeted to eliminate the V1 representation of the right horizontal meridian between $\sim 2\text{--}7^\circ$ of visual eccentricities (red) while leaving lower vertical meridian representation intact (blue). **C**, Stimuli close to the right horizontal meridian inside the lesion-affected visual space are labeled “scotoma stimuli” and stimuli close to the vertical meridian are labeled “control stimuli.” **D**, Coronal section of V1 for Monkey B (left) and F (right). Scale bars, 5 mm.

inferior occipital sulcus. Each microelectrode was 1.5 mm long with a tip radius ranging from 3 to 5 μm , and an interelectrode spacing of 400 μm . After array implantation, dura and bone flap were sutured back in place and covered with the skin. In a subsequent surgery, following the first period of recordings, V1 was lesioned using procedures as described previously (Schmid et al., 2010).

Behavioral task and visual stimulation. Eye movements were monitored either using the scleral search coil technique or via infrared-based tracking of the pupil. To delineate the outline of the visual deficit (“scotoma”) in the part of the visual field containing the V4-receptive fields, monkeys were trained on a simple perimetry task before lesioning. To this end, monkeys learned to initially fixate a small centrally placed dot (0.4° diameter). If the monkeys maintained fixation for 500 ms within maximally $1.5\text{--}2^\circ$ diameter of the fixation spot, a second dot (0.4° diameter) was presented in addition to the fixation spot for 1000–2000 ms in one of 10×10 possible target positions of a virtual grid in the lower right visual field quadrant (-1° to 9° , grid resolution 1°). To receive reward, monkeys had to execute a single saccade and acquire fixation for 500 ms within a new fixation window of 2° diameter around the target.

To probe for visually elicited neuronal responses, monkeys were trained to maintain passive fixation within $1.5\text{--}2^\circ$ diameter of a fixation spot while the various visual stimuli were displayed on the screen. Visual stimuli were generated using OpenGL-based custom written software (ESS/STIM, courtesy of Dr. D. Sheinberg, Brown University) running on industrial PCs (Kontron) with NVIDIA Quadro FX 3000 graphics boards. Stimuli were presented with a screen refresh rate of 60 Hz on a single LCD Samsung monitor (height 40 cm, width 65 cm) positioned at a viewing distance of 100 cm. All stimuli were presented for 500 ms on a dark gray background. Typical stimulus presentations per session were between 1000 and 1300.

For receptive field mapping, random dot kinematographs with a diameter of $1\text{--}1.5^\circ$ were presented at pseudo-randomly selected stimulus locations on an 8×8 virtual grid in the lower right visual field quadrant ($0^\circ\text{--}7^\circ$, grid resolution 1°). The direction of dot movement (upward or downward) was randomly varied on a trial-by-trial basis while the mo-

tion strength was kept constant at 100% dot coherence. Individual dots were white and moved with a speed of $6^\circ/\text{s}$.

Grating stimuli had a diameter of 1° or 1.5° and were displayed at either one of the following positions: $(0^\circ, -3.5^\circ)$, $(3^\circ, -3^\circ)$, $(3.5^\circ, 0^\circ)$. The first and the last of these positions were used as control and scotoma stimulus in this study, respectively. The gratings were either static or slowly drifting at 0.3 or $0.5^\circ/\text{s}$ and varied with respect to spatial frequency ($0.7\text{--}10^\circ/\text{s}$), orientation ($0^\circ, 90^\circ, 180^\circ, 270^\circ$ with two of these orientations resulting in equal stimuli for static gratings), and luminance contrast (low vs high, only high contrast considered here).

For the assessment of directional motion tuning, random dot kinematographs with four randomly selected directions of motion ($0^\circ, 90^\circ, 180^\circ, 270^\circ$) were presented at the same stimulus positions as the gratings described above. They varied with respect to coherence (10%, 50%, or 100%, only 100% considered here) and color (red, green, blue, or yellow, all considered here). Speed and size were the same as for the receptive field mapping.

Neurophysiological recordings. Electrical reference was a wire located subdurally over the parietal cortex. We recorded from a random selection of 64 channels of the 96 channels available from the array. Electrode impedances ranged between 150 and $1\text{ M}\Omega$ at 1 kHz. Extracellular voltages were amplified, filtered between 0.1 Hz and 12 kHz, and digitized at 24,414.1 Hz using a 64-channel RZ2 recording system (Tucker Davis Technologies).

Data analysis. All data were analyzed with the MATLAB (R2011a, MathWorks) toolbox FieldTrip (Oostenveld et al., 2011) and custom-written scripts. To obtain an estimate of MUA, the field potential was bandpass-filtered between 300 Hz and 12 kHz, rectified, low-pass filtered at 120 Hz with a fourth order zero-phase Butterworth filter, and downsampled to 256 Hz, yielding a quasi-continuous measure of high-frequency field power. Data from each trial were then normalized to their respective 250 ms prestimulus period and expressed as percentage change from baseline throughout the paper. Data were pooled across sessions, except for the direction of motion analysis. Responses were estimated by averaging the normalized MUA signal between 50 and 500 ms. For presentation purposes, the MUA time courses were smoothed by convolution with a Gaussian kernel of 125 ms SD. The array receptive field (RF) was determined by averaging the individual receptive fields of all visually responsive electrodes and interpolating to a resolution of 0.5° . Tuning for direction of motion was assessed by comparing the average responses of the preferred feature (i.e., the one resulting in strongest response) to the nonpreferred feature (i.e., with minimal response). Tuning strength is quantified with a tuning index d' as follows:

$$d' = \frac{\text{MUA}_{\text{PF}} - \text{MUA}_{\text{nonPF}}}{\hat{\sigma}}$$

where $\hat{\sigma} = \sqrt{(\sigma_{\text{PF}}^2 + \sigma_{\text{nonPF}}^2)/2}$ is the pooled SD of the two response distributions. Significance was assessed by comparing actual d' values against a surrogate distribution obtained by randomly shuffling trial labels 10,000 times.

Results

To delineate the effect of permanent V1 lesions on electrophysiological responses in macaque ventral-stream visual cortex, we longitudinally monitored V4 MUA during the presentation of various spatially restricted stimuli over a period of several weeks

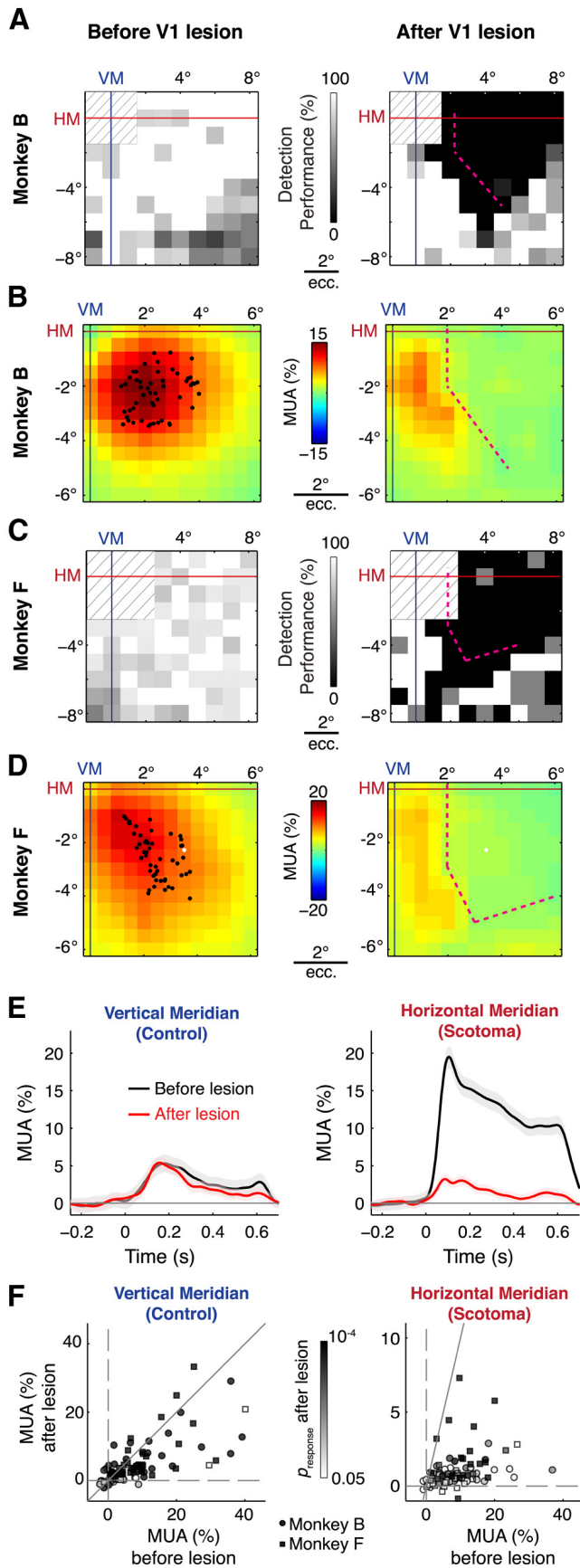


Figure 2. V4 responses to scotoma stimuli are severely degraded but not abolished. **A**, Detection performance of Monkey B in a perimetry task at various stimulus positions in the lower right visual field during the week before (left, $n = 532$ trials from 2 sessions) and after (right, $n = 705$ trials from 3 sessions) the V1 lesion. Dashed magenta line indicates scotoma

using chronically implanted multielectrode arrays (Fig. 1). Following detailed presurgical retinotopic mapping by fMRI (Fig. 1A), we first implanted electrode arrays into area V4 at a position where the average receptive field of neurons was centered at $\sim 3^\circ$ of eccentricity. After ~ 2 weeks of initial electrophysiological assessment with V1 intact, we carried out permanent V1 lesions by aspirating V1's gray matter from the representation of the fovea laterally up to $\sim 7^\circ$ medially, straddling most of the upper and lower visual field representations around the horizontal meridian (Fig. 1B). Importantly, however, a section of approximately 5 mm near the lunate sulcus representing the visual vertical meridian (including the boundary to area V2) was not aspirated to allow for control conditions with V1 intact (Fig. 1B,C). For the experiments described below, this enabled us to compare neuronal responses with V1 intact versus V1 lesioned, regardless of the time point of assessment (Fig. 1C). Postmortem histological assessment of the brains of both monkeys confirmed complete loss of gray matter in the lesioned area of V1 and the preservation of the region of cortex that served as a control in the experiments (Fig. 1D).

Behavioral performance

During the week after the lesion, we assessed the animals' behavioral ability to detect visual stimuli and recorded V4 spiking responses to visual stimuli presented at different positions in the visual field. As expected, the V1 lesion resulted in a circumscribed scotoma: there was a severe deficit in detecting visual stimuli in a zone surrounding the horizontal meridian, whereas vision at the vertical meridian remained largely intact (Fig. 2A, C).

Spatial organization of V4 responses with respect to scotoma

We next assessed the effects of the V1 lesion on the large-scale visuotopic RF organization of the sampled V4 population by presenting stimuli at various locations in the lower right visual field. The longitudinal design of our study allowed for a direct comparison of the RFs from precisely the same cortical location before and after the lesion. In both monkeys, the array RF (i.e., the average RF across all visually responsive electrodes) showed a strong reduction in response amplitude for stimuli around the horizontal meridian that closely matched the behavioral scotoma (compare Fig. 2A, C with Fig. 2B, D, respectively), whereas the responses close to the vertical meridian remained mostly intact. On average, MUA responses to stimuli presented near the horizontal meridian were reduced from $8 \pm 1.0\%$ before the lesion to $0.70 \pm 0.076\%$ after the lesioning Monkey B ($n = 53$ electrodes, $p < 10^{-9}$, Wilcoxon signed rank

border estimate. **B**, V4 MUA array RF of Monkey B before (left, $n = 3524$ trials from $n = 5$ sessions) and after (right, $n = 4882$ trials from $n = 7$ sessions) V1 lesion ($n = 53$ electrodes). Black dots indicate RF centers of individual electrodes. **C**, Detection performance as in **A** for Monkey F before ($n = 1344$ trials from 3 sessions) and after V1 lesion ($n = 206$ trials from 1 session). **D**, V4 array RF as in **B** for Monkey F ($n = 47$ electrodes, $n = 2193$ and 4530 trials from $n = 3$ and 6 sessions from before and after V1 lesion, respectively). White dot indicates RF center of example electrode shown in **E**. **E**, MUA response from example electrode with large RF coverage in Monkey F to stimuli close to vertical meridian (left, $x = 0$ to 1° , $y = -3$ to -4°) and horizontal meridian (right, $x = 3$ to 4° , $y = -2$ to 0°) before and after V1 lesion. Shading indicates SEM. **F**, Distribution of MUA responses to stimuli close to vertical meridian (left) and horizontal meridian (right). Each dot indicates the average MUA response of a recording site before and after V1 lesion. Color shading indicates p value of postlesion responses (Wilcoxon signed rank test compared with prestimulus period). Solid gray lines indicate identical prelesion and postlesion responses. ecc., Eccentricity.

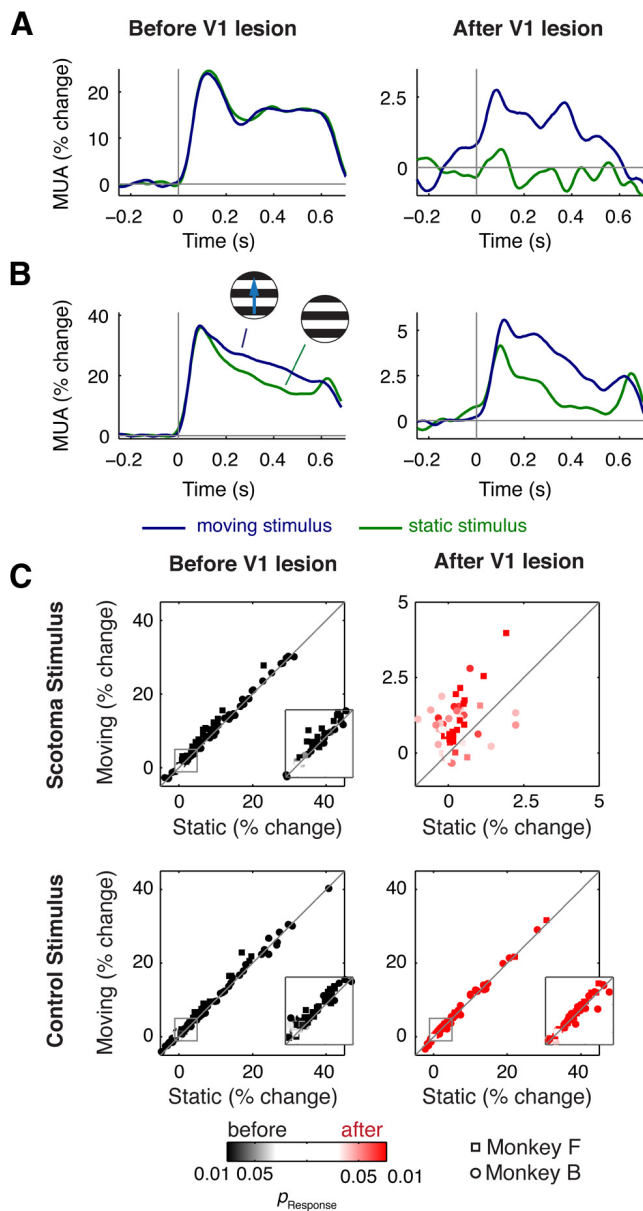


Figure 3. V4 MUA responses to scotoma stimuli show sensitivity for motion. **A, B**, Example MUA time courses for moving (blue) and static (green) gratings before (left) and after (right) V1 lesion from Monkey B (**A**) and Monkey F (**B**). **C**, Distribution of responses to moving and static gratings of all recording sites for scotoma (top row) and control (bottom row) stimuli. Each dot represents the average MUA response of a recording site, before the lesion (black symbols, left column; Monkey B: $n = 7$ sessions; Monkey F: $n = 4$ sessions) or after (red symbols, right column; Monkey B: $n = 3$ sessions, 5–9 d after lesion; Monkey F: $n = 5$ sessions, 9–18 d after lesion). Insets, Magnified view of the gray box.

test) and from $8.4 \pm 0.87\%$ before lesioning to $1.1 \pm 0.23\%$ after lesioning in Monkey F ($n = 47$ electrodes, $p < 10^{-8}$). Despite these greatly reduced activity levels in V1 after the V1 lesion, several sites continued to show significant MUA responses to visual stimuli presented to the scotoma (e.g., see Fig. 2E): 26 of 43 and 33 of 46 electrodes in Monkey B and F, respectively, remained responsive to visual stimulation close to the horizontal meridian ($p < 0.05$, Wilcoxon signed rank test compared with baseline). In contrast, for stimuli close to the vertical meridian (the control region outside the scotoma), virtually all recording sites remained responsive (39 of 39 electrodes in Monkey B, 42 of 47 in Monkey F).

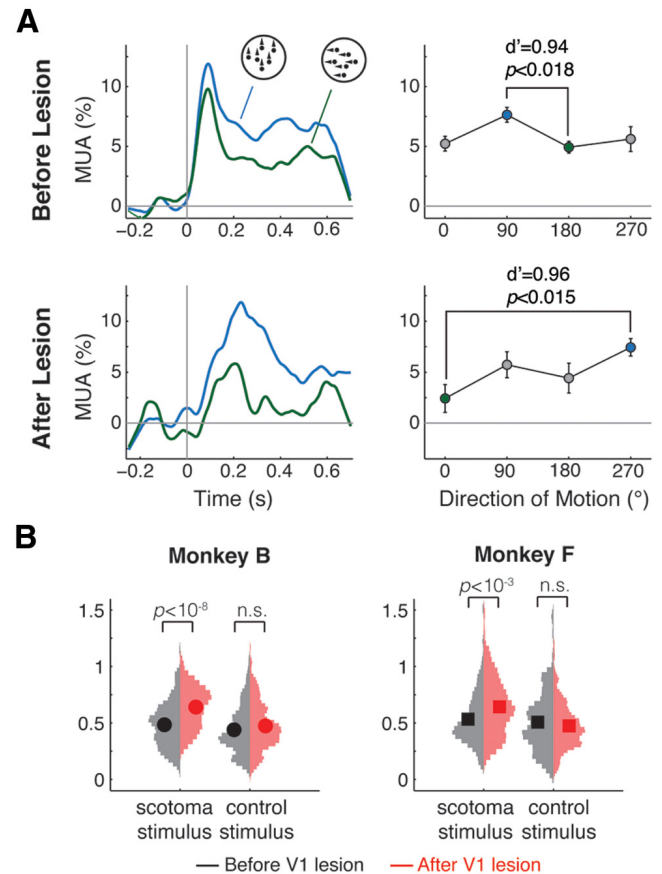


Figure 4. V1-independent tuning for direction of motion in V4. **A**, MUA time courses (left column) and tuning profile (right column) from example sessions before (top row) and after (bottom row) V1 lesion of Monkey F. Tuning is quantified by taking the d' value between the maximum (blue) and minimum (green) MUA response. Error bars indicate SEM. **B**, Smoothed histograms of d' values for direction of motion tuning from all responsive recording sites and sessions before (gray, Monkey B: $n = 5$ sessions, Monkey F: $n = 3$ sessions) and after (red, Monkey B: $n = 4$ sessions, Monkey F: $n = 11$ sessions) the V1 lesion for scotoma or control stimuli. Larger symbols indicate mean values. n.s. indicates a difference not significant at $p < 0.05$ (Mann–Whitney U test).

Motion sensitivity of residual neuronal responses to scotoma restricted stimuli

The residual responses to stimuli in the lesion-affected visual space demonstrate V1-independent transmission of visual information to area V4. To further characterize the nature of these responses with respect to the preserved motion detection that characterizes the phenomenon of blindsight after V1 injury (Zeki and Ffytche, 1998), we assessed the extent of neural motion sensitivity in our V4 sample. In a first step, we compared V4 responses to moving versus static gratings (Fig. 3). After the lesion, almost all of the recording sites with residual neuronal responses ($MUA > 0.05\%$ and $p < 0.05$ Wilcoxon signed rank test against prestimulus period) of both monkeys revealed a preference for moving gratings (Fig. 3C, top right; Monkey B: $p < 0.04$, $n = 11$ sites; Monkey F: $p < 0.0012$, $n = 18$ sites, Wilcoxon signed rank test), indicating a residual sensitivity of V1-deafferented V4 neurons for visual motion.

To test whether V4’s preference for moving stimuli after lesioning V1 includes directional tuning, we analyzed spiking responses to random dot patterns that coherently moved in one of four different directions of motion (Fig. 4). Before the V1 lesion, 16 of 190 (8.4%) and 11 of 106 (10.4%) recordings from responsive sites ($MUA > 1\%$ and $p < 0.05$, Wilcoxon signed rank test)

in Monkey B and Monkey F, respectively, showed significant ($p < 0.05$, trial label shuffling test, see Materials and Methods) tuning for direction of motion (Fig. 4A, top). Surprisingly, significant directional tuning could also be observed after V1 removal (Fig. 4A, bottom). Indeed, the number of significantly motion-tuned V4 sites increased, resulting in 19 of 81 (23.5%) and 30 of 129 (23.3%) significantly tuned recordings in Monkey B and Monkey F, respectively. To further quantify the tuning strength, we calculated d' between the multiunit responses of the preferred and the least preferred stimulus (Fig. 4A). In both monkeys, d' for motion direction increased after the V1 lesion (Fig. 4B, Mann–Whitney U test), yet only for the scotoma-directed stimuli and not for the control stimuli (Fig. 4B), thus highlighting the dependence on absent V1 input for this effect.

Discussion

Our results demonstrate visually driven V4 neuronal responses in the absence of V1 input, which are sensitive for stimulus motion. We discuss these findings in the context of V4's role in motion processing, the pathways that may contribute to V1-independent visual functions, and the implications for blindsight.

Motion processing in V4: dependence on V1 input and plasticity

V4 neurons have been implicated in a wide range of stimulus features, including orientation, color, shape, and motion (Roe et al., 2012). In our experiments, we have assessed motion sensitivity in V4 with and without V1 input. With respect to the strength of motion selectivity, our measures with V1 intact are at the lower end of the reported effects for V4 (Desimone and Schein, 1987; Ferrera et al., 1994; Tolias et al., 2005). However, as recent data from optical imaging suggest a modular organization of V4 with discrete patches of cortex dedicated to motion tuning (Li et al., 2013), it is conceivable that our electrode arrays may have undersampled these patches. Such a potential bias notwithstanding, we used a longitudinal recording approach, which permitted us to sample from the same cortical tissue at multiple time points before and after lesioning V1. We found increased directional selectivity in both the number of tuned electrode sites as well as in the d' values (Fig. 4B) when there was no input from V1 to V4. It is possible that this increased sensitivity is the result of local unmasking: the balance of neurons that are interconnected via inhibitory synapses but are tuned to different stimulus features due to diverse inputs might have shifted toward motion processing after the V1 lesion. As this plastic process may take some time to take effect, it could explain the differences between previous electrophysiological assessments of V4 activity during V1 cooling (Girard et al., 1991) and the ones by fMRI under chronic lesion conditions (Baseler et al., 1999; Goebel et al., 2001; Schmid et al., 2010).

V1-independent pathways to V4

The observation of V1-independent responses to visual stimuli in area V4 implies a subcortical pathway that bypasses V1 and relays information from the retina to visual association cortex. The superior colliculus, which receives direct retinal input and whose neurons exhibit motion sensitivity (Marrocco and Li, 1977), is a likely contributor to such a pathway projecting directly to the visual thalamus (Harting et al., 1991). This projection is often considered to be a component of one or more secondary visual pathways that circumvent V1 to reach extrastriate cortex, including areas V4 and V5/MT, via relays in LGN and pulvinar (Benevento and Rezak, 1976; Benevento and Yoshida, 1981; Ly-

sakowski et al., 1988; Rodman et al., 2001). Although the role of the pulvinar for V1-independent processing remains uncertain, the superior colliculus and LGN have been demonstrated to be critical structures for mediating blindsight-related effects (Mohler and Wurtz, 1977; Rodman et al., 1990; Schmid et al., 2010; Kato et al., 2011). Alternatively, or more likely in addition to the direct subcortical route to V4, intracortical projections from motion-sensitive area V5/MT to V4 may contribute to the effects we observed (Maunsell and van Essen, 1983). It is attractive to implicate V5/MT in mediating the responses we observed in V4 due to the robust input V5/MT receives from the LGN (Sincich et al., 2004), as well as MT's prominent motion sensitivity (Albright et al., 1984). Input from higher areas other than V5/MT remains also a viable option for contributing to our observations in V4.

Implications for blindsight

The term "blindsight" was coined by Weiskrantz and colleagues to describe visual capacities that survive V1 injury that exist in the absence of conscious visual experience (Cowey, 2010). A prominent feature of blindsight in both humans and monkeys is the ability to detect moving stimuli (Zeki and Ffytche, 1998). Typically, the preserved sensitivity for motion in blindsight has been associated with area V5/MT because of this area's high proportion of motion-selective neurons (Albright et al., 1984) and because of several reports of preserved brain activity in MT after V1 damage (Rodman et al., 1989; Zeki and Ffytche, 1998; Azzopardi et al., 2003). The remarkable motion capacities that survive V1 injury are, however, in strong contrast with the deteriorating deficits of a V1 lesion with respect to color or shape judgments (Cowey, 2010), functions that are typically associated with the cortical ventral stream, including area V4 (Roe et al., 2012). Whereas for the present data the monkeys' V1-independent detection capacities remain unclear, our electrophysiological results appear to be in good agreement with the general phenotype of blindsight.

Together, our findings lend neurophysiological support for previous observations made by fMRI of extrastriate visual responses after V1 damage (Baseler et al., 1999; Goebel et al., 2001; Schmid et al., 2010): V4 spiking can be visually driven in the absence of V1 input.

References

- Albright TD, Desimone R, Gross CG (1984) Columnar organization of directionally selective cells in visual area MT of the macaque. *J Neurophysiol* 51:16–31. [Medline](#)
- Azzopardi P, Fallah M, Gross CG, Rodman HR (2003) Response latencies of neurons in visual areas MT and MST of monkeys with striate cortex lesions. *Neuropsychologia* 41:1738–1756. [CrossRef Medline](#)
- Baseler HA, Morland AB, Wandell BA (1999) Topographic organization of human visual areas in the absence of input from primary cortex. *J Neurosci* 19:2619–2627. [Medline](#)
- Benevento LA, Rezak M (1976) The cortical projections of the inferior pulvinar and adjacent lateral pulvinar in the rhesus monkey (*Macaca mulatta*): an autoradiographic study. *Brain Res* 108:1–24. [CrossRef Medline](#)
- Benevento LA, Yoshida K (1981) The afferent and efferent organization of the lateral geniculo-prestriate pathways in the macaque monkey. *J Comp Neurol* 203:455–474. [CrossRef Medline](#)
- Cowey A (2010) The blindsight saga. *Exp Brain Res* 200:3–24. [CrossRef Medline](#)
- Desimone R, Schein SJ (1987) Visual properties of neurons in area V4 of the macaque: sensitivity to stimulus form. *J Neurophysiol* 57:835–868. [Medline](#)
- Felleman DJ, van Essen DC (1991) Distributed hierarchical processing in the primate cerebral cortex. *Cereb Cortex* 1:1–47. [CrossRef Medline](#)
- Ferrera VP, Rudolph KK, Maunsell JH (1994) Responses of neurons in the

- parietal and temporal visual pathways during a motion task. *J Neurosci* 14:6171–6186. [Medline](#)
- Girard P, Salin PA, Bullier J (1991) Visual activity in macaque area V4 depends on area 17 input. *Neuroreport* 2:81–84. [CrossRef](#) [Medline](#)
- Goebel R, Muckli L, Zanella FE, Singer W, Stoerig P (2001) Sustained extrastriate cortical activation without visual awareness revealed by fMRI studies of hemianopic patients. *Vision Res* 41:1459–1474. [CrossRef](#) [Medline](#)
- Harting JK, Huerta MF, Hashikawa T, van Lieshout DP (1991) Projection of the mammalian superior colliculus upon the dorsal lateral geniculate nucleus: organization of tectogeniculate pathways in nineteen species. *J Comp Neurol* 304:275–306. [CrossRef](#) [Medline](#)
- Kato R, Takaura K, Ikeda T, Yoshida M, Isa T (2011) Contribution of the retino-tectal pathway to visually guided saccades after lesion of the primary visual cortex in monkeys. *Eur J Neurosci* 33:1952–1960. [CrossRef](#) [Medline](#)
- Li P, Zhu S, Chen M, Han C, Xu H, Hu J, Fang Y, Lu HD (2013) A motion direction preference map in monkey V4. *Neuron* 78:376–388. [CrossRef](#) [Medline](#)
- Lysakowski A, Standage GP, Benevento L (1988) An investigation of collateral projections of the dorsal lateral geniculate nucleus and other subcortical structures to cortical areas V1 and V4 in the macaque monkey: a double label retrograde tracer study. *Exp Brain Res* 69:651–661. [Medline](#)
- Marrocco RT, Li RH (1977) Monkey superior colliculus: properties of single cells and their afferent inputs. *J Neurophysiol* 40:844–860. [Medline](#)
- Maunsell JH, van Essen DC (1983) The connections of the middle temporal visual area (MT) and their relationship to a cortical hierarchy in the macaque monkey. *J Neurosci* 3:2563–2586. [Medline](#)
- Mohler CW, Wurtz RH (1977) Role of striate cortex and superior colliculus in visual guidance of saccadic eye movements in monkeys. *J Neurophysiol* 40:74–94. [Medline](#)
- Oostenveld R, Fries P, Maris E, Schoffelen JM (2011) FieldTrip: open source software for advanced analysis of MEG, EEG, and invasive electrophysiological data. *Comput Intell Neurosci* 2011:156869. [CrossRef](#) [Medline](#)
- Rodman HR, Gross CG, Albright TD (1989) Afferent basis of visual response properties in area MT of the macaque: I. Effects of striate cortex removal. *J Neurosci* 9:2033–2050. [Medline](#)
- Rodman HR, Gross CG, Albright TD (1990) Afferent basis of visual response properties in area MT of the macaque: II. Effects of superior colliculus removal. *J Neurosci* 10:1154–1164. [Medline](#)
- Rodman HR, Sorenson KM, Shim AJ, Hexter DP (2001) Calbindin immunoreactivity in the geniculo-extrastriate system of the macaque: implications for heterogeneity in the koniocellular pathway and recovery from cortical damage. *J Comp Neurol* 431:168–181. [CrossRef](#) [Medline](#)
- Roe AW, Chelazzi L, Connor CE, Conway BR, Fujita I, Gallant JL, Lu H, Vanduffel W (2012) Toward a unified theory of visual area V4. *Neuron* 74:12–29. [CrossRef](#) [Medline](#)
- Schmid MC, Mrowka SW, Turchi J, Saunders RC, Wilke M, Peters AJ, Ye FQ, Leopold DA (2010) Blindsight depends on the lateral geniculate nucleus. *Nature* 466:373–377. [CrossRef](#) [Medline](#)
- Sincich LC, Park KF, Wohlgemuth MJ, Horton JC (2004) Bypassing V1: a direct geniculate input to area MT. *Nat Neurosci* 7:1123–1128. [CrossRef](#) [Medline](#)
- Tolias AS, Keliris GA, Smirnakis SM, Logothetis NK (2005) Neurons in macaque area V4 acquire directional tuning after adaptation to motion stimuli. *Nat Neurosci* 8:591–593. [CrossRef](#) [Medline](#)
- Zeki S, Ffytche DH (1998) The Riddoch syndrome: insights into the neurobiology of conscious vision. *Brain* 121:25–45. [CrossRef](#) [Medline](#)

CHAPTER

6

**Beta oscillation dynamics in
extrastriate cortex after removal of
primary visual cortex**

Erklärung zu den Autorenanteilen

an der Publikation: Beta oscillation dynamics in extrastriate cortex after removal of V1

Status: in press

Name der Zeitschrift: The Journal of Neuroscience

Beteiligte Autoren:

- | | |
|--|-----------------------------|
| - Joscha T. Schmiedt (Promovierender) | - Richard C. Saunders (RCS) |
| - Alexander Maier (AM) | - David A. Leopold (DAL) |
| - Pascal Fries (PF) | - Michael C. Schmid (MCS) |

Was hat der/die Promovierende bzw. was haben die Co-Autoren/Autorinnen beigetragen?

(1) zu Entwicklung und Planung

Promovierender 30%

MCS 60%, DAL 10%

(2) zur Durchführung der einzelnen Untersuchungen und Experimente

MCS: Aufnahme der Daten (90%)

DAL: Durchführung der OPs (5%)

RCS: Durchführung der OPs (5%)

(3) zur Erstellung der Datensammlung und Abbildungen

Promovierender: Erstellung aller Abbildungen (80%)

DAL: Aufbau des Setups (5%)

MCS: Aufbau des Setups (15%)

(4) zur Analyse und Interpretation der Daten

Promovierender: Analyse und Interpretation aller Daten (100%)

(5) zur Verfassung des Manuskripts

Promovierender 70%:

MCS 30%

Beta Oscillation Dynamics in Extrastriate Cortex after Removal of Primary Visual Cortex

Joscha T. Schmiedt,¹ Alexander Maier,² Pascal Fries,^{1,3} Richard C. Saunders,⁴ David A. Leopold,^{4,5} and Michael C. Schmid¹

¹Ernst Strüngmann Institute (ESI) for Neuroscience in Cooperation with Max Planck Society, 60528 Frankfurt, Germany, ²Vanderbilt University, Department of Psychology, Nashville, Tennessee 37240, ³Donders Institute for Brain, Cognition and Behaviour, Radboud University, 6525 EN Nijmegen, The Netherlands, ⁴Laboratory of Neuropsychology, National Institute of Mental Health, Bethesda, Maryland 20892, and ⁵Neurophysiology Imaging Facility, National Institute of Mental Health, National Institute of Neurological Disorders and Stroke, and National Eye Institute, Bethesda, Maryland 20892

The local field potential (LFP) in visual cortex is typically characterized by the following spectral pattern: before the onset of a visual stimulus, low-frequency oscillations (beta, 12–20 Hz) dominate, whereas during the presentation of a stimulus these oscillations diminish and are replaced by fluctuations at higher frequencies (gamma, >30 Hz). The origin of beta oscillations *in vivo* remains unclear, as is the basis of their suppression during visual stimulation. Here we investigate the contribution of ascending input from primary visual cortex (V1) to beta oscillation dynamics in extrastriate visual area V4 of behaving monkeys. We recorded LFP activity in V4 before and after resecting a portion of V1. After the surgery, the visually induced gamma LFP activity in the lesion projection zone of V4 was markedly reduced, consistent with previously reported spiking responses (Schmid et al., 2013). In the beta LFP range, the lesion had minimal effect on the normal pattern of spontaneous oscillations. However, the lesion led to a surprising and permanent reversal of the normal beta suppression during visual stimulation, with visual stimuli eliciting beta magnitude increases up to 50%, particularly in response to moving stimuli. This reversed beta activity pattern was specific to stimulus locations affected by the V1 lesion. Our results shed light on the mechanisms of beta activity in extrastriate visual cortex: The preserved spontaneous oscillations point to a generation mechanism independent of the geniculostriate pathway, whereas the positive beta responses support the contribution of visual information to V4 via direct thalamo-extrastriate projections.

Key words: blindsight; cortex; monkey; neurophysiology; oscillation; V4

Introduction

Neuronal oscillations often appear in both mesoscopic and macroscopic electric field measurements. They are thought to largely reflect synchronous subthreshold synaptic activity generated by local or remote input into an area (Buzsáki et al., 2012) and are an ubiquitous feature of sensory and motor systems (Buzsáki, 2006). The frequencies of these rhythmic phenomena tend to vary in a state-dependent manner, ranging from slow/delta rhythms (0.5–4 Hz) during sleep (Crunelli and Hughes, 2010) to high-frequency oscillations in the gamma frequency range during states of active stimulus processing (Fries, 2009). The intermediate beta frequency range (12–20 Hz) has seen increased interest in

recent years as these rhythms are frequently observed in both sensorimotor (Kilavik et al., 2013) and visual cortex (Engel and Fries, 2010) but have not been conclusively attributed to specific functions. In mammalian visual cortex, beta range fluctuations in the local field potential (LFP) are prominent during the deployment of top-down attention (Lopes da Silva et al., 1970a; Bekisz and Wróbel, 2003; Buschman and Miller, 2007; Bosman et al., 2012; Grothe et al., 2012), working memory allocation (Tallon-Baudry et al., 2004; Salazar et al., 2012), subjective stimulus visibility (Wilke et al., 2006; Maier et al., 2008), and other tasks aimed at probing cognitive processes (Engel and Fries, 2010).

The precise mechanism underlying the generation of beta oscillations in visual cortex is not well understood; in particular, it remains unknown how beta rhythms are shaped by local and/or remote neural sources. It has been suggested that bottom-up (i.e., stimulus-driven) input to an area causes a reduction in oscillatory activity in the beta frequency range, whereas top-down (i.e., endogenously generated) input leads to an enhancement (Engel and Fries, 2010). By combining selective lesions of primary visual cortex (V1) with longitudinal recordings in higher-order visual area 4 (V4) of behaving macaque monkeys, we directly address here the influence of cortical V1 feedforward input on the formation of beta oscillations in the LFP of area V4. Whereas V4 spiking (Schmid et al., 2013) and gamma range activity show a strong reduction following V1 lesions, beta oscillations follow a surpris-

Received Feb. 5, 2014; revised July 16, 2014; accepted July 22, 2014.

Author contributions: D.A.L. and M.C.S. designed research; R.C.S. and M.C.S. performed research; A.M., P.F., and D.A.L. contributed unpublished reagents/analytic tools; J.T.S. analyzed data; J.T.S. and M.C.S. wrote the paper.

This work was supported by the Intramural Research Program of the National Institute of Mental Health and Deutsche Forschungsgemeinschaft Emmy Noether Grant Schm 2806/1-1 to M.C.S. and Whitehall and Alfred P. Sloan Foundation Grants to A.M. We thank Charles Zhu, David Hu, Alex Cummins, Andy Mitz, Katy Smith, and James Yu for technical assistance and Andy Peters for help with the experiments.

The authors declare no competing financial interests.

This article is freely available online through the JNeurosci Author Open Choice option.

Correspondence should be addressed to Dr. Michael C. Schmid, Ernst Strüngmann Institute (ESI) for Neuroscience in Cooperation with Max Planck Society, Deutschordenstrasse 46, 60528 Frankfurt, Germany. E-mail: michael.schmid@esi-frankfurt.de.

DOI:10.1523/JNEUROSCI.0509-14.2014

Copyright © 2014 the authors 0270-6474/14/3411857-08\$15.00/0

ingly different pattern. Removing the major feedforward sensory input to V4 (Barone et al., 2000) did not eliminate spontaneously occurring beta oscillations. Instead, visual stimulation of V4 in the absence of V1 input led to an enhancement of beta oscillations that was sensitive to the particular parameters of the stimulus. We will discuss this finding and its implications for the generation and possible functional roles of beta oscillations in the context of feedforward and feedback signals along the visual pathway.

Materials and Methods

Subjects. Two healthy adult female rhesus monkeys (*Macaca mulatta*, Monkey B and Monkey F) with prior V1 lesions in the right hemisphere were used in the study. All procedures were in accordance with the Institute for Laboratory Animal Research Guide for the Care and Use of Laboratory Animals and approved by the Animal Care and Use Committee of the National Institute of Mental Health.

Surgical procedures. As described by Schmid et al. (2013), briefly, a chronic “Utah” array of 1.5-mm-long microelectrodes (Blackrock Microsystems) was implanted on the prelunate gyrus in visual area V4. Two weeks later, following the first period of recordings, the part of V1 corresponding to horizontal meridian was lesioned by aspiration while the representation of the vertical meridian was left intact.

Behavioral task and visual stimulation. Visuomotor capacities before and after the V1 lesion (see Fig. 1E) were assessed with a detection task. After a fixation period of 1 s, a 0.2° diameter dot of one of four contrast levels could appear either on the vertical meridian (3.5°–4° eccentricity), on the horizontal meridian (3.5°–5.3° eccentricity), or no stimulus appeared (catch trial). Animals were rewarded if they performed a single saccade to the appearing dot or kept fixating during catch trials.

Visual stimulation with parallel electrical recording was performed in a passive fixation task as described by Schmid et al. (2013). Briefly, monkeys were trained to maintain fixation for at least 2 s within maximally 1° radius of a centrally presented fixation spot while various visual stimuli were displayed on the screen. Animals were rewarded after the presentation of 3 or 4 stimuli. Stimuli were presented for 500 ms and consisted of square-wave gratings with a diameter of 1° or 1.5°, displayed at either one of the following positions: (0°, –3.5°); (3°, –3°); (3.5°, 0°), of which in this study the first position near the vertical meridian was used as control and the last position near the horizontal meridian within the lesion-affected part of the visual field (“lesion stimulus”). The gratings were either static or slowly drifting at 0.3°/s or 0.5°/s and varied with respect to spatial frequency (0.7°/s–10°/s), direction (0°, 90°, 180°, 270° with two being equal for static gratings) and luminance contrast (low vs high, only high contrast considered here). Typical numbers of stimulus presentations per session were between 1000 and 1300. The data presented here comprise periods during which the monkeys had V1 intact and were fully acquainted with the detection task (Monkey F: 5 sessions from 10 to 1 d before the lesion, Monkey B: 7 sessions from 15 to 1 d before the lesion) and a period of several weeks after the V1 lesion surgery when visual detection was reestablished (13 sessions from 30 to 72 d after the lesion, 5 sessions from 40 to 53 d after the lesion).

Neurophysiological recordings. All electrophysiological recording sessions were carried out in an electromagnetically shielded cabin. Voltages were measured against a reference wire located subdurally over parietal cortex. The impedance of the recording electrodes ranged between 150 k Ω and 1 M Ω at 1 kHz. Extracellular voltages were amplified, filtered between 0.1 Hz and 12 kHz, and digitized at 24,414.1 Hz using a 64 channel RZ2 recording system (Tucker Davis Technologies). Electrodes were selected for data analysis if at least three recording sessions before and after the V1 lesion showed a noise and artifact-free signal.

Data analysis. All data were analyzed with the MATLAB (R2011a, MathWorks) toolbox FieldTrip (Oostenveld et al., 2011) (<http://fieldtrip.fcdonders.nl>) and custom-written routines. LFPs were extracted from raw signals by downsampling to 1017.25 Hz. LFP wavelet time-frequency analysis was performed with a Morlet wavelet of 7 cycles length (Field-Trip parameter “width,” corresponding to a spectral bandwidth of 2.14 Hz at 15 Hz) at 89 logarithmically spaced frequencies between 7.6 and

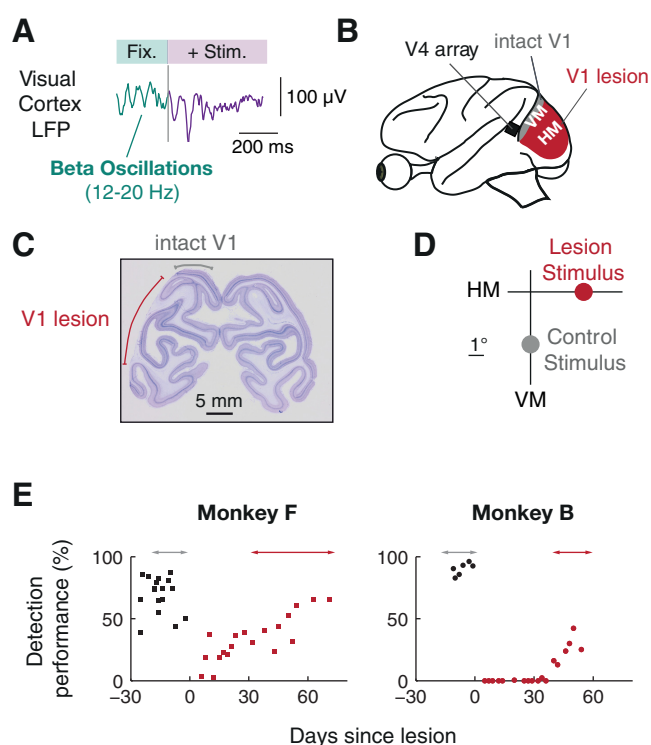


Figure 1. Longitudinal investigation of beta rhythms (12–20 Hz) in the LFP of area V4 with and without V1 input by selective ablation of V1. **A**, During task periods without transient sensory input, such as active fixation (Fix.) before the onset of a stimulus (Stim.), the LFP in visual cortex of behaving subjects is often dominated by rhythmic fluctuations in the beta frequency range (12–20 Hz). **B**, To investigate the role of bottom-up input for the generation of these beta oscillations, we recorded from midlevel area V4 with chronically implanted arrays before and after a targeted aspiration lesion in V1. The lesion was placed to eliminate the V1 representation of the horizontal meridian (HM) between ~ 2 – 7° of visual eccentricities (red) while leaving the lower vertical meridian (VM) representation, close to lunale sulcus, intact (gray). **C**, Example coronal section of V1 showing extent of lesioned (red line) and intact (gray line) tissue for Monkey B. Note the loss of gray matter in the targeted area. **D**, Stimulus locations throughout the paper are labeled lesion stimulus (LS) for stimuli inside the lesion-affected visual space around the HM and control stimulus (CS) for stimuli outside, close to the VM. **E**, Behavioral performance in a detection task before and after V1 lesion with dot stimuli around the lesion stimulus location. Arrows indicate time period of LFP recordings.

400 Hz. Stimulus-induced power changes were quantified as percentage change from the 250 ms baseline power averaged across trials. Power in a time-frequency window was determined by averaging across time and frequency. The latency of the stimulus-induced beta power changes were determined as the first time point reaching 90% of the peak value in the session-averaged beta power time course. For all prelesion and control stimulus data, the peak was defined as the minimum value in the 50–400 ms window after stimulus onset. For the lesion stimulus after lesion, the peak was defined as the maximum power value in the same time window.

Results

The goal of our experiments was to directly test the effect of permanent V1 lesions on the spectral properties of visual responses in area V4 (Fig. 1A) of macaque extrastriate cortex. Detailed retinotopic assessment of V1 and V4 by fMRI guided the planning of our surgical procedures (Schmid et al., 2013). We first implanted multielectrode arrays into the dorsal part of area V4 at a position responsive to parafoveal visual stimulation in the lower right quadrant of the visual field. After recovery from the implantation, over the course of 2 weeks, we obtained LFP recordings during visual task performance, as a baseline with intact V1. Subsequently, we surgically removed V1 gray matter straddling the horizontal meridian representation (Fig. 1B). Care was

taken to spare a section of the cortex ~ 5 mm in width along the lunate sulcus (which corresponds to the visual representation of the visual vertical meridian and the boundary to area V2). Using this selective lesioning approach, our study contrasted V4 LFP responses to visual stimuli with V1 input intact versus V1 removed, regardless of the time point of assessment (Fig. 1C,D). Postmortem histological assessment of the occipital lobes of both monkeys confirmed the complete loss of gray matter in the targeted area of V1 as well as the preservation of striate cortex in the control region (Fig. 1C).

To assess the impact of the V1 lesion on the monkeys' visuomotor capacities, we tested the monkeys on a simple task in which they had to detect and saccade toward a small patch of light. While both monkeys achieved very good performance under V1 intact conditions, lesioning V1 had a detrimental effect on performance, that is, the monkeys were unable to detect stimuli presented at the horizontal meridian (lesion stimulus) (Fig. 1E). However, following a recovery period of 30–40 d with daily testing on the detection task, both monkeys had partially recovered their detection capabilities and reached performance values ranging from 23%–66% in Monkey F and 13%–42% in Monkey B.

For the electrophysiological assessment, we focused our analysis on the time periods before and >30 d after the surgical intervention (i.e., when the monkeys had regained some of their visuomotor capacities; Monkey F: 30–72 d after lesion; Monkey B: 40–53 d after lesion). The basic testing procedure across all experimental conditions entailed passive fixation on a centrally presented spot, while stimuli were shown on a screen. After 250 ms of fixation, a drifting or static square-wave grating stimulus (high contrast, varying drift direction, and spatial frequency, 70–90 presentations per session) was presented in parafoveal regions to elicit visually triggered LFP responses while the monkey continued to fixate. Stimuli were either placed in the lesion-affected part of visual space, that is, the horizontal meridian (lesion stimulus), or on the vertical meridian (control stimulus). During the times when testing was performed under V1 intact conditions, the prestimulus LFP was often dominated by voltage fluctuations in the beta frequency range (12–20 Hz; Fig. 2A,D, left). Following stimulus onset and a brief broadband response, these low-frequency fluctuations decreased in amplitude, and a mixture of broadband and oscillatory high-frequency gamma activity (>50 Hz) instead dominated the LFP (for an example, see Fig. 3A). The resulting spectral change of the LFP was evident as a decrease in the baseline-normalized beta power and an increase in gamma band power. This effect of visual stimulation causing a shift from high-amplitude, low-frequency activity toward low-amplitude, high-frequency activity has been observed in a large number of studies on visual cortical responses (Gray and Singer, 1989; Taylor et al., 2005; Ray and Maunsell, 2011).

Prestimulus beta rhythms in V4 are still present after V1 lesion

Following the V1 lesion and subsequent partial behavioral recovery (Monkey F: 30–72 d after lesion; Monkey B: 40–53 d after lesion) beta oscillations during the prestimulus period (Fig. 2) were prominent in the raw LFP (Fig. 2A,D, right) and manifested as peaks in the power spectra ~ 15 and 14 Hz in Monkey F and Monkey B, respectively (Fig. 2B,E). The mean amplitude of the oscillation was unchanged in Monkey F (Fig. 2A–C, $p > 0.05$, $n = 47$ electrodes averaged across 5 sessions prelesion and 11–13 sessions after lesion, Wilcoxon signed rank test) and enhanced by $23 \pm 4.4\%$ in Monkey B (Fig. 2D–F, $p < 10^{-5}$, $n = 53$ electrodes averaged across 7 sessions prelesion and 3–5 sessions after lesion).

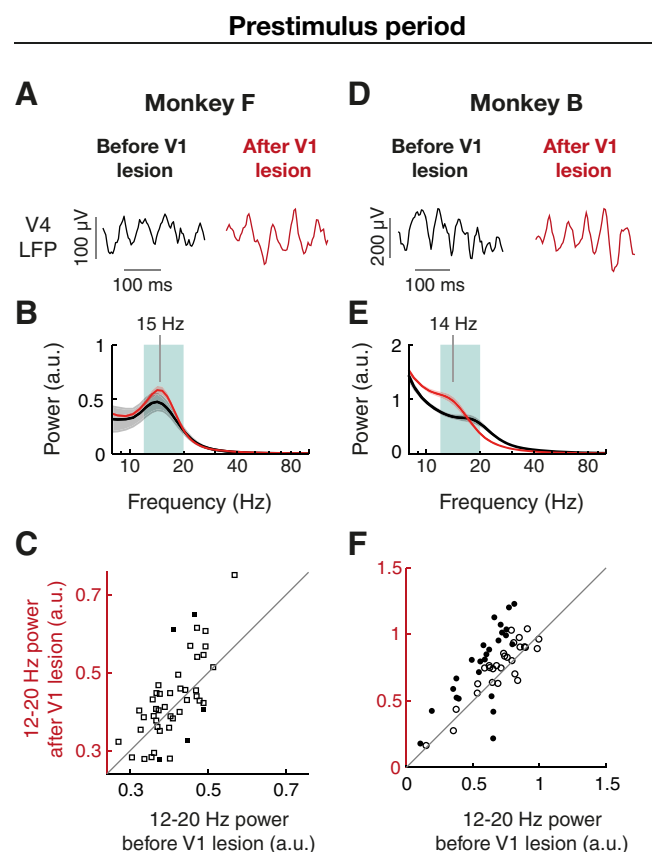


Figure 2. Beta oscillations during active fixation in area V4 are preserved after selective removal of V1. **A**, Example prestimulus beta oscillations of the unfiltered V4 LFP before (black, left) and after V1 lesion (red, right). **B**, Absolute power spectrum of the prestimulus period before (black, $n = 5$ sessions, each comprising 1000–1300 trials) and after (red, $n = 13$ sessions) from an example V4 electrode in Monkey F, averaged across trials and sessions. Gray and red shadings represent SEM across sessions before and after lesion, respectively. **C**, Distribution of power in the beta frequency range (12–20 Hz, green shading in **B**) during prestimulus period before and after V1 lesion. Each dot represents the beta-band power at a recording site averaged across sessions. Filled and open symbols represent recording sites with significant or nonsignificant changes in power ($p < 0.05$, independent samples t test), respectively. Gray line indicates identical prelesion and postlesion power. **D–F**, Example beta oscillations (**D**), wavelet spectrum (**E**), and beta power distribution (**F**) for Monkey B before ($n = 7$ sessions) and after ($n = 5$ sessions) V1 lesion.

On the individual electrode level, in Monkey F only a small fraction showed significant changes in beta power, with a decrease in 2 (4%) electrodes and increase in other 2 (4%) electrodes (independent samples t test, $p < 0.05$, electrodes and sessions as before). In Monkey B, 21 (40%) electrodes showed a significant increase and 3 (6%) electrodes a decrease in beta power. These findings demonstrate that the generation of V4 beta oscillations is not dependent on input from V1.

Differential effects of V1 lesion on V4 beta and gamma dynamics

Under normal conditions, the presentation of a visual stimulus leads to a reduction in the amplitude of beta LFP oscillations (Fig. 3A). Following the lesion, however, there was a notable reversal of this effect: visual stimulation with a slowly drifting grating in the lesion-affected visual space now led to a beta power enhancement (Fig. 3B). This postlesion stimulus-induced beta power enhancement was significantly different from zero in both monkeys ($p < 10^{-6}$, Wilcoxon signed rank test, $n = 47$ and 53 electrodes in Monkey F and Monkey B, respectively). Compared with the pre-

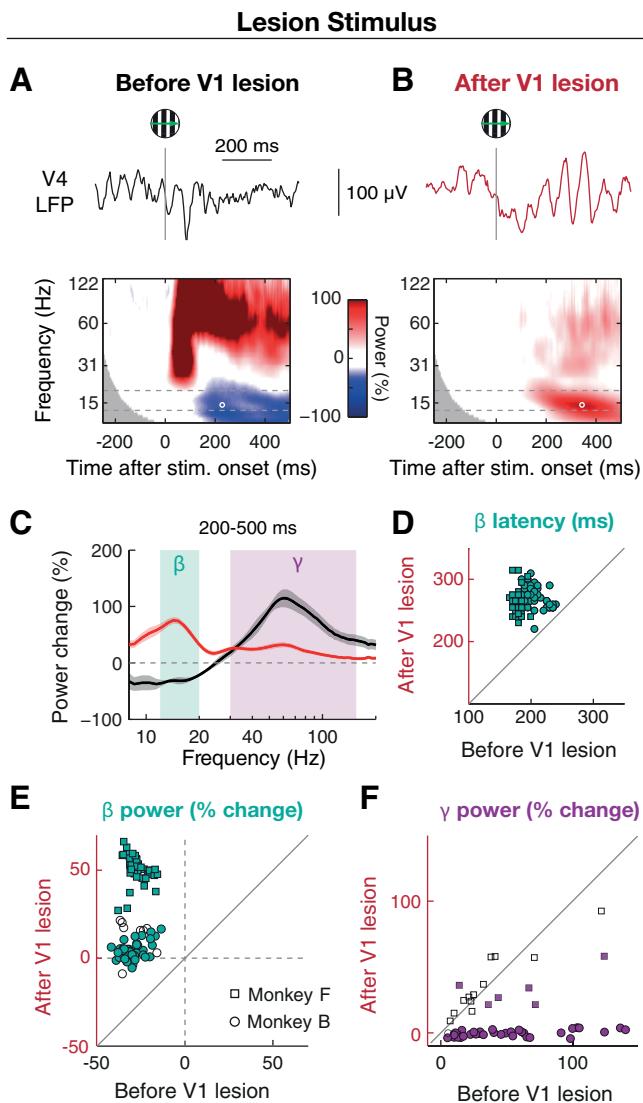


Figure 3. Visual stimulation in lesion-affected visual space induces strong beta (12–20 Hz) oscillations in V4 instead of decreasing beta power. **A**, Example LFP responses to a moving grating stimulus (high contrast, varying spatial frequency, and drift direction) in the lesion-affected part of visual space from a recording site in Monkey F before the V1 lesion. Upper row, Single trial LFP trace. Gray line indicates stimulus onset. Lower row, Session-averaged ($n = 5$), baseline-normalized wavelet power spectra from an example electrode in Monkey F (data as in Fig. 2). White circle represents peak latency within the beta frequency band (dashed lines). **B**, Same as **A** for data from after the V1 lesion ($n = 11$ sessions). Note the unusual stimulus-induced beta oscillations visible in both single trials and average. **C**, Baseline-normalized power spectra from example recording site in **A** averaged across 200–500 ms period and sessions for lesion stimulus, before (black) and after (red) V1 lesion. Shadings surrounding curves represent SEM across sessions. **D**, Distribution of beta power peak latency before and after V1 lesion. **E**, Distribution of baseline-normalized power in beta band before and after V1 lesion for lesion stimulus. Each dot represents a power value from one recording site averaged across the beta band, 200–500 ms period, and sessions. **F**, Same as **E** for the gamma frequency band (30–150 Hz). **E**, **F**, Open and filled symbols represent recording sites with nonsignificant and significant changes in power on the individual electrode level ($p < 0.05$, independent samples t test), respectively.

lesion condition, the baseline-normalized beta power in the 200–500 ms and 12–20 Hz time-frequency window increased from $-27.1 \pm 0.84\%$ to $51 \pm 1.1\%$ in Monkey F ($p < 10^{-8}$, $n = 47$ electrodes, Wilcoxon signed rank test) and from $-29 \pm 0.9\%$ to $5 \pm 0.9\%$ in Monkey B ($p < 10^{-9}$, $n = 53$ electrodes) (Fig. 3C). On the individual electrode level, 47 of 47 (100%) and 43 of 53 (81%) electrodes showed a significant increase in stimulus-induced

beta power (independent samples t test, $p < 0.05$, sessions as above) (Fig. 3E). Thus, lack of V1 input appeared to unmask the stimulus-induced modulation of beta oscillations.

To obtain more information with respect to mechanistic changes that may have contributed to this effect, we compared the latencies of the stimulus-induced beta modulation before and after the V1 lesion. The beta power enhancement observed under V1 lesion conditions reached its peak at 260 ± 2.8 ms and 274 ± 2.3 ms after stimulus onset (Fig. 3D; see 5A) for Monkey F and Monkey B, respectively. In comparison, the stimulus induced beta power decrease under V1 intact conditions had a latency of 179 ± 1.0 ms and 207 ± 2.1 ms in Monkey F and Monkey B, respectively. This means that the postlesion positive beta peak occurred by ~ 65 –85 ms significantly later than the negative peak before the lesion ($p < 10^{-9}$ in both monkeys, Wilcoxon signed rank test).

In addition to the changes in the beta oscillation dynamics, we also examined the effects of the V1 lesion on faster LFP oscillatory activity (i.e., in the gamma range, which is thought to be strongly dependent on feedforward input) (Bosman et al., 2012). In contrast to the general increase in the stimulus-induced beta power, effects on the stimulus-induced gamma power (30–150 Hz, late time window 200–500 ms, same sessions and trials as for beta) were more spatially confined. In sites that were well activated by the stimulus before the lesion (power increase from baseline $>25\%$, $p < 0.05$, independent samples t test), gamma power was reduced after the V1 lesion (Fig. 3C,F). In Monkey B, stimulus-elicited gamma power was drastically decreased from $70 \pm 7.3\%$ prelesion to $0.3 \pm 0.4\%$ postlesion ($n = 23$ electrodes, Wilcoxon signed rank test, $p < 10^{-7}$, sessions as above), which was significant in 23 of 23 (100%) individual recording sites (independent samples t test, $p < 0.05$). In Monkey F, this gamma decrease was less pronounced, from $64 \pm 11\%$ prelesion to $44 \pm 6\%$ postlesion ($p = 0.037$, Wilcoxon signed rank test, $n = 10$ electrodes) with 4 of 10 electrodes showing significant decreases ($p < 0.05$, independent samples t test).

Reversal of beta oscillation dynamics is restricted to lesion-affected visual space

Importantly, the lesion-induced reversal of beta dynamics was specific to stimuli that were presented in the lesion-affected visual space and was not seen for the identical control stimuli that invoked visual processing in V1 as they were presented outside the lesion zone (Fig. 1D). Stimulation at the vertical meridian resulted in a decrease in low frequency and an increase in high-frequency power (Fig. 4). In contrast to the stimulus in the lesion-affected space, beta power values for the control stimulation (Fig. 4E) were either further decreased from the prelesion baseline in Monkey F, from $-21.9 \pm 0.83\%$ to $-45 \pm 1.2\%$ ($p < 10^{-8}$, Wilcoxon signed rank test, $n = 47$ electrodes) or minimally increased in Monkey B with $-34 \pm 1.2\%$ before and $-32 \pm 1.1\%$ after the lesion ($p = 0.025$, Wilcoxon signed rank test, $n = 53$ electrodes). On the individual electrode level, in Monkey F 44 of 47 (94%) electrodes showed a significant decrease of stimulus-induced beta power, whereas in Monkey B 8 of 53 (15%) showed a significant increase and 1 of 53 (2%) a significant decrease (independent samples t test, sessions as before). The gamma frequency range was also affected with an increase from $40 \pm 3.6\%$ to $74 \pm 8.9\%$ in Monkey F ($p = 0.016$, $n = 7$ electrodes, Wilcoxon signed rank test; significant change in 5 (71%) electrodes, independent samples t test) and a decrease in Monkey B from $75 \pm 9.4\%$ to $58 \pm 8.0\%$ ($p = 0.008$, $n = 13$ electrodes; significant change in 2 (15%) electrodes).

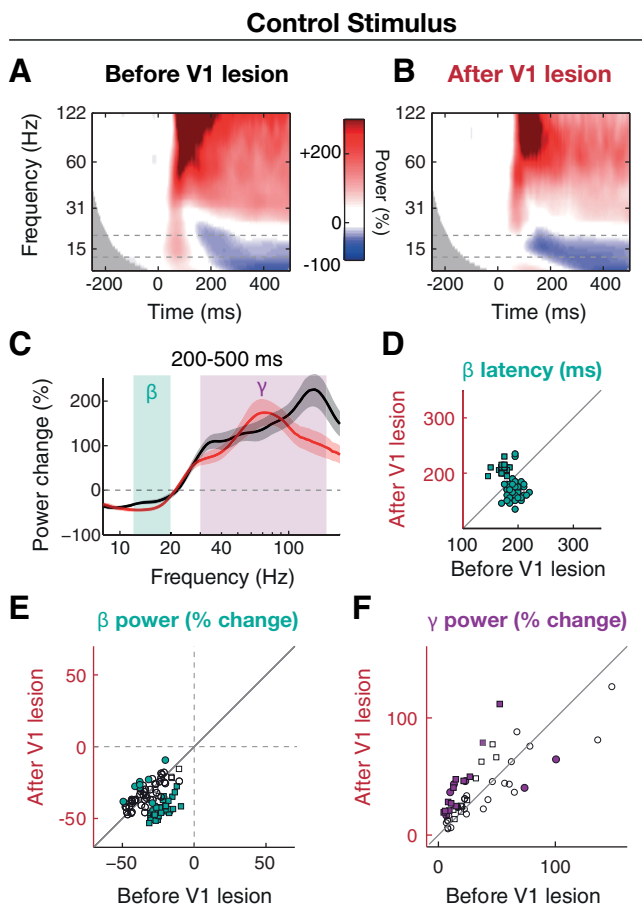


Figure 4. Reversal of stimulus-induced beta oscillation dynamics is restricted to visual stimulation in lesion-affected space. **A, B**, Session-averaged, baseline-normalized wavelet power spectra from an example electrode in Monkey B around visual stimulation with drifting grating stimulus (high contrast, varying spatial frequency, and drift correction) at the control stimulus location before (**A**, $n = 7$ sessions) and after (**B**, $n = 4$ sessions) the V1 lesion. **C**, Baseline-normalized power spectra from example recording site in **A, B** averaged across 200–500 ms period and sessions for lesion stimulus, before (black) and after (red) V1 lesion. Shadings surrounding curves represent SEM across sessions. **D**, Distribution of beta power peak latency before and after V1 lesion. **E**, Distribution of baseline-normalized power in beta band before and after V1 lesion for lesion stimulus. Each dot represents a power value from one recording site averaged across the beta band, 200–500 ms period, and sessions. **F**, Same as **E** for the gamma frequency band (30–150 Hz). **E, F**, Open and filled symbols represent recording sites with nonsignificant and significant changes in power on the individual electrode level ($p < 0.05$, independent samples t test), respectively.

Stimulus-induced beta oscillations reflect stimulus content

We previously observed residual, V1-independent spiking activity in V4 that was unusually sensitive to stimulus motion (Schmid et al., 2013). In an effort to assess whether beta oscillations similarly reflected feature-dependent processing of the stimulus, we compared their magnitude following the presentation of static versus slowly drifting gratings (Fig. 5). In both monkeys, the stimulus-driven beta power increase in V4 was significantly stronger for moving than for static stimuli ($p < 10^{-8}$ for both monkeys, Wilcoxon signed rank test), indicating that the observed responses showed some level of stimulus specificity.

Discussion

Our results demonstrate that beta-band oscillations in area V4 are preserved in the absence of V1 input, indicating that they are not generated by a feedforward drive from V1. Moreover, following the ablation of V1, the stimulus-driven power decrease in the beta frequency band was replaced by stimulus-driven power in-

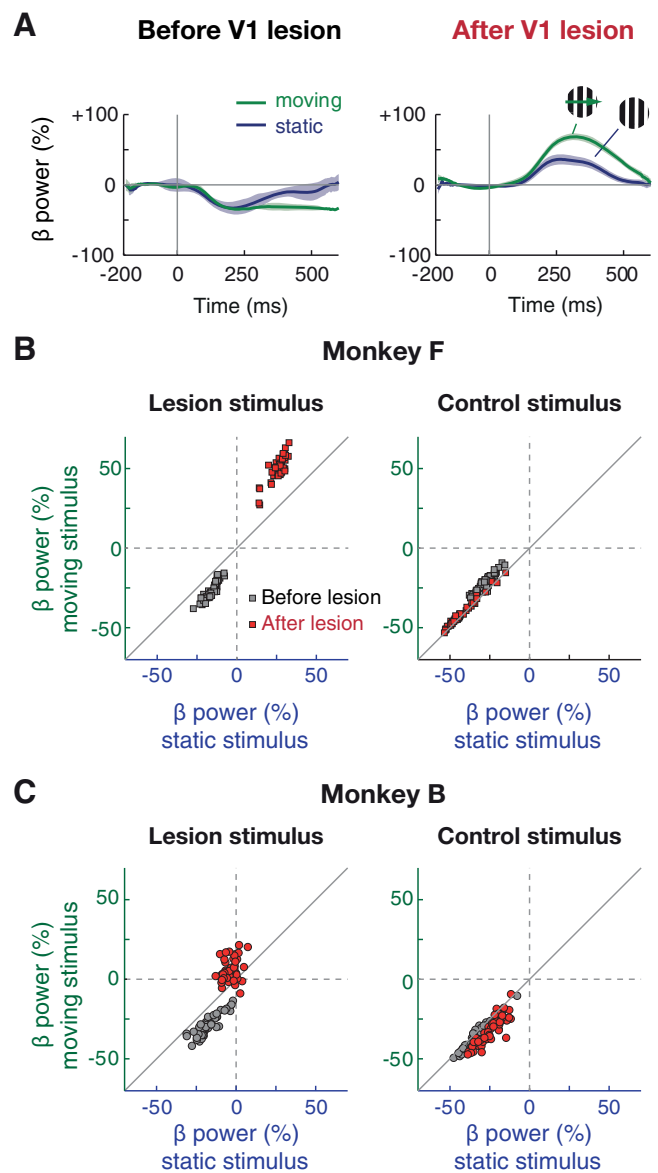


Figure 5. V1-independent beta oscillations are sensitive to motion. **A**, Time course of baseline-normalized power in beta (12–20 Hz) band from example recording site and sessions in Monkey F for moving (green) and static (blue) grating stimuli (high contrast, varying drift direction/orientation, and spatial frequency for both) at the lesion stimulus location. Shading represents SEM. **B**, Distribution of beta power values (200–500 ms) for moving versus static stimuli for lesion (left) and control stimulus (right) from Monkey F (data as in Figs. 3 and 4). **C**, Same as **B** for Monkey B.

crease occurring ~ 300 ms after stimulus onset. As this effect was limited to the lesion-affected part of visual space, passive volume conduction as a potential contributor to the observed effect can be largely excluded. In addition, stimulus-induced beta power modulation in V1-deafferented V4 was sensitive to stimulus motion, indicating that these changes of the LFP are related to active feature-dependent stimulus processing. In the following, we discuss our findings in the context of what is known about the generation of beta oscillations and their putative contribution to cortical processing.

Beta rhythm in infragranular cortical layers

Beta oscillations in the visual system were described early in the occipital cortex of dogs actively attending a screen (Lopes da Silva et al., 1970a). Yet, compared with other brain rhythms, to date

very little is known about their generation and function in the visual system (Steriade, 1993; Engel and Fries, 2010). On the cellular level, *in vitro* results from rat auditory and somatosensory cortex showed that layer 5 cortical pyramidal neurons can generate beta rhythms (Roopun et al., 2006, 2010). Consistent with this finding are observations from studies showing that alpha to beta band oscillations measured in primate visual cortex are most prominent in the infragranular layers (Sun and Dan, 2009; Buffalo et al., 2011; Maier et al., 2011; Xing et al., 2012). Given an estimated average cortical thickness of ~ 2 mm and our electrode lengths of 1.5 mm, it is likely that we have primarily sampled beta activity from V4's deep layers. A common observation in studies that assessed oscillatory activity in visual cortex is that the LFP is usually dominated by low-frequency fluctuations before the presentation of salient visual stimuli, which are then reduced during stimulus presentation (Gray and Singer, 1989; Taylor et al., 2005; Fries et al., 2008; Ray and Maunsell, 2011). This effect of stimulus-induced cortical excitation is also evident in our data from area V4 in the V1 intact condition (Figs. 3 and 4). *In vitro* slice studies suggest that an excitatory glutamatergic or cholinergic drive is needed to generate beta oscillations (Roopun et al., 2006, 2010). What might be the source of the V4 beta oscillation and its modulation by visual input?

Beta oscillations may reflect unmasked input from thalamus or neighboring cortex

Our data argue against a contribution of a bottom-up V1 drive contributing to V4 beta oscillations because prestimulus beta power was not affected or, if anything, increased under the lesion condition. Surprisingly, after the lesion, beta power in V4 was no longer diminished following visual input, but instead, beta oscillations were enhanced following the presentation of a stimulus. It is likely that this effect reflects some form of unmasking or plasticity that results from the lack of V1 input and may involve either local or remote circuits. For example, it is conceivable that neurons in layer 4 of V4 release their inhibitory impact on processes in deeper layers when their driving input from V1 is removed. Alternatively, the enhanced beta modulation may indicate the unmasking of alternative input projections. It is likely that at some point these processes invoke the thalamus. The lateral geniculate nucleus (LGN) directly projects to multiple extrastriate areas, including V4 (Fries, 1981; Lysakowski et al., 1988; Rodman et al., 2001; Lyon and Rabideau, 2012), and has been shown to be crucial for V1-independent responses in extrastriate areas (Schmid et al., 2009, 2010). Interestingly, the geniculate input to V4 appears to target primarily the deeper layers (Benevento and Yoshida, 1981) from which we likely recorded and where beta oscillations are most prominent. It is possible that V4 inherits beta oscillatory activity via this projection from LGN as beta oscillations have also been recorded in LGN (Lopes da Silva et al., 1970b, 1970a; Bekisz and Wróbel, 2003; Bastos et al., 2014). This geniculate beta-drive to V4 may get unmasked or even upregulated following the V1 lesion. Other thalamic nuclei are also possible candidate sources for beta rhythmicity in visual cortex, in particular the pulvinar and lateral posterior complex. These higher-order nuclei have been shown to engage in rhythmic activity in the alpha/beta frequency range (Wróbel et al., 2007; Saalmann et al., 2012). The pulvinar, which receives visual input from superior colliculus and projects to visual cortex (Harting et al., 1980; Stepniewska et al., 1999; Adams et al., 2000; Lyon et al., 2010), could trigger a stimulus-related increase in oscillatory activity.

A possible argument against a thalamic origin of V1-independent beta modulations is the relatively long peak latency

of 300 ms after stimulus onset. It is therefore conceivable that the beta oscillations are triggered by input from other cortical areas, including feedback projections, which reach to the infragranular layers of area V4 as well (Barone et al., 2000). The idea of cortical beta oscillations as a spectral signature of top-down feedback signals has gained support from a number of studies that reported beta-band modulation associated with attention (Bekisz and Wróbel, 2003; Buschman and Miller, 2007; Bosman et al., 2012), working memory allocation (Tallon-Baudry et al., 2004; Salazar et al., 2012), or subjective stimulus visibility (Wilke et al., 2006; Maier et al., 2008). In some of these studies, beta oscillations resulted in increased interareal coherence (Buschman and Miller, 2007; Bosman et al., 2012; Salazar et al., 2012) and were most pronounced in cortical layers 5 and 6 (Maier et al., 2008; Sun and Dan, 2009; Buffalo et al., 2010). However, a recent study reported beta oscillations that did not exhibit attentional modulation in area V4 of monkeys with prefrontal cortex lesions (Gregoriou et al., 2014). Therefore, areas other than prefrontal cortex likely contribute to the observed beta oscillation dynamics in our results.

Irrespective of the ultimate neuronal mechanism leading to the formation of beta oscillations, it appears to become unmasked or perhaps even plastically upregulated after lesioning V1. As the changes in beta oscillation dynamics were observed during a time period when visuomotor detection capacities had substantially recovered after the surgery (Mohler and Wurtz, 1977), it is tempting to speculate that the beta increase may reflect or perhaps even directly contribute to the observed behavioral recovery.

Dependence of gamma range activity on feedforward input

In contrast to LFP beta oscillations in visual cortex that are present before the onset of a visual stimulus, oscillatory activity in the gamma frequency band is usually associated with the presence of a visual stimulus (Gray and Singer, 1989; Fries, 2009; Ray and Maunsell, 2011). It was hypothesized that gamma oscillations could be related to or even mediate feedforward processing (Bosman et al., 2012) of visual stimuli. In our data, similar to previous assessment of spiking and fMRI activity in V4 after removal of V1 input (Schmid et al., 2010, 2013), LFP activity in the gamma range in V4 was decreased or abolished following the V1 lesion. Therefore, feedforward input from V1 appears to be necessary for the full emergence of gamma oscillations at the level of V4.

Distinguishing alpha from beta oscillations

The beta oscillations and their modulation by the stimulus that we observed were ~ 15 Hz in both monkeys (Figs. 2A,E and 3C,D). This frequency lies at the lower end of the classical beta 13–30 Hz (Kilavik et al., 2013) frequency band, raising the question whether the generative mechanism of the beta oscillations in our study is distinct from the one for alpha oscillations, which are usually considered to be in the 8–12 Hz range in both humans (Haegens et al., 2014) and monkeys (Bollimunta et al., 2008) as well as other species. One important difference between the two frequency bands in previous studies seemed to be that beta rhythms were enhanced in attentive behavior (Lopes da Silva et al., 1970a; Bekisz and Wróbel, 1993), whereas alpha rhythms were strongest when attention was away from visual stimuli (Lopes da Silva et al., 1980; Bollimunta et al., 2011; Haegens et al., 2014). In our case, the monkeys were attentively fixating on the screen to receive reward and were also trained on other visual tasks that required attention to the visual domain. This makes it conceivable that the rhythm observed in our data is rather asso-

ciated with an activated state. However, based only on frequency range, without more targeted experimental manipulations, it is difficult to delineate whether the underlying mechanism has greater overlap with the alpha-generating or beta-generating networks.

A final conclusion on the origin of the beta rhythm withstanding, our data conclusively demonstrate that the feedforward drive from V1 is not necessary for the initiation and maintenance of V4 rhythmic activity in the beta range. Rather, V1 input seems to be required to break low-frequency rhythms and evoke an activated state (for a similar mechanism in the thalamocortical system, compare Castro-Alamancos, 2004; Poulet et al., 2012).

References

- Adams MM, Hof PR, Gattass R, Webster MJ, Ungerleider LG (2000) Visual cortical projections and chemoarchitecture of macaque monkey pulvinar. *J Comp Neurol* 419:377–393. [CrossRef Medline](#)
- Barone P, Batardiere A, Knoblauch K, Kennedy H (2000) Laminar distribution of neurons in extrastriate areas projecting to visual areas V1 and V4 correlates with the hierarchical rank and indicates the operation of a distance rule. *J Neurosci* 20:3263–3281. [Medline](#)
- Bastos AM, Briggs F, Alitto HJ, Mangun GR, Usrey WM (2014) Simultaneous recordings from the primary visual cortex and lateral geniculate nucleus reveal rhythmic interactions and a cortical source for gamma-band oscillations. *J Neurosci* 34:7639–7644. [CrossRef Medline](#)
- Bekisz M, Wróbel A (1993) 20 Hz rhythm of activity in visual system of perceiving cat. *Acta Neurobiol Exp (Wars)* 53:175–182. [Medline](#)
- Bekisz M, Wróbel A (2003) Attention-dependent coupling between beta activities recorded in the cat's thalamic and cortical representations of the central visual field. *Eur J Neurosci* 17:421–426. [CrossRef Medline](#)
- Benevento LA, Yoshida K (1981) The afferent and efferent organization of the lateral geniculate-prestriate pathways in the macaque monkey. *J Comp Neurol* 203:455–474. [CrossRef Medline](#)
- Bollimunta A, Chen Y, Schroeder CE, Ding M (2008) Neuronal mechanisms of cortical alpha oscillations in awake-behaving macaques. *J Neurosci* 28:9976–9988. [CrossRef Medline](#)
- Bollimunta A, Mo J, Schroeder CE, Ding M (2011) Neuronal mechanisms and attentional modulation of corticothalamic alpha oscillations. *J Neurosci* 31:4935–4943. [CrossRef Medline](#)
- Bosman CA, Schoffelen JM, Brunet N, Oostenveld R, Bastos AM, Womelsdorf T, Rubehn B, Stieglitz T, De Weerd P, Fries P (2012) Attentional stimulus selection through selective synchronization between monkey visual areas. *Neuron* 75:875–888. [CrossRef Medline](#)
- Buffalo EA, Fries P, Landman R, Liang H, Desimone R (2010) A backward progression of attentional effects in the ventral stream. *Proc Natl Acad Sci U S A* 107:361–365. [CrossRef Medline](#)
- Buffalo EA, Fries P, Landman R, Buschman TJ, Desimone R (2011) Laminar differences in gamma and alpha coherence in the ventral stream. *Proc Natl Acad Sci U S A* 108:11262–11267. [CrossRef Medline](#)
- Buschman TJ, Miller EK (2007) Top-down versus bottom-up control of attention in the prefrontal and posterior parietal cortices. *Science* 315:1860–1862. [CrossRef Medline](#)
- Buzsáki G (2006) *Rhythms of the brain*. Oxford: Oxford UP.
- Buzsáki G, Anastassiou CA, Koch C (2012) The origin of extracellular fields and currents: EEG, ECoG, LFP and spikes. *Nat Rev Neurosci* 13:407–420. [CrossRef Medline](#)
- Castro-Alamancos MA (2004) Dynamics of sensory thalamocortical synaptic networks during information processing states. *Prog Neurobiol* 74:213–247. [CrossRef Medline](#)
- Crunelli V, Hughes SW (2010) The slow (<1 Hz) rhythms of non-REM sleep: a dialogue between three cardinal oscillators. *Nat Neurosci* 13:9–17. [CrossRef Medline](#)
- Engel AK, Fries P (2010) beta-band oscillations: signalling the status quo? *Curr Opin Neurobiol* 20:156–165. [CrossRef Medline](#)
- Fries P (2009) Neuronal gamma-band synchronization as a fundamental process in cortical computation. *Annu Rev Neurosci* 32:209–224. [CrossRef Medline](#)
- Fries P, Womelsdorf T, Oostenveld R, Desimone R (2008) The effects of visual stimulation and selective visual attention on rhythmic neuronal synchronization in macaque area V4. *J Neurosci* 28:4823–4835. [CrossRef Medline](#)
- Fries W (1981) The projection from the lateral geniculate nucleus to the prestriate cortex of the macaque monkey. *Proc R Soc Lond B Biol Sci* 213:73–86. [CrossRef Medline](#)
- Gray CM, Singer W (1989) Stimulus-specific neuronal oscillations in orientation columns of cat visual cortex. *Proc Natl Acad Sci U S A* 86:1698–1702. [CrossRef Medline](#)
- Gregoriou GG, Rossi AF, Ungerleider LG, Desimone R (2014) Lesions of prefrontal cortex reduce attentional modulation of neuronal responses and synchrony in V4. *Nat Neurosci* 17:1003–1011. [CrossRef Medline](#)
- Grothe I, Neitzel SD, Mandon S, Kreiter AK (2012) Switching neuronal inputs by differential modulations of gamma-band phase-coherence. *J Neurosci* 32:16172–16180. [CrossRef Medline](#)
- Haegens S, Cousijn H, Wallis G, Harrison PJ, Nobre AC (2014) Inter- and intra-individual variability in alpha peak frequency. *Neuroimage* 92:46–55. [CrossRef Medline](#)
- Harting JK, Huerta MF, Frankfurter AJ, Strominger NL, Royce GJ (1980) Ascending pathways from the monkey superior colliculus: an autoradiographic analysis. *J Comp Neurol* 192:853–882. [CrossRef Medline](#)
- Kilavik BE, Zaepffel M, Brovelli A, MacKay WA, Riehle A (2013) The ups and downs of beta oscillations in sensorimotor cortex. *Exp Neurol* 245:15–26. [CrossRef Medline](#)
- Lopes da Silva FH, van Rotterdam A, Storm van Leeuwen W, Tielen AM (1970a) Dynamic characteristics of visual evoked potentials in the dog: II. beta frequency selectivity in evoked potentials and background activity. *Electroencephalogr Clin Neurophysiol* 29:260–268. [CrossRef Medline](#)
- Lopes da Silva FH, van Rotterdam A, Storm van Leeuwen W, Tielen AM (1970b) Dynamic characteristics of visual evoked potentials in the dog: I. Cortical and subcortical potentials evoked by sine wave modulated light. *Electroencephalogr Clin Neurophysiol* 29:246–259. [CrossRef Medline](#)
- Lopes da Silva FH, Vos JE, Mooibroek J, Van Rotterdam A (1980) Relative contributions of intracortical and thalamo-cortical processes in the generation of alpha rhythms, revealed by partial coherence analysis. *Electroencephalogr Clin Neurophysiol* 50:449–456. [CrossRef Medline](#)
- Lyon DC, Rabideau C (2012) Lack of robust LGN label following transneuronal rabies virus injections into macaque area V4. *J Comp Neurol* 520:2500–2511. [CrossRef Medline](#)
- Lyon DC, Nassi JJ, Callaway EM (2010) A disinaptic relay from superior colliculus to dorsal stream visual cortex in macaque monkey. *Neuron* 65:270–279. [CrossRef Medline](#)
- Lysakowski A, Standage GP, Benevento LA (1988) An investigation of colateral projections of the dorsal lateral geniculate nucleus and other subcortical structures to cortical areas V1 and V4 in the macaque monkey: a double label retrograde tracer study. *Exp Brain Res* 69:651–661. [Medline](#)
- Maier A, Wilke M, Aura C, Zhu C, Ye FQ, Leopold DA (2008) Divergence of fMRI and neural signals in V1 during perceptual suppression in the awake monkey. *Nat Neurosci* 11:1193–1200. [CrossRef Medline](#)
- Maier A, Aura CJ, Leopold DA (2011) Infragranular sources of sustained local field potential responses in macaque primary visual cortex. *J Neurosci* 31:1971–1980. [CrossRef Medline](#)
- Mohler CW, Wurtz RH (1977) Role of striate cortex and superior colliculus in visual guidance of saccadic eye movements in monkeys. *J Neurophysiol* 40:74–94. [Medline](#)
- Oostenveld R, Fries P, Maris E, Schoffelen JM (2011) FieldTrip: open source software for advanced analysis of MEG, EEG, and invasive electrophysiological data. *Comput Intell Neurosci* 2011:156869. [CrossRef Medline](#)
- Poulet JF, Fernandez LM, Crochet S, Petersen CC (2012) Thalamic control of cortical states. *Nat Neurosci* 15:370–372. [CrossRef Medline](#)
- Ray S, Maunsell JH (2011) Different origins of gamma rhythm and high-gamma activity in macaque visual cortex. *PLoS Biol* 9:e1000610. [CrossRef Medline](#)
- Rodman HR, Sorenson KM, Shim AJ, Hexter DP (2001) Calbindin immunoreactivity in the geniculate-extrastriate system of the macaque: implications for heterogeneity in the koniocellular pathway and recovery from cortical damage. *J Comp Neurol* 431:168–181. [CrossRef Medline](#)
- Roopun AK, Middleton SJ, Cunningham MO, Lebeau FE, Bibbig A, Whittington MA, Traub RD (2006) A beta2-frequency (20–30 Hz) oscillation in nonsynaptic networks of somatosensory cortex. *Proc Natl Acad Sci U S A* 103:15646–15650. [CrossRef Medline](#)
- Roopun AK, Lebeau FE, Rammell J, Cunningham MO, Traub RD, Whittington MA (2010) Cholinergic neuromodulation controls directed tempo-

- ral communication in neocortex in vitro. *Front Neural Circuits* 4:8. [CrossRef Medline](#)
- Saalmann YB, Pinsk MA, Wang L, Li X, Kastner S (2012) The pulvinar regulates information transmission between cortical areas based on attention demands. *Science* 337:753–756. [CrossRef Medline](#)
- Salazar RF, Dotson NM, Bressler SL, Gray CM (2012) Content-specific fronto-parietal synchronization during visual working memory. *Science* 338:1097–1100. [CrossRef Medline](#)
- Schmid MC, Panagiotaropoulos T, Augath MA, Logothetis NK, Smirnakis SM (2009) Visually driven activation in macaque areas V2 and V3 without input from the primary visual cortex. *PLoS One* 4:e5527. [CrossRef Medline](#)
- Schmid MC, Mrowka SW, Turchi J, Saunders RC, Wilke M, Peters AJ, Ye FQ, Leopold DA (2010) Blindsight depends on the lateral geniculate nucleus. *Nature* 466:373–377. [CrossRef Medline](#)
- Schmid MC, Schmiedt JT, Peters AJ, Saunders RC, Maier A, Leopold DA (2013) Motion-sensitive responses in visual area v4 in the absence of primary visual cortex. *J Neurosci* 33:18740–18745. [CrossRef Medline](#)
- Stepniewska I, Qi HX, Kaas JH (1999) Do superior colliculus projection zones in the inferior pulvinar project to MT in primates? *Eur J Neurosci* 11:469–480. [CrossRef Medline](#)
- Steriade M (1993) Cellular substrates of brain rhythms. In: *Electroencephalography: basic principles, clinical applications, and related fields*, Ed 3 (Niedermeyer E, Lopes da Silva FH, eds), pp 27–62. Baltimore: Williams and Wilkins.
- Sun W, Dan Y (2009) Layer-specific network oscillation and spatiotemporal receptive field in the visual cortex. *Proc Natl Acad Sci U S A* 106:17986–17991. [CrossRef Medline](#)
- Tallon-Baudry C, Mandon S, Freiwald WA, Kreiter AK (2004) Oscillatory synchrony in the monkey temporal lobe correlates with performance in a visual short-term memory task. *Cereb Cortex* 14:713–720. [CrossRef Medline](#)
- Taylor K, Mandon S, Freiwald WA, Kreiter AK (2005) Coherent oscillatory activity in monkey area v4 predicts successful allocation of attention. *Cereb Cortex* 15:1424–1437. [Medline](#)
- Wilke M, Logothetis NK, Leopold DA (2006) Local field potential reflects perceptual suppression in monkey visual cortex. *Proc Natl Acad Sci U S A* 103:17507–17512. [CrossRef Medline](#)
- Wróbel A, Ghazaryan A, Bekisz M, Bogdan W, Kamiński J (2007) Two streams of attention-dependent beta activity in the striate recipient zone of cat's lateral posterior-pulvinar complex. *J Neurosci* 27:2230–2240. [CrossRef Medline](#)
- Xing D, Yeh CI, Burns S, Shapley RM (2012) Laminar analysis of visually evoked activity in the primary visual cortex. *Proc Natl Acad Sci U S A* 109:13871–13876. [CrossRef Medline](#)

Part IV

Appendix

Bibliography

- B. B. Averbeck, P. E. Latham, and A. Pouget. Neural correlations, population coding and computation. *Nat. Rev. Neurosci.*, 2006.
- A. M. Bastos, F. Briggs, H. J. Alitto, G. R. Mangun, and W. M. Usrey. Simultaneous recordings from the primary visual cortex and lateral geniculate nucleus reveal rhythmic interactions and a cortical source for gamma-band oscillations. *J. Neurosci.*, 2014.
- A. M. Bastos, J. Vezoli, C. A. Bosman, J.-M. Schoffelen, R. Oostenveld, J. R. Dowdall, P. De Weerd, H. Kennedy, and P. Fries. Visual Areas Exert Feedforward and Feedback Influences through Distinct Frequency Channels. *Neuron*, 2015.
- D. B. Bender. Retinotopic organization of macaque pulvinar. *J. Neurophysiol.*, 1981.
- D. B. Bender and M. Youakim. Effect of Attentive Fixation in Macaque Thalamus and Cortex. *J. Neurophysiol.*, 2001.
- H. Berger. *Über das Elektroencephalogramm des Menschen*. Archiv für Psychiatrie und Nervenkrankheiten, 1929.
- S. E. Boehnke and D. D. Rasmusson. Time course and effective spread of lidocaine and tetrodotoxin delivered via microdialysis: an electrophysiological study in cerebral cortex. *J. Neurosci. Meth.*, 2001.
- C. A. Bosman, J.-M. Schoffelen, N. Brunet, R. Oostenveld, A. M. Bastos, T. Womelsdorf, B. Rubehn, T. Stieglitz, P. De Weerd, and P. Fries. Attentional Stimulus Selection through Selective Synchronization between Monkey Visual Areas. *Neuron*, 2012.
- E. A. Buffalo, P. Fries, R. Landman, T. J. Buschman, and R. Desimone. Laminar differences in gamma and alpha coherence in the ventral stream. *Proc. Natl. Acad. Sci. U.S.A.*, 2011.
- G. Buzsáki. *Rhythms of the Brain*. Oxford University Press, USA, 2006.
- G. Buzsáki and X.-J. Wang. Mechanisms of Gamma Oscillations. *Annu. Rev. Neurosci.*, 2012.
- G. Buzsáki, N. Logothetis, and W. Singer. Scaling brain size, keeping timing: evolutionary preservation of brain rhythms. *Neuron*, 2013.
- M. A. Castro-Alamancos and M. E. Calcagnotto. High-pass filtering of corticothalamic activity by neuromodulators released in the thalamus during arousal: in vitro and in vivo. *J. Neurophysiol.*, 2001.
- F. Clascá, P. Rubio-Garrido, and D. Jabaudon. Unveiling the diversity of thalamocortical neuron subtypes. *Eur. J. Neurosci.*, 2012.
- C. M. Constantinople and R. M. Bruno. Deep Cortical Layers Are Activated Directly by Thalamus. *Science*, 2013.

BIBLIOGRAPHY

- J. W. Cooley and J. W. Tukey. An algorithm for the machine calculation of complex Fourier series. *Math. Comp.*, 1965.
- R. Courtemanche, N. Fujii, and A. M. Graybiel. Synchronous, focally modulated beta-band oscillations characterize local field potential activity in the striatum of awake behaving monkeys. *J. Neurosci.*, 2003.
- A. Cowey. The blindsight saga. *Exp. Brain Res.*, 2010.
- S. Crochet and C. C. H. Petersen. Correlating whisker behavior with membrane potential in barrel cortex of awake mice. *Nat. Neurosci.*, 2006.
- V. Crunelli and S. W. Hughes. The slow (<1 Hz) rhythms of non-REM sleep: a dialogue between three cardinal oscillators. *Nat. Neurosci.*, 2010.
- V. Crunelli, S. Lightowler, and C. E. Pollard. A T-type Ca²⁺ current underlies low-threshold Ca²⁺ potentials in cells of the cat and rat lateral geniculate nucleus. *J. Physiol.*, 1989.
- V. Crunelli, F. David, M. L. Lőrincz, and S. W. Hughes. The thalamocortical network as a single slow wave-generating unit. *Curr. Opin. Neurobiol.*, 2014.
- F. David and J. T. Schmiedt. Thalamus and cortex: inseparable partners in shaping sleep slow waves? *J. Neurosci.*, 2014.
- F. David, J. T. Schmiedt, H. L. Taylor, G. Orbán, G. Di Giovanni, V. N. Uebele, J. J. Renger, R. C. Lambert, N. Leresche, and V. Crunelli. Essential thalamic contribution to slow waves of natural sleep. *J. Neurosci.*, 2013.
- M. Deschenes, J. P. Roy, and M. Steriade. Thalamic bursting mechanism: an inward slow current revealed by membrane hyperpolarization. *Brain. Res.*, 1982.
- S. Diekelmann and J. Born. The memory function of sleep. *Nat. Rev. Neurosci.*, 2010.
- R. Eckhorn, R. Bauer, W. Jordan, M. Brosch, W. Kruse, M. Munk, and H. J. Reitboeck. Coherent oscillations: a mechanism of feature linking in the visual cortex? Multiple electrode and correlation analyses in the cat. *Biol Cybern.*, 1988.
- A. K. Engel and P. Fries. Beta-band oscillations—signalling the status quo? *Curr. Opin. Neurobiol.*, 2010.
- D. J. Felleman and D. C. Van Essen. Distributed Hierarchical Processing in the Primate Cerebral Cortex. *Cereb. Cortex*, 1991.
- P. Fries. A mechanism for cognitive dynamics: neuronal communication through neuronal coherence. *Trends Cogn. Sci. (Regul. Ed.)*, 2005.
- P. Fries. Neuronal gamma-band synchronization as a fundamental process in cortical computation. *Annu. Rev. Neurosci.*, 2009.
- P. Fries. Rhythms for Cognition: Communication through Coherence. *Neuron*, 2015.
- K. Fujimura and Y. Matsuda. Autogenous oscillatory potentials in neurons of the guinea pig substantia nigra pars compacta in vitro. *Neurosci. Lett.*, 1989.
- J. M. Fuster and G. E. Alexander. Firing changes in cells of the nucleus medialis dorsalis associated with delayed response behavior. *Brain. Res.*, 1973.
- C. D. Gilbert and W. Li. Adult visual cortical plasticity. *Neuron*, 2012.

-
- R. Goutagny, J. Jackson, and S. Williams. Self-generated theta oscillations in the hippocampus. *Nature Publishing Group*, 2009.
- A. A. Grace and S. P. Onn. Morphology and electrophysiological properties of immunocytochemically identified rat dopamine neurons recorded in vitro. *J. Neurosci.*, 1989.
- C. M. Gray and W. Singer. Stimulus-specific neuronal oscillations in orientation columns of cat visual cortex. *Proc. Natl. Acad. Sci. U.S.A.*, 1989.
- C. Gutierrez, A. Yaun, and C. G. Cusick. Neurochemical subdivisions of the inferior pulvinar in macaque monkeys. *J. Comp. Neurol.*, 1995.
- C. Gutierrez, M. G. Cola, B. Seltzer, and C. Cusick. Neurochemical and connective organization of the dorsal pulvinar complex in monkeys. *J. Comp. Neurol.*, 2000.
- N. C. Harris, C. Webb, and S. A. Greenfield. A possible pacemaker mechanism in pars compacta neurons of the guinea-pig substantia nigra revealed by various ion channel blocking agents. *Neuroscience*, 1989.
- S. H. C. Hendry and R. C. Reid. The Koniocellular Pathway in Primate Vision. *Annu. Rev. Neurosci.*, 2000.
- J. I. Hubbard, R. R. Llinás, and D. M. J. Quastel. *Electrophysiological analysis of synaptic transmission*. Edward Arnold, 1969.
- D. H. Hubel and T. N. Wiesel. Receptive fields of single neurones in the cat's striate cortex. *J. Physiol.*, 1959.
- S. A. Huettel, A. W. Song, and G. McCarthy. *Functional Magnetic Resonance Imaging*. Sinauer Associates Incorporated, 2009.
- S. W. Hughes, D. W. Cope, K. L. Blethyn, and V. Crunelli. Cellular mechanisms of the slow (<1Hz) oscillation in thalamocortical neurons in vitro. *Neuron*, 2002.
- S. W. Hughes, M. Lörincz, D. W. Cope, K. L. Blethyn, K. A. Kékesi, H. R. Parri, G. Juhász, and V. Crunelli. Synchronized Oscillations at α and θ Frequencies in the Lateral Geniculate Nucleus. *Neuron*, 2004.
- H. Jahnsen and R. Llinás. Electrophysiological properties of guinea-pig thalamic neurones: an in vitro study. *J. Physiol.*, 1984a.
- H. Jahnsen and R. Llinás. Ionic basis for the electro-responsiveness and oscillatory properties of guinea-pig thalamic neurones in vitro. *J. Physiol.*, 1984b.
- E. G. Jones. The thalamic matrix and thalamocortical synchrony. *Trends Neurosci.*, 2001.
- E. G. Jones. *The Thalamus*. Springer Science & Business Media, 2012.
- T. Kanamaru. Van der Pol oscillator. *Scholarpedia*, 2007.
- J. Keener and J. Sneyd. *Mathematical Physiology*. Springer Science & Business Media, 2009.
- P. Khanna and J. M. Carmena. Neural oscillations: beta band activity across motor networks. *Curr. Opin. Neurobiol.*, 2015.
- B. E. Kilavik, M. Zaepffel, A. Brovelli, W. A. MacKay, and A. Riehle. The ups and downs of β oscillations in sensorimotor cortex. *Exp. Neurol.*, 2013.
- A. K. Kreiter. How do we model attention-dependent signal routing? *Neural Netw*, 2006.

BIBLIOGRAPHY

- A. N. Landau and P. Fries. Attention samples stimuli rhythmically. *Curr. Biol.*, 2012.
- A. N. Landau, H. M. Schreyer, S. van Pelt, and P. Fries. Distributed Attention Is Implemented through Theta-Rhythmic Gamma Modulation. *Curr. Biol.*, 2015.
- M. Lemieux, J.-Y. Chen, P. Lonjers, M. Bazhenov, and I. Timofeev. The impact of cortical deafferentation on the neocortical slow oscillation. *J. Neurosci.*, 2014.
- R. Llinás and H. Jahnsen. Electrophysiology of mammalian thalamic neurones in vitro. *Nature*, 1982.
- R. R. Llinás and M. Steriade. Bursting of thalamic neurons and states of vigilance. *J. Neurophysiol.*, 2006.
- S. G. Lomber. The advantages and limitations of permanent or reversible deactivation techniques in the assessment of neural function. *J. Neurosci. Meth.*, 1999.
- F. H. Lopes da Silva, A. van Rotterdam, W. Storm van Leeuwen, and A. M. Tielen. Dynamic characteristics of visual evoked potentials in the dog. II. Beta frequency selectivity in evoked potentials and background activity. *Electro. Clin. Neuro.*, 1970.
- M. L. Lőrincz, K. A. Kékesi, G. Juhász, V. Crunelli, and S. W. Hughes. Temporal Framing of Thalamic Relay-Mode Firing by Phasic Inhibition during the Alpha Rhythm. *Neuron*, 2009.
- D. C. Lyon and C. Rabideau. Lack of robust LGN label following transneuronal rabies virus injections into macaque area V4. *J. Comp. Neurol.*, 2012.
- A. Maier, C. J. Aura, and D. A. Leopold. Infragranular sources of sustained local field potential responses in macaque primary visual cortex. *J. Neurosci.*, 2011.
- N. T. Markov, M. Ercsey-Ravasz, D. C. Van Essen, K. Knoblauch, Z. Toroczkai, and H. Kennedy. Cortical High-Density Counterstream Architectures. *Science*, 2013.
- D. A. McCormick and H. C. Pape. Properties of a hyperpolarization-activated cation current and its role in rhythmic oscillation in thalamic relay neurones. *J. Physiol.*, 1990.
- P. Mitra and H. Bokil. *Observed Brain Dynamics*. Oxford University Press, 2007.
- R. Y. Moore and V. B. Eichler. Loss of a circadian adrenal corticosterone rhythm following suprachiasmatic lesions in the rat. *Brain. Res.*, 1972.
- R. S. Morison and D. L. Bassett. Electrical activity of the thalamus and basal ganglia in decorticate cats. *J. Neurophysiol.*, 1945.
- V. Mountcastle. The evolution of ideas concerning the function of the neocortex. *Cereb. Cortex*, 1995.
- R. C. Mureşan, O. F. Jurjuţ, V. V. Moca, W. Singer, and D. Nikolic. The oscillation score: an efficient method for estimating oscillation strength in neuronal activity. *J. Neurophysiol.*, 2008.
- R. K. Nakamura and M. Mishkin. Blindness in monkeys following non-visual cortical lesions. *Brain. Res.*, 1980.
- Y. Nir, R. J. Staba, T. Andrillon, V. V. Vyazovskiy, C. Cirelli, I. Fried, and G. Tononi. Regional slow waves and spindles in human sleep. *Neuron*, 2011.
- P. L. Nunez and R. Srinivasan. *Electric Fields of the Brain*. Oxford University Press, 2006.
- J. Olszewski. *The Thalamus of the Macaca Mulatta*. Karger, 1952.

-
- R. Oostenveld, P. Fries, E. Maris, and J.-M. Schoffelen. FieldTrip: Open source software for advanced analysis of MEG, EEG, and invasive electrophysiological data. *Comput. Intell. Neurosci.*, 2011.
- A. M. Packer, B. Roska, and M. Häusser. Targeting neurons and photons for optogenetics. *Nat. Neurosci.*, 2013.
- H. C. Pape. Queer current and pacemaker: the hyperpolarization-activated cation current in neurons. *Annu. Rev. Physiol.*, 1996.
- C. C. H. Petersen, T. T. G. Hahn, M. Mehta, A. Grinvald, and B. Sakmann. Interaction of sensory responses with spontaneous depolarization in layer 2/3 barrel cortex. *Proc. Natl. Acad. Sci. U.S.A.*, 2003.
- S. E. Petersen, D. L. Robinson, and W. Keys. Pulvinar nuclei of the behaving rhesus monkey: visual responses and their modulation. *J. Neurophysiol.*, 1985.
- S. E. Petersen, D. L. Robinson, and J. D. Morris. Contributions of the pulvinar to visual spatial attention. *Neuropsychologia*, 1987.
- A. Pikovsky and M. Rosenblum. Synchronization. *Scholarpedia*, 2007.
- A. Pikovsky, M. Rosenblum, and J. Kurths. *Synchronization: A Universal Concept in Nonlinear Sciences*. Cambridge University Press, 2008.
- S. Pluta, A. Naka, J. Veit, G. Telian, L. Yao, R. Hakim, D. Taylor, and H. Adesnik. A direct translaminal inhibitory circuit tunes cortical output. *Nat. Neurosci.*, 2015.
- R. Q. Quiroga, L. Reddy, G. Kreiman, C. Koch, and I. Fried. Invariant visual representation by single neurons in the human brain. *Nature*, 2005.
- E. J. Ramcharan, J. W. Gnadt, and S. M. Sherman. Burst and tonic firing in thalamic cells of unanesthetized, behaving monkeys. *Vis. Neurosci.*, 2000.
- E. J. Ramcharan, J. W. Gnadt, and S. M. Sherman. Higher-order thalamic relays burst more than first-order relays. *Proc. Natl. Acad. Sci. U.S.A.*, 2005.
- D. L. Robinson and R. J. Cowie. The Primate Pulvinar: Structural, Functional, and Behavioral Components of Visual Saliency. In *Thalamus*. 1997.
- D. L. Robinson and S. E. Petersen. The pulvinar and visual saliency. *Trends Neurosci.*, 1992.
- K. S. Rockland, J. Andresen, R. J. Cowie, and D. L. Robinson. Single axon analysis of pulvinocortical connections to several visual areas in the Macaque. *J. Comp. Neurol.*, 1999.
- H. R. Rodman, K. M. Sorenson, A. J. Shim, and D. P. Hexter. Calbindin immunoreactivity in the geniculo-extrastriate system of the macaque: implications for heterogeneity in the koniocellular pathway and recovery from cortical damage. *J. Comp. Neurol.*, 2001.
- A. K. Roopun, M. A. Kramer, L. M. Carracedo, M. Kaiser, C. H. Davies, R. D. Traub, N. J. Kopell, and M. A. Whittington. Temporal Interactions between Cortical Rhythms. *Front. Neurosci.*, 2008.
- O. Ruiz, D. Royal, G. Sáry, X. Chen, J. D. Schall, and V. A. Casagrande. Low-threshold Ca²⁺-associated bursts are rare events in the LGN of the awake behaving monkey. *J. Neurophysiol.*, 2006.
- Y. B. Saalmann and S. Kastner. Cognitive and perceptual functions of the visual thalamus. *Neuron*, 2011.

BIBLIOGRAPHY

- Y. B. Saalmann, M. A. Pinsk, L. Wang, X. Li, and S. Kastner. The pulvinar regulates information transmission between cortical areas based on attention demands. *Science*, 2012.
- R. Sachdev, N. Gaspard, and J. L. Gerrard. Delta rhythm in wakefulness: evidence from intracranial recordings in human beings. *J. Neurophysiol.*, 2015.
- K. S. Saleem and N. K. Logothetis. *A Combined MRI and Histology Atlas of the Rhesus Monkey Brain in Stereotaxic Coordinates*. Academic Press, 2012.
- M. V. Sanchez-Vives and D. A. McCormick. Cellular and network mechanisms of rhythmic recurrent activity in neocortex. *Nat. Neurosci.*, 2000.
- M. C. Schmid, T. Panagiotaropoulos, M. A. Augath, N. K. Logothetis, and S. M. Smirnakis. Visually driven activation in macaque areas V2 and V3 without input from the primary visual cortex. *PLoS ONE*, 2009.
- M. C. Schmid, S. W. Mrowka, J. Turchi, R. C. Saunders, M. Wilke, A. J. Peters, F. Q. Ye, and D. A. Leopold. Blindsight depends on the lateral geniculate nucleus. *Nature*, 2010.
- M. C. Schmid, J. T. Schmiedt, A. J. Peters, R. C. Saunders, A. Maier, and D. A. Leopold. Motion-sensitive responses in visual area V4 in the absence of primary visual cortex. *J. Neurosci.*, 2013.
- J. T. Schmiedt, A. Maier, P. Fries, R. C. Saunders, D. A. Leopold, and M. C. Schmid. Beta oscillation dynamics in extrastriate cortex after removal of primary visual cortex. *J. Neurosci.*, 2014.
- S. M. Sherman. A wake-up call from the thalamus. *Nat. Neurosci.*, 2001.
- S. M. Sherman and R. W. Guillery. *Exploring the Thalamus and Its Role in Cortical Function*. MIT Press (MA), 2009.
- S. Shipp. The functional logic of cortico-pulvinar connections. *Phil. Trans. R. Soc. B*, 2003.
- L. C. Sincich, K. F. Park, M. J. Wohlgemuth, and J. C. Horton. Bypassing V1: a direct geniculate input to area MT. *Nat. Neurosci.*, 2004.
- S. M. Smirnakis, A. A. Brewer, M. C. Schmid, A. S. Tolia, A. Schüz, M. Augath, W. Inhoffen, B. A. Wandell, and N. K. Logothetis. Lack of long-term cortical reorganization after macaque retinal lesions. *Nature*, 2005.
- J. C. Snow, H. A. Allen, R. D. Rafal, and G. W. Humphreys. Impaired attentional selection following lesions to human pulvinar: Evidence for homology between human and monkey. *Proc. Natl. Acad. Sci. U.S.A.*, 2009.
- E. Spaak, F. P. de Lange, and O. Jensen. Local Entrainment of Alpha Oscillations by Visual Stimuli Causes Cyclic Modulation of Perception. *J. Neurosci.*, 2014.
- F. K. Stephan and I. Zucker. Circadian rhythms in drinking behavior and locomotor activity of rats are eliminated by hypothalamic lesions. *Proc. Natl. Acad. Sci. U.S.A.*, 1972.
- M. Steriade. Cellular Substrates of Brain Rhythms. In *Electroencephalography: Basic Principles, Clinical Applications, and Related Fields*. 1993.
- M. Steriade. To burst, or rather, not to burst. *Nat. Neurosci.*, 2001a.
- M. Steriade. *The Intact and Sliced Brain*. MIT Press, 2001b.
- M. Steriade and M. Deschenes. The thalamus as a neuronal oscillator. *Brain Res. Rev.*, 1984.

- M. Steriade, M. Deschenes, L. Domich, and C. Mulle. Abolition of spindle oscillations in thalamic neurons disconnected from nucleus reticularis thalami. *J. Neurophysiol.*, 1985.
- M. Steriade, D. Contreras, R. Curró Dossi, and A. Nuñez. The slow (<1 Hz) oscillation in reticular thalamic and thalamocortical neurons: scenario of sleep rhythm generation in interacting thalamic and neocortical networks. *J. Neurosci.*, 1993a.
- M. Steriade, D. A. McCormick, and T. J. Sejnowski. Thalamocortical oscillations in the sleeping and aroused brain. *Science*, 1993b.
- M. Steriade, A. Nuñez, and F. Amzica. Intracellular analysis of relations between the slow (<1 Hz) neocortical oscillation and other sleep rhythms of the electroencephalogram. *J. Neurosci.*, 1993c.
- M. Steriade, A. Nuñez, and F. Amzica. A novel slow (<1 Hz) oscillation of Neocortical neurons in vivo: depolarizing and hyperpolarizing components. *J. Neurosci.*, 1993d.
- S. H. Strogatz. *Nonlinear Dynamics and Chaos*. Westview Press, 2014.
- W. Sun and Y. Dan. Layer-specific network oscillation and spatiotemporal receptive field in the visual cortex. *Proc. Natl. Acad. Sci. U.S.A.*, 2009.
- H. A. Swadlow and A. G. Gusev. The impact of 'bursting' thalamic impulses at a neocortical synapse. *Nat. Neurosci.*, 2001.
- M. Thieffry, Y. Burnod, Y. Poussart, and J. Calvet. Synchronous modifications in the cortical and pulvinar unit activity during slow wave sleep. *Exp. Neurol.*, 1977.
- A. Thiele, L. S. Delicato, M. J. Roberts, and M. A. Gieselmann. A novel electrode-pipette design for simultaneous recording of extracellular spikes and iontophoretic drug application in awake behaving monkeys. *J. Neurosci. Meth.*, 2006.
- C. Torrence and G. P. Compo. A practical guide to wavelet analysis. *Bull. Amer. Meteor. Soc.*, 1998.
- L. G. Ungerleider and C. A. Christensen. Pulvinar lesions in monkeys produce abnormal scanning of a complex visual array. *Neuropsychologia*, 1979.
- T. van Kerkoerle, M. W. Self, B. Dagnino, M. A. Gariel-Mathis, J. Poort, C. van der Togt, and P. R. Roelfsema. Alpha and gamma oscillations characterize feedback and feedforward processing in monkey visual cortex. *Proc. Natl. Acad. Sci. U.S.A.*, 2014.
- V. V. Vyazovskiy and K. D. Harris. Sleep and the single neuron: the role of global slow oscillations in individual cell rest. *Nat. Rev. Neurosci.*, 2013.
- V. V. Vyazovskiy, U. Olcese, E. C. Hanlon, Y. Nir, C. Cirelli, and G. Tononi. Local sleep in awake rats. *Nature*, 2011.
- A. E. Walker. The primate thalamus. 1938.
- X. J. Wang. Neural oscillations. *Encyclopedia of cognitive science*, 2003.
- H. Wässle. Parallel processing in the mammalian retina. *Nat. Rev. Neurosci.*, 2004.
- H. Wei, M. Bonjean, H. M. Petry, T. J. Sejnowski, and M. E. Bickford. Thalamic burst firing propensity: a comparison of the dorsal lateral geniculate and pulvinar nuclei in the tree shrew. *J. Neurosci.*, 2011.
- M. Wilke, K. M. Mueller, and D. A. Leopold. Neural activity in the visual thalamus reflects perceptual suppression. *Proc. Natl. Acad. Sci. U.S.A.*, 2009.

BIBLIOGRAPHY

- C. D. Woody, E. Gruen, and X. F. Wang. Electrical properties affecting discharge of units of the mid and posterolateral thalamus of conscious cats. *Neuroscience*, 2003.
- A. Wróbel. Beta activity: a carrier for visual attention. *Acta Neurobiol. Exp. (Wars)*, 2000.
- R. H. Wurtz and E. R. Kandel. Central Visual Pathways. In *Principles of neural science*. 2000.
- A. Yamadori. Role of the spindles in the onset of sleep. *Kobe J. Med. Sci.*, 1971.
- J. Zihl and D. von Cramon. The contribution of the 'second' visual system to directed visual attention in man. *Brain*, 1979.

List of publications

Peer-reviewed publications

- Shapcott KA, **Schmiedt JT**, Saunders RC, Maier A, Leopold DA, Schmid MC (in review) Correlated activity of cortical neurons in the absence of feedforward sensory input.
- Schmiedt JT**, Maier A, Fries P, Saunders RC, Leopold DA, Schmid MC (2014) Beta oscillation dynamics in extrastriate cortex after removal of primary visual cortex. *J Neurosci* 34:11857–11864.
- David F & **Schmiedt JT** (2014) Thalamus and cortex: inseparable partners in shaping sleep slow waves? *J Neurosci* 34:11517–11518.
- Taylor H*, **Schmiedt JT***, Çarçak N, Onat F, Di Giovanni G, Lambert R, Leresche N, Crunelli V, David F (2014) Investigating local and long-range neuronal network dynamics by simultaneous optogenetics, reverse microdialysis and silicon probe recordings *in vivo*. *J Neurosci Methods* 235C:83–91.
- Schmid MC*, **Schmiedt JT***, Peters AJ, Saunders RC, Maier A, Leopold DA (2013) Motion-sensitive responses in visual area V4 in the absence of primary visual cortex. *J Neurosci* 33:18740–18745.
- Albers C, **Schmiedt JT**, Pawelzik KR (2013) Theta-specific susceptibility in a model of adaptive synaptic plasticity. *Front Comput Neurosci* 7:170.
- David F*, **Schmiedt JT***, Taylor HL, Orban G, Di Giovanni G, Uebele VN, Renger JJ, Lambert RC, Leresche N, Crunelli V (2013) Essential thalamic contribution to slow waves of natural sleep. *J Neurosci* 33:19599–19610.
- Mathes B, **Schmiedt JT**, Schmiedt-Fehr C, Pantelis C, Basar-Eroglu Ç (2012) New rather than old? For working memory tasks with abstract patterns the P3 and the single-trial delta response are larger for modified than identical probe stimuli. *Psychophysiology* 49:920–932.
- Schmiedt JT**, Albers C, Pawelzik K (2010) Spike timing-dependent plasticity as dynamic filter. *NIPS*:2110–2118.

*Authors contributed equally.

Other publications

- Schmiedt JT** & Schmid MC (2014) Sehen ohne Bewusstsein – was und warum sehen Blindseher?. *Max Planck Jahrbuch*.

Acknowledgements

Science thrives on inspiration. Inspiration for me always came through the great teachers I had the honor to be taught by. I would like to thank Canan Basar-Eroglu, Klaus Pawelzik, Vincenzo Crunelli and Michael Schmid who all gave me their complementary perspectives on how the brain might work. I am truly grateful for the opportunities and support that I was given such that I could learn and pursue all the ideas I had.

With the teachers came welcoming, inspiring and helpful communities, which I enjoyed to be part of; thank you (in no particular but roughly historical order), Stini, Edwin, Jan, Birgit, Wilfried, Evgenij, David, Udo, Christian, Ingo, Agnes, Marcus, Cian, François, Kleo, Katharine, Ricardo, Carsten, Sabrina, Marieke, Hermann, Alina, Pascal, Chris, Craig, Ayelet, Jianguang, Giorgos S. & M., Jarrod, Julien, Thomas, Patrick, Andre, Hanka, Sylvia, Andreea, Nina, Liane.

*Science thrives on scientists who actually are humans first.*¹ I would like to thank my (by now large) family and friends for their everlasting love and support. Without you I would not have been a happy scientist. Most importantly, Iris and Myrthe, thank you for being the love of my life.

¹A great insight borrowed from Andreea and Pascal

CV

JOSCHA T. SCHMIEDT

EDUCATION

11/2011 to date	PhD in Biosciences at Ernst Strüngmann Institute (ESI) for Neuroscience in Cooperation with Max Planck Society and Goethe University (Frankfurt/Main, Germany) <i>Thesis:</i> Thalamic and cortical contributions to physiological brain rhythms <i>in vivo</i> . <i>Supervisor:</i> Michael Schmid
10/2009 - 09/2011	MSc in Neurosciences at University of Bremen (Germany) / Cardiff University (UK) / Weizmann Institute (IL) <i>Thesis:</i> The effect of the selective T-type calcium channel blocker TTA-P2 on physiological brain rhythms <i>Supervisor:</i> Vincenzo Crunelli
10/2008 - 09/2009	Medical Studies at Hannover Medical School (Germany)
10/2005 - 09/2008	BSc in Physics at University of Bremen (Germany) <i>Thesis:</i> Classification of bistable perception by based on EEG data <i>Supervisors:</i> Canan Basar-Eroglu and Klaus Pawelzik
08/2004	Abitur at Ökumenisches Gynasium zu Bremen (Germany)

PEER-REVIEWED PUBLICATIONS

- Schmiedt JT, Maier A, Fries P, Saunders RC, Leopold DA, Schmid MC (2014) Beta oscillation dynamics in extrastriate cortex after removal of primary visual cortex. *J Neurosci* 34:11857–11864.
- David F & Schmiedt JT (2014) Thalamus and cortex: inseparable partners in shaping sleep slow waves? *J Neurosci* 34:11517–11518.
- Taylor H*, Schmiedt JT*, Çarçak N, Onat F, Di Giovanni G, Lambert R, Leresche N, Crunelli V, David F (2014) Investigating local and long-range neuronal network dynamics by simultaneous optogenetics, reverse microdialysis and silicon probe recordings *in vivo*. *J Neurosci Methods* 235C:83–91.
- Schmid MC*, Schmiedt JT*, Peters AJ, Saunders RC, Maier A, Leopold DA (2013) Motion-sensitive responses in visual area V4 in the absence of primary visual cortex. *J Neurosci* 33:18740–18745.
- Albers C, Schmiedt JT, Pawelzik KR (2013) Theta-specific susceptibility in a model of adaptive synaptic plasticity. *Front Comput Neurosci* 7:170.
- David F*, Schmiedt JT*, Taylor HL, Orbán G, Di Giovanni G, Uebele VN, Renger JJ, Lambert RC, Leresche N, Crunelli V (2013) Essential thalamic contribution to slow waves of natural sleep. *J Neurosci* 33:19599–19610.
- Mathes B, Schmiedt JT, Schmiedt-Fehr C, Pantelis C, Basar-Eroglu C (2012) New rather than old? For working memory tasks with abstract patterns the P3 and the single-trial delta response are larger for modified than identical probe stimuli. *Psychophysiology* 49:920–932.
- Schmiedt JT, Albers C, Pawelzik K (2010) Spike timing-dependent plasticity as dynamic filter. *NIPS*:2110–2118.

*equal contribution

CONFERENCE ABSTRACTS AND TALKS

- Schmiedt JT**, Saunders RC, Maier A, Leopold D, & Schmid MC. Low-frequency oscillations in extrastriate cortex: contributions of V1 and pulvinar. Poster at SfN Meeting, Washington, DC, USA, 2014.
- Schmiedt JT**, Peters AJ, Saunders RC, Maier A, Leopold D, & Schmid MC. Blindsight: insights from neuronal responses in macaque V4 after V1 injury. Talk at ECVP, Bremen, Germany, 2013.
- Schmiedt JT**. Neuronal organization of V4 after V1 injury. Invited talk at NIN, Amsterdam, Netherlands, 2013.
- Schmid MC, Peters AJ, **Schmiedt JT**, Saunders RC, Maier A, & Leopold D. Organization of neural responses in macaque area V4 without input from V1. Poster at SfN Meeting, New Orleans, USA, 2012.
- David F*, **Schmiedt JT***, Taylor HL, Orban G, Di Giovanni G, Uebele VN, Renger JJ, Lambert RC, Leresche N, & Crunelli V. T-type calcium channels of thalamocortical neurons are necessary for the full expression of sleep slow waves in the EEG. Poster at SfN Meeting, New Orleans, USA, 2012.
- Albers C, **Schmiedt J**, & Pawelzik KR. Inclusion of NMDA receptor like interactions into the contribution dynamics of synaptic plasticity captures adaptation phenomena in spike timing dependent plasticity. Poster at BCCN, Freiburg, Germany, 2011.
- Albers C, **Schmiedt JT**, & Pawelzik KR. Theta rhythmicity enhances learning in adaptive STDP. Poster at Cosyne, Salt Lake City, USA, 2011.
- Schmiedt JT**, Albers C, & Pawelzik K. Spike timing-dependent plasticity as dynamic filter. Poster at NIPS, Vancouver, Canada, 2010.
- Schmiedt JT**, Rotermund D, Basar-Eroglu C, & Pawelzik KR. High EEG-gamma-power codes perceptual states of ambiguous motion. Poster at CNS, Berlin, Germany, 2009.
- Schmiedt JT**, Pawelzik KR, & Basar-Eroglu C. Prediction of Cognitive States in Bistable Perception from EEG Data. Poster at ICON X, Bodrum, Turkey, 2008.

AWARDS AND SCHOOLS

12/2013	FENS-IBRO-Hertie Winter School on Thalamus and Thalamocortical Interactions (Oberurgl, Austria)
03/2012	G-Node Winter Course in Neural Data Analysis (Munich, Germany)
2006 - 2011	5 year study grant of the German National Academic Foundation (GNAF)
12/2010	NIPS travel award
09/2009	Minerva Workshop at the Weizmann Institute of Science (Rehovot, Israel)
09/2008	Summer School of the GNAF (Guidel, France) on "Music and Brain"
09/2005	Summer School of the GNAF (Alpbach, Austria) on "Learning Brains"
2002 - 2004	Study scholarship of the Ökumenisches Gymnasium (Bremen, Germany)
1995 - 2004	Several prizes in the national music competition "Jugend musiziert" (accordion, piano)